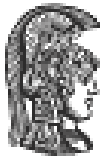

ΚΑΡΔΙΟΜΕΤΑΒΟΛΙΚΗ ΙΑΤΡΙΚΗ

ΕΛΛΗΝΙΚΗ ΔΗΜΟΚΡΑΤΙΑ
Εθνικόν και Καποδιστριακόν Πανεπιστήμιον Αθηνών
ΙΔΡΥΘΕΝ ΤΟ 1837
ΙΑΤΡΙΚΗ ΣΧΟΛΗ ΑΘΗΝΩΝ

ΠΜΣ: Καρδιομεταβολική Ιατρική
Απεικόνιση αθηρωματικής πλάκας

Κωνσταντίνος Κατωγιάννης, MD, PhD

Καρδιολόγος, Επιμελητής ΕΣΥ

ΠΓΝ «ΑΤΤΙΚΟΝ»

- Atherosclerosis is an inflammatory disease that causes most myocardial infarctions, strokes and acute coronary syndromes.
- The risk of atherosclerotic plaque rupture is not well correlated with stenosis severity.
- Lumenography has a central place for defining the site and severity of vascular stenosis as a prelude to intervention for relief of symptoms due to blood flow limitation.

Eur Heart J Cardiovasc Imaging. 2014 Jul;15(7):730-5. doi: 10.1093/ehjci/jeu094

- Atherosclerosis develops within the arterial wall.
- This is **not imaged by lumenography** and hence **it provides no information regarding underlying processes that may lead to plaque rupture.**

We must rely on other ***imaging modalities*** such as:

1. ultrasound,
2. computed tomography (CT),
3. magnetic resonance imaging,
4. nuclear imaging methods.

These are capable of reporting on the ***underlying pathology***, in particular:

- the presence of inflammation,
- calcification,
- neovascularization and
- intraplaque haemorrhage.

Additionally, non-invasive imaging can now be used to track the effect of anti-atherosclerosis therapy.

Eur Heart J Cardiovasc Imaging. 2014 Jul;15(7):730-5. doi: 10.1093/ehjci/jeu094

Vulnerable coronary artery plaques

- thin fibrous cap (<65 μm),
- large lipid-rich necrotic core,
- superficial spotty microcalcification,
- high macrophage density and expansive remodelling.

Stable coronary artery plaques

- thick fibrous cap
- macroscopic calcifications.

Histological studies on ruptured coronary plaques with active inflammation

- macrophage infiltration, neovascularization,
- intraplaque haemorrhage,
- platelet aggregation,
- proteolytic remodelling of the extracellular matrix,
- hypoxia,
- apoptosis
- smooth muscle proliferation

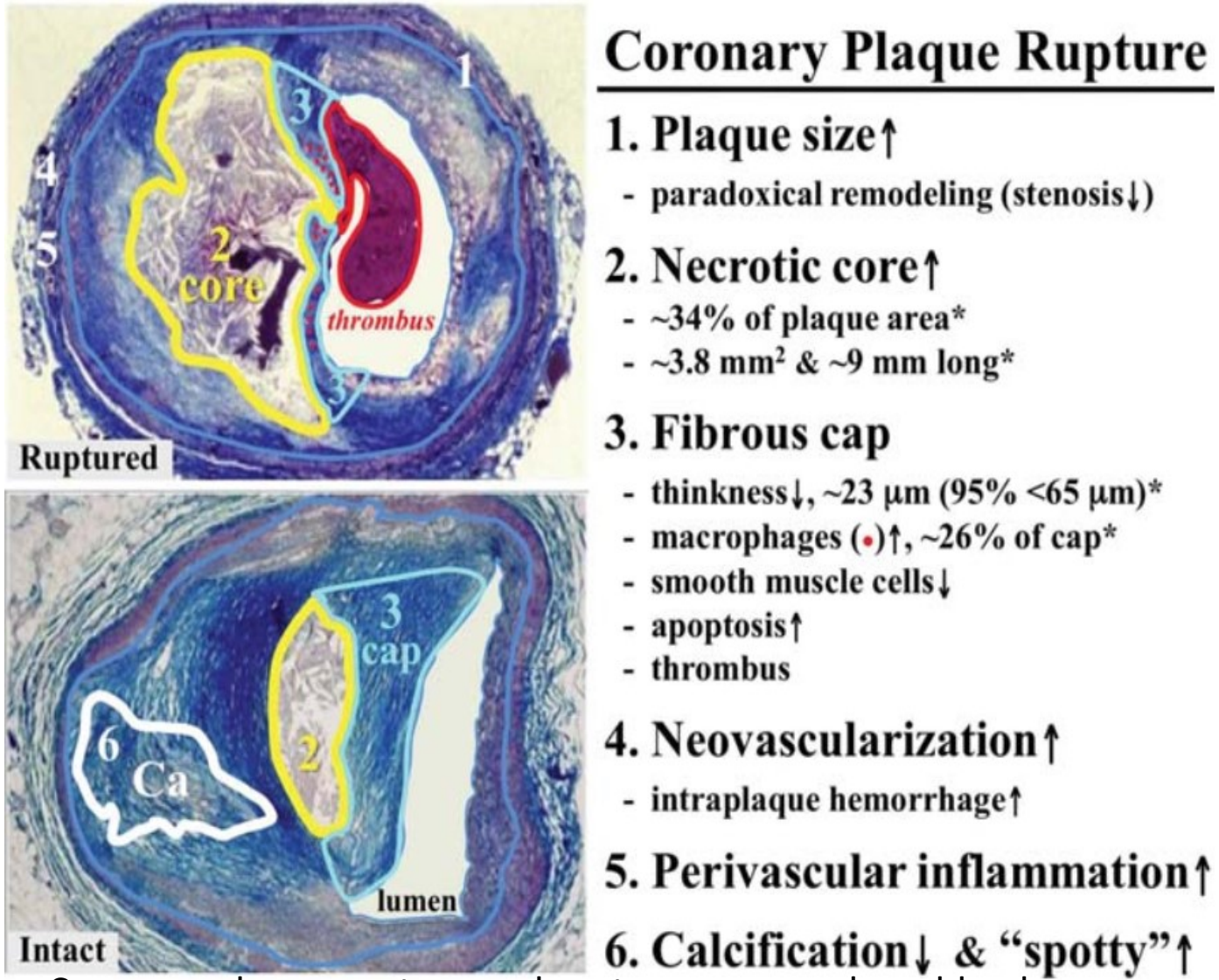

Coronary plaque rupture and rupture-prone vulnerable plaques.

Eur Heart J Cardiovasc Imaging. 2014 Jul;15(7):730-5. doi: 10.1093/ehjci/jeu094

Imaging of atherosclerosis by Ultrasound

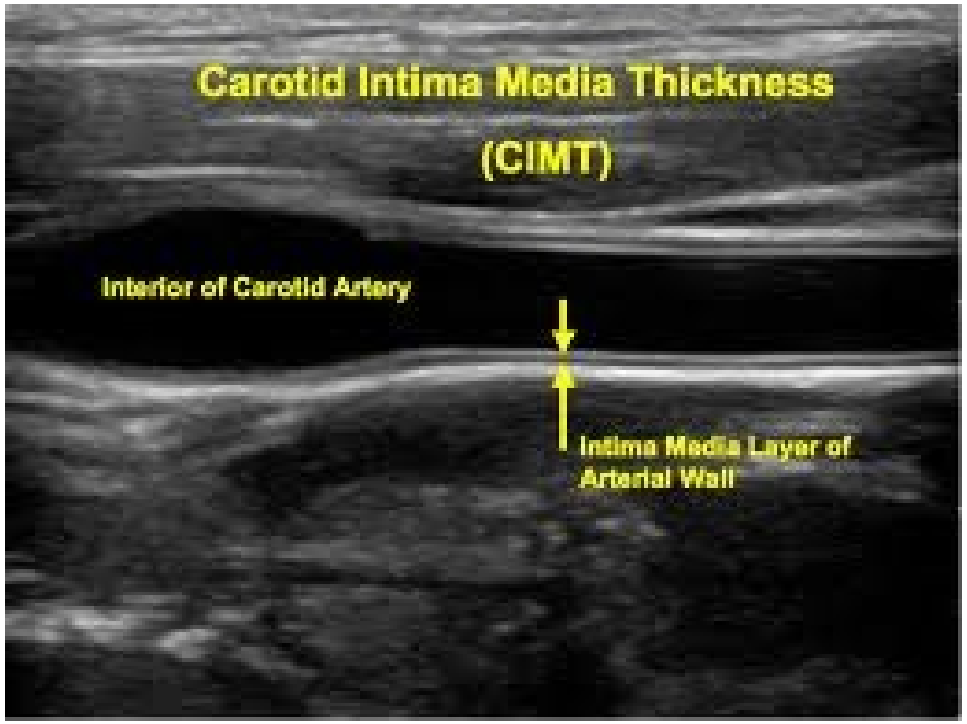

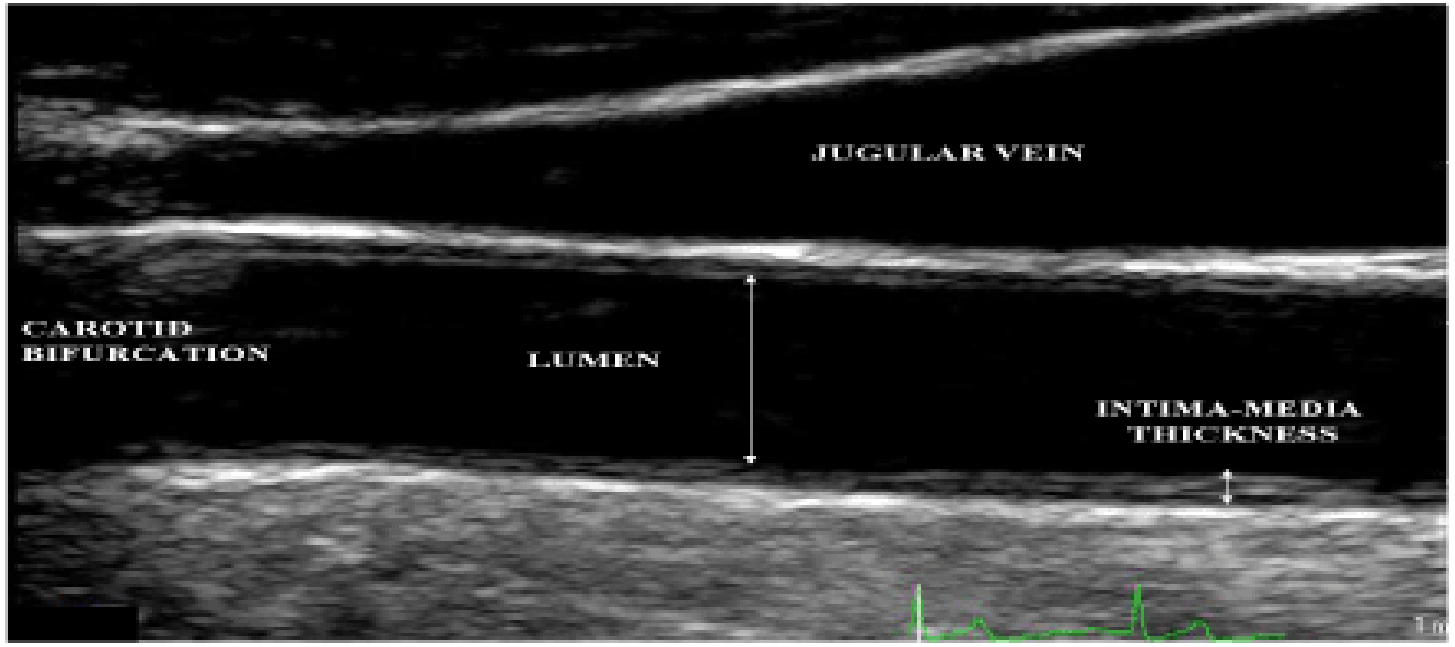

- Prospective data have shown CIMT correlates with cardiovascular risk, even in asymptomatic individuals.
- The Atherosclerosis Risk in the Community (ARIC) study demonstrated that for each 0.19 mm increase in CIMT, the risk of death or myocardial infarction increased by 36% in a middle-aged cohort.
- CIMT has been used to demonstrate the arterial response to therapy; the REGRESS study found that a 0.05 mm reduction in CIMT in patients treated with pravastatin was associated with a 10% decrease of the absolute risk of cardiovascular events over 2 years.

Eur Heart J Cardiovasc Imaging. 2014 Jul;15(7):730-5. doi: 10.1093/ehjci/jeu094

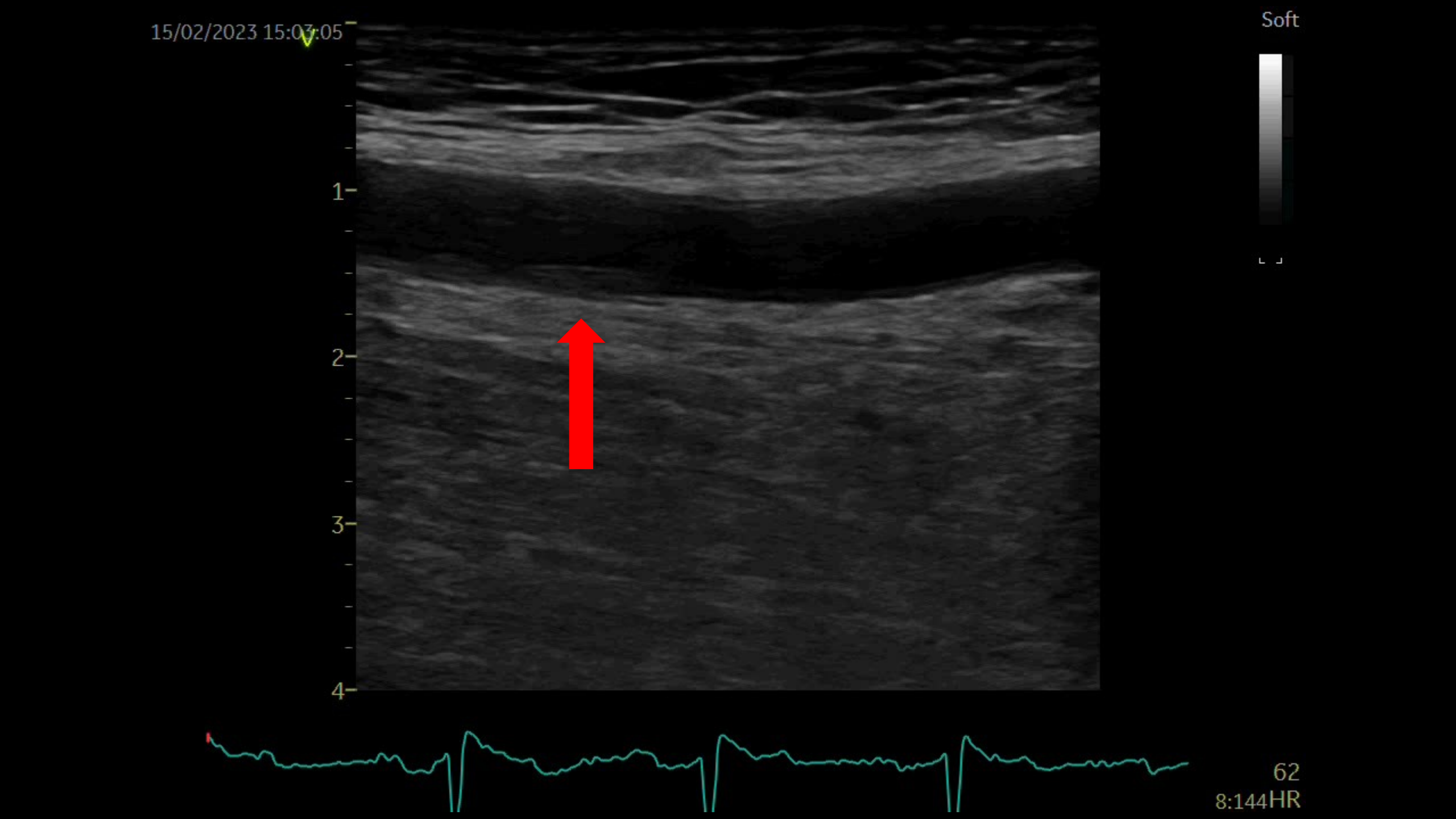
15/02/2023 15:03:05
Soft
1
2
3
4
62
8:144HR

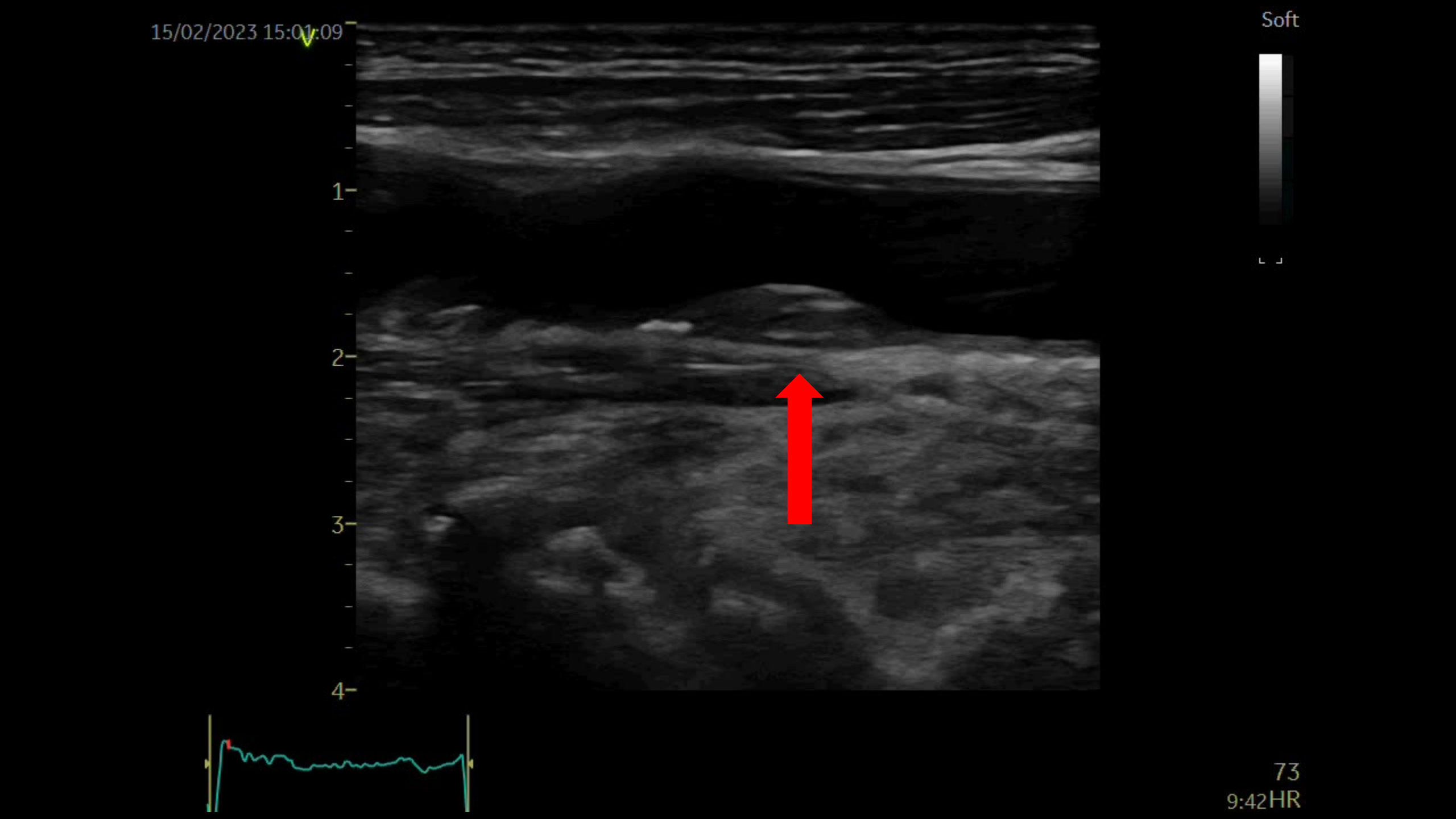
15/02/2023 15:01:09
Soft
1
2
3
4
73
9:42 HR

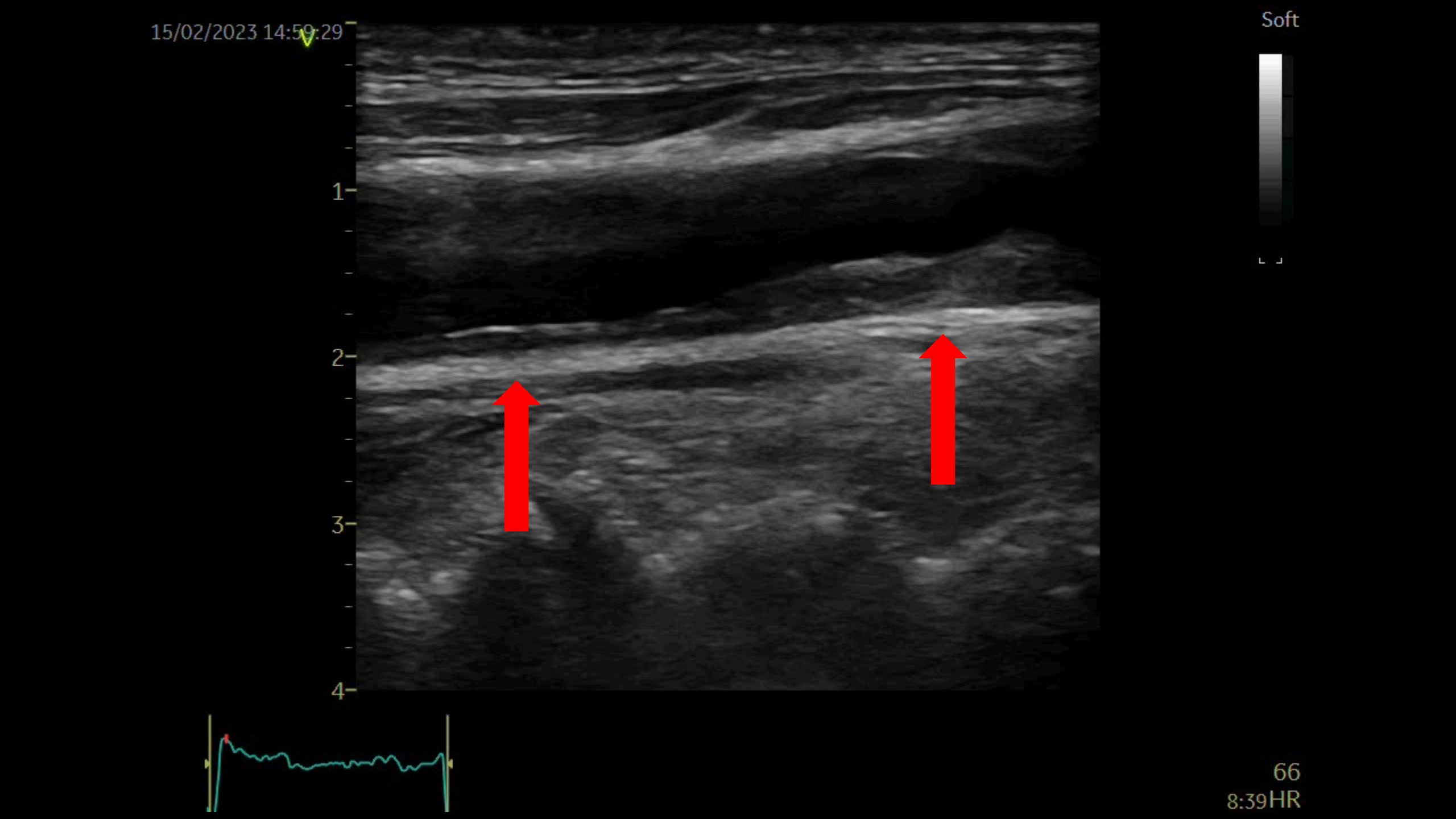
15/02/2023 14:59:29
Soft
1
2
3
4
66
8:39 HR

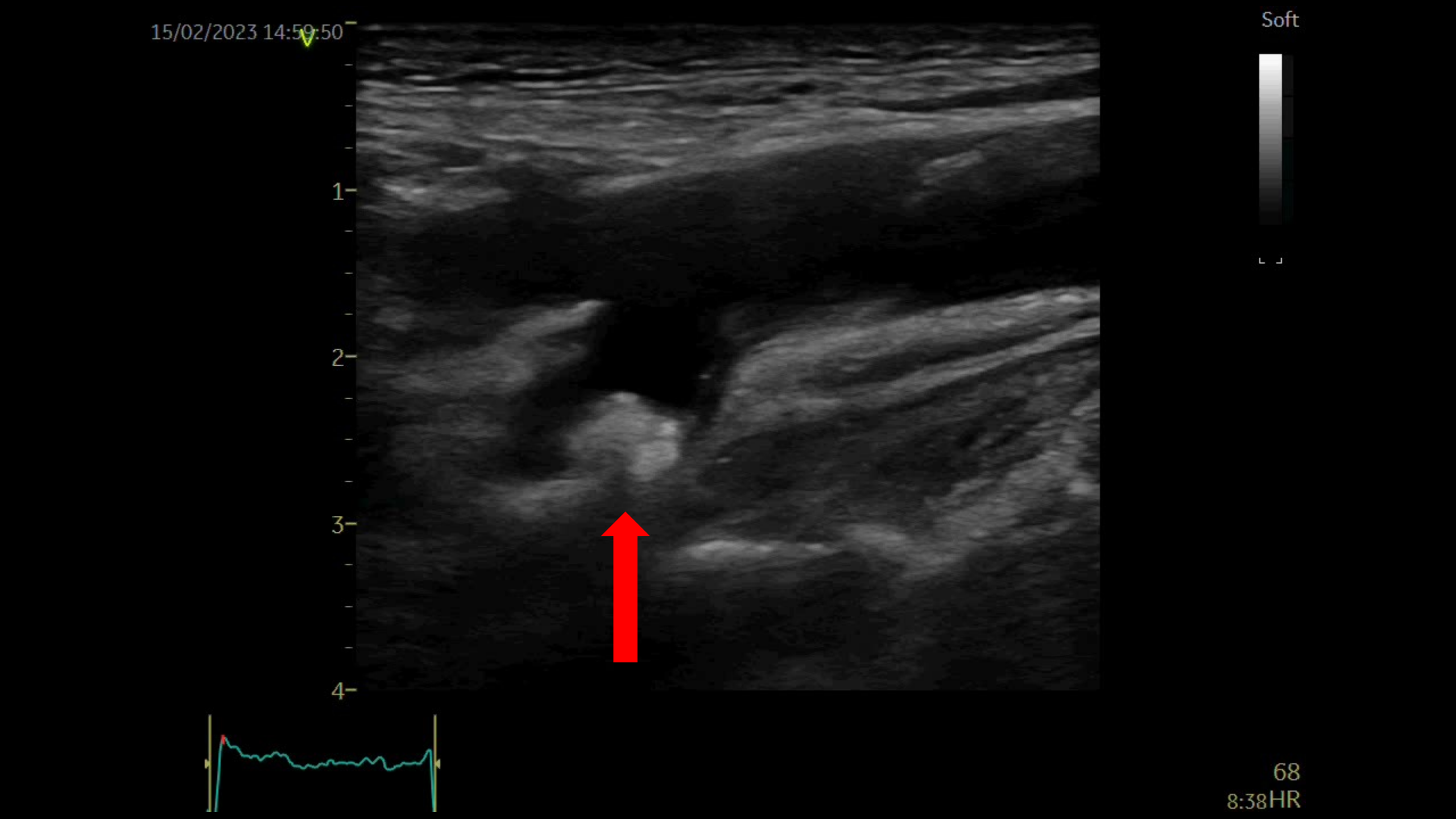
15/02/2023 14:59:50
Soft
1
2
3
4
68
8:38 HR

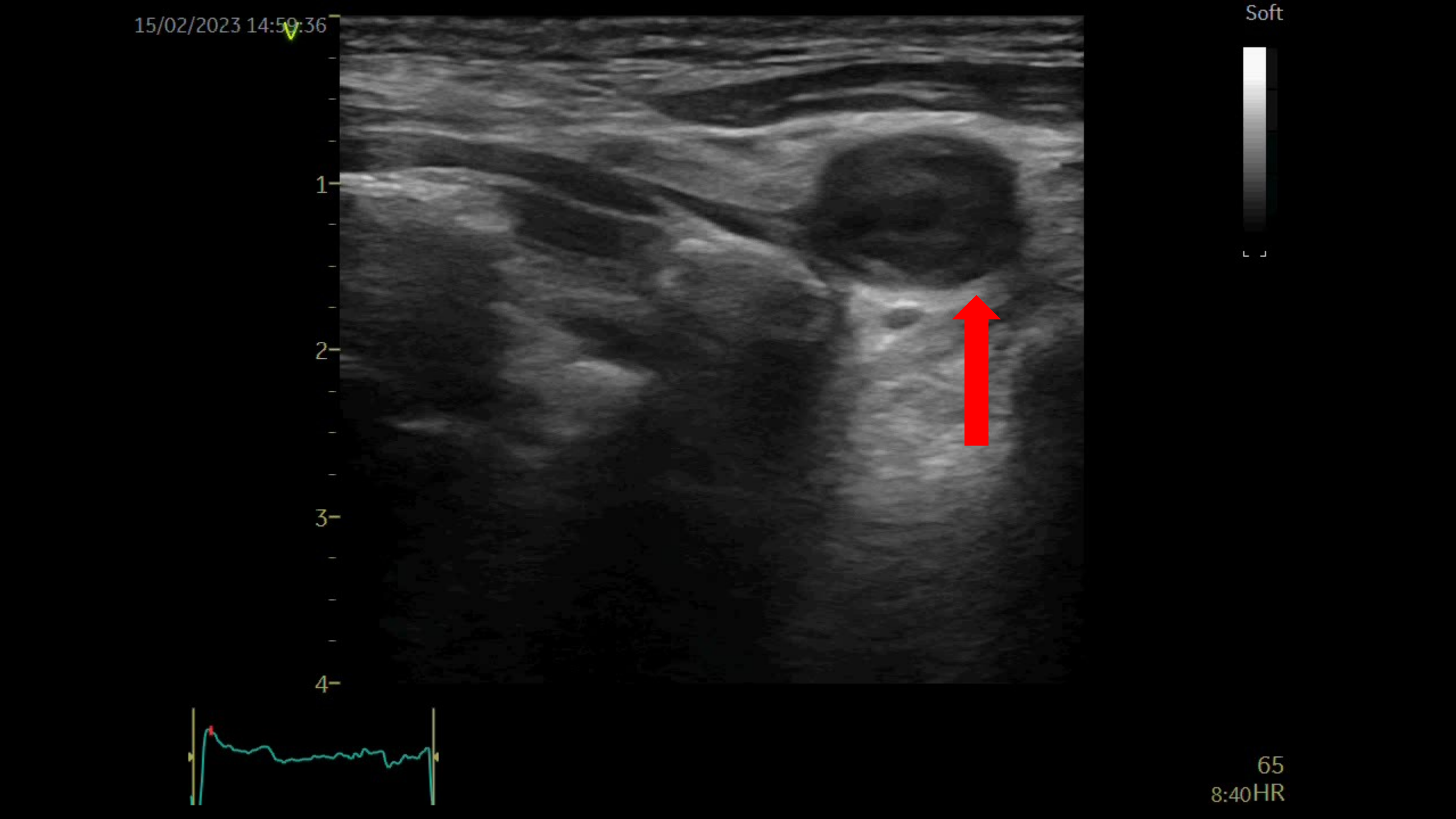
15/02/2023 14:59:36
Soft
1
2
3
4
65
8:40 HR

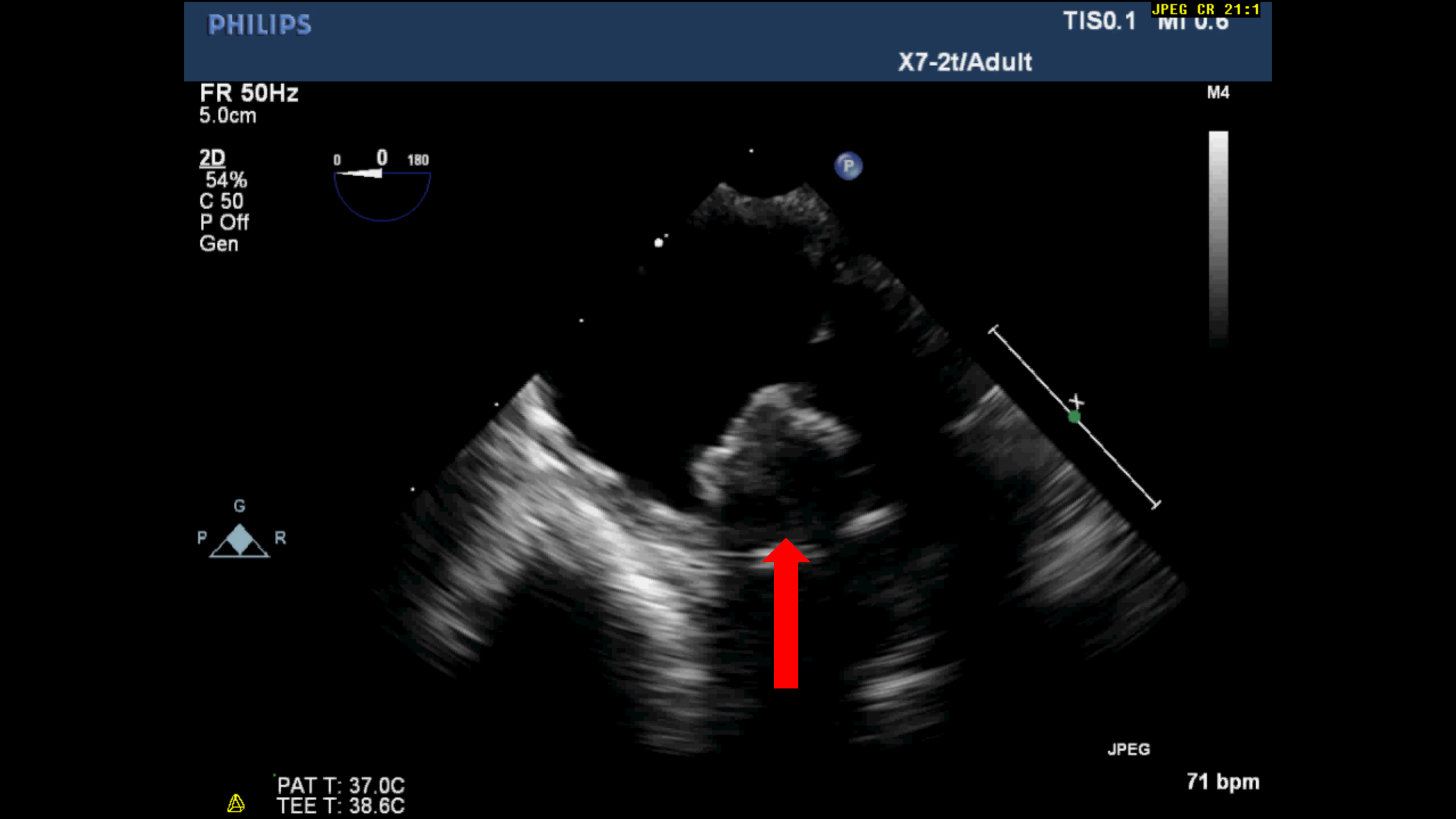
PHILIPS
TIS0.1
JPEG CR 21:1
X7-2t/Adult
FR 50Hz
5.0cm
M4
2D
54%
C 50
P Off
Gen
0
0
180
P
G
P
R
JPEG
71 bpm
PAT T: 37.0C
TEE T: 38.6C

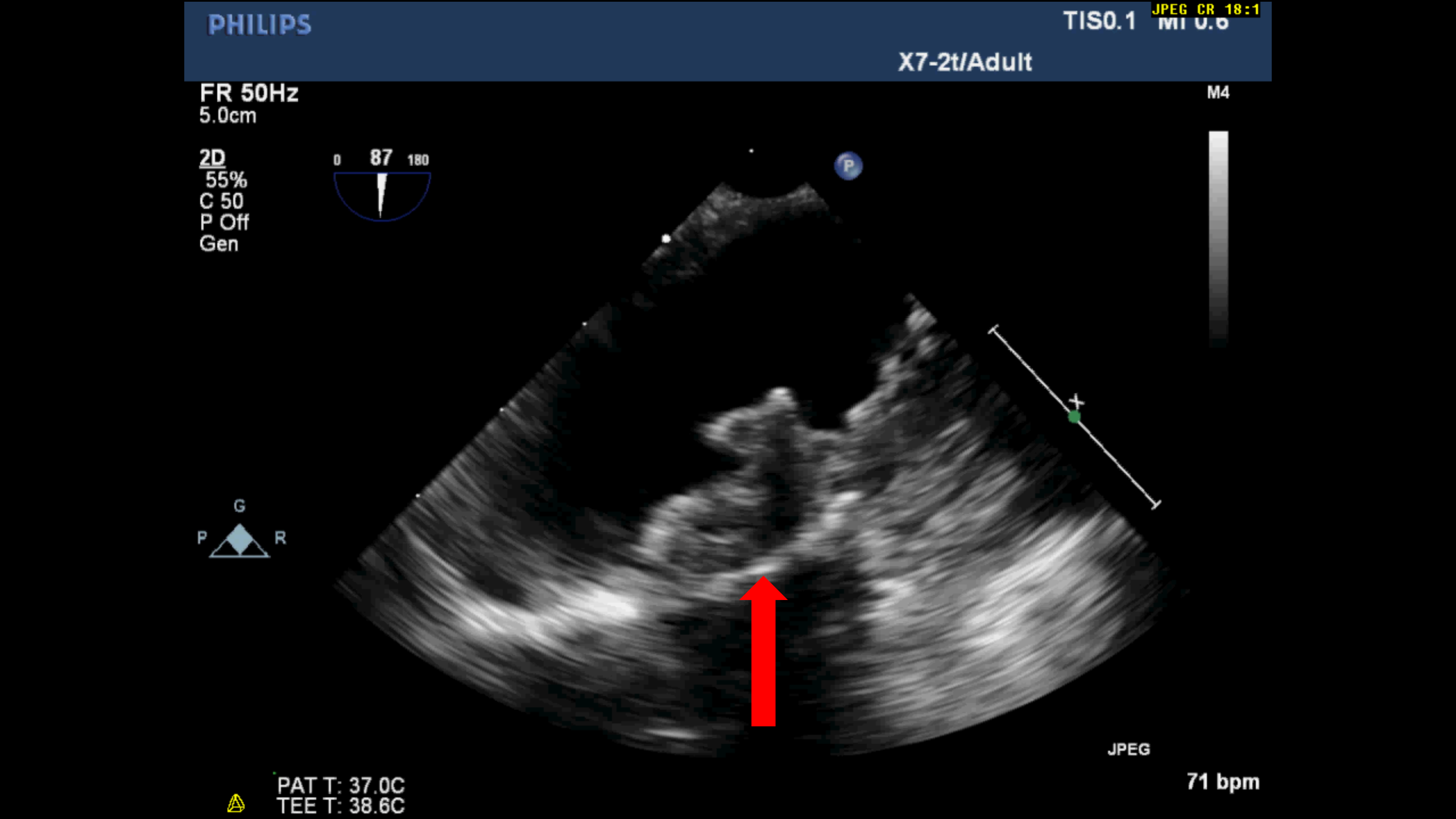
PHILIPS
JPEG CR 18:1
TIS0.1
X7-2t/Adult
FR 50Hz
5.0cm
M4
2D
55%
C 50
P Off
Gen
0
87
180
G
P
R
JPEG
71 bpm
PAT T: 37.0C
TEE T: 38.6C

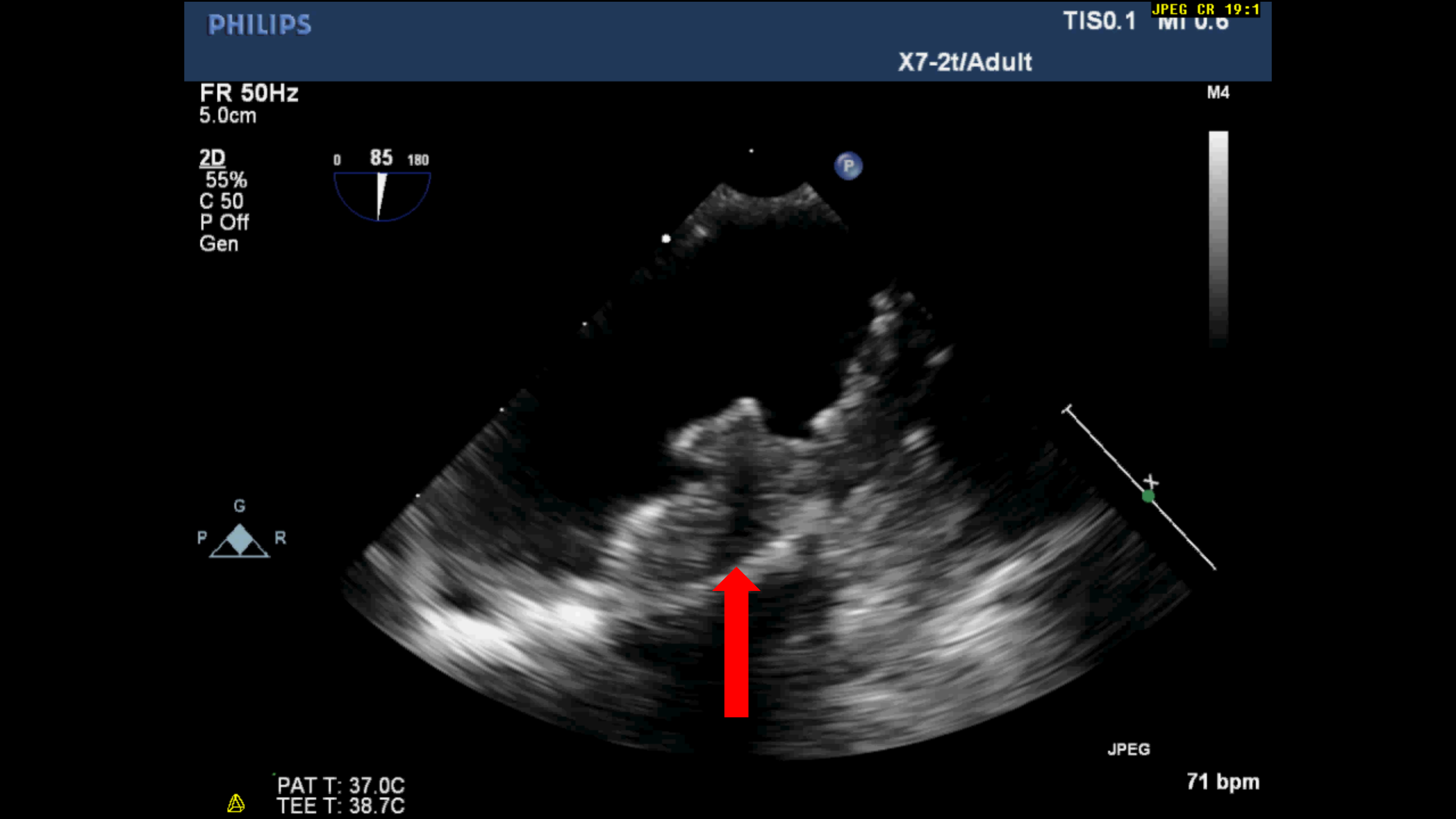
PHILIPS
TIS0.1
JPEG CR 19:1
X7-2t/Adult
FR 50Hz
5.0cm
M4
2D
55%
C 50
P Off
Gen
0
85
180
G
P
R
JPEG
71 bpm
PAT T: 37.0C
TEE T: 38.7C

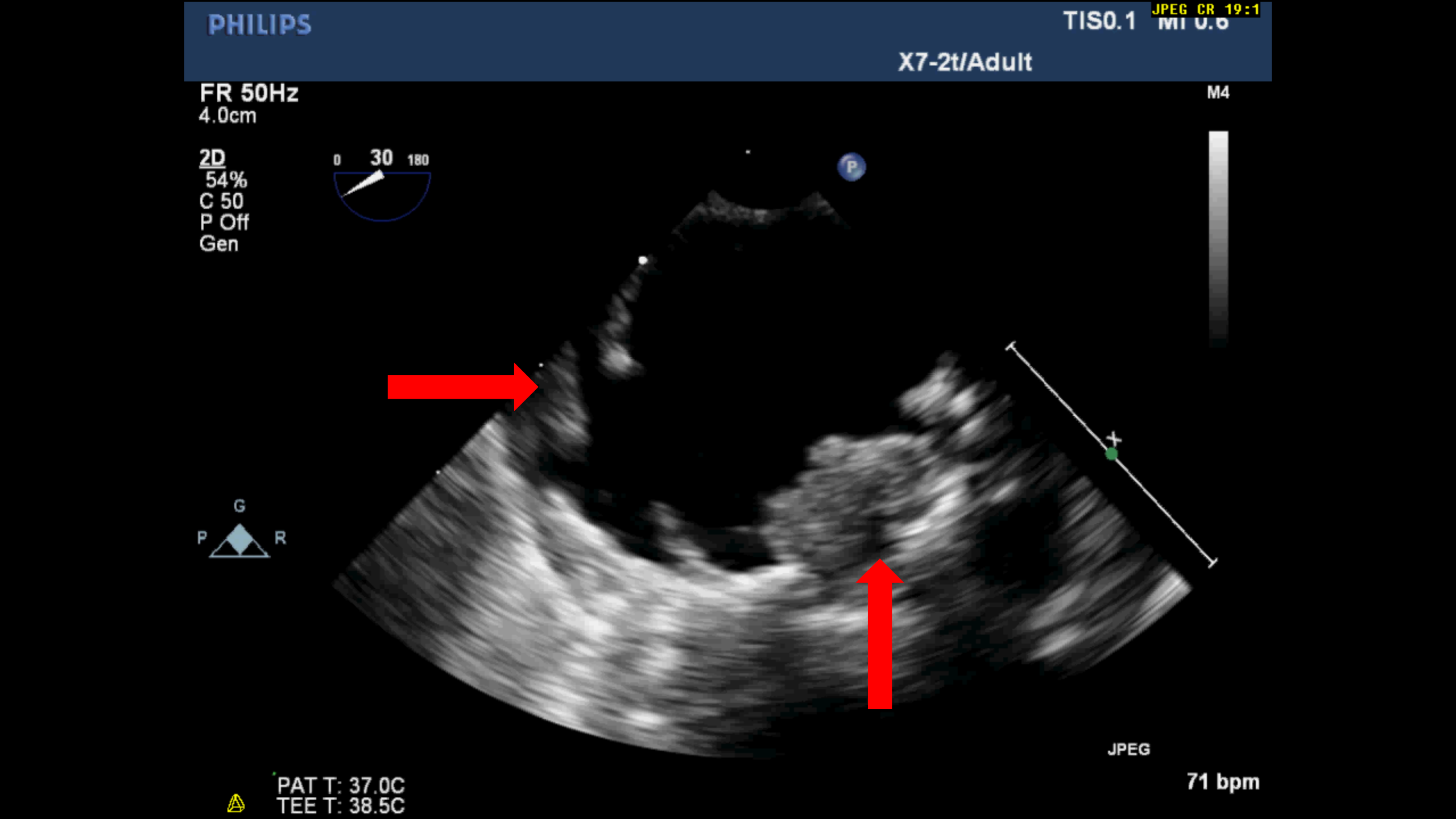
PHILIPS
TIS0.1
JPEG CR 19:1
X7-2t/Adult
FR 50Hz
4.0cm
M4
2D
54%
C 50
P Off
Gen
0
30
180
G
P
R
JPEG
71 bpm
PAT T: 37.0C
TEE T: 38.5C

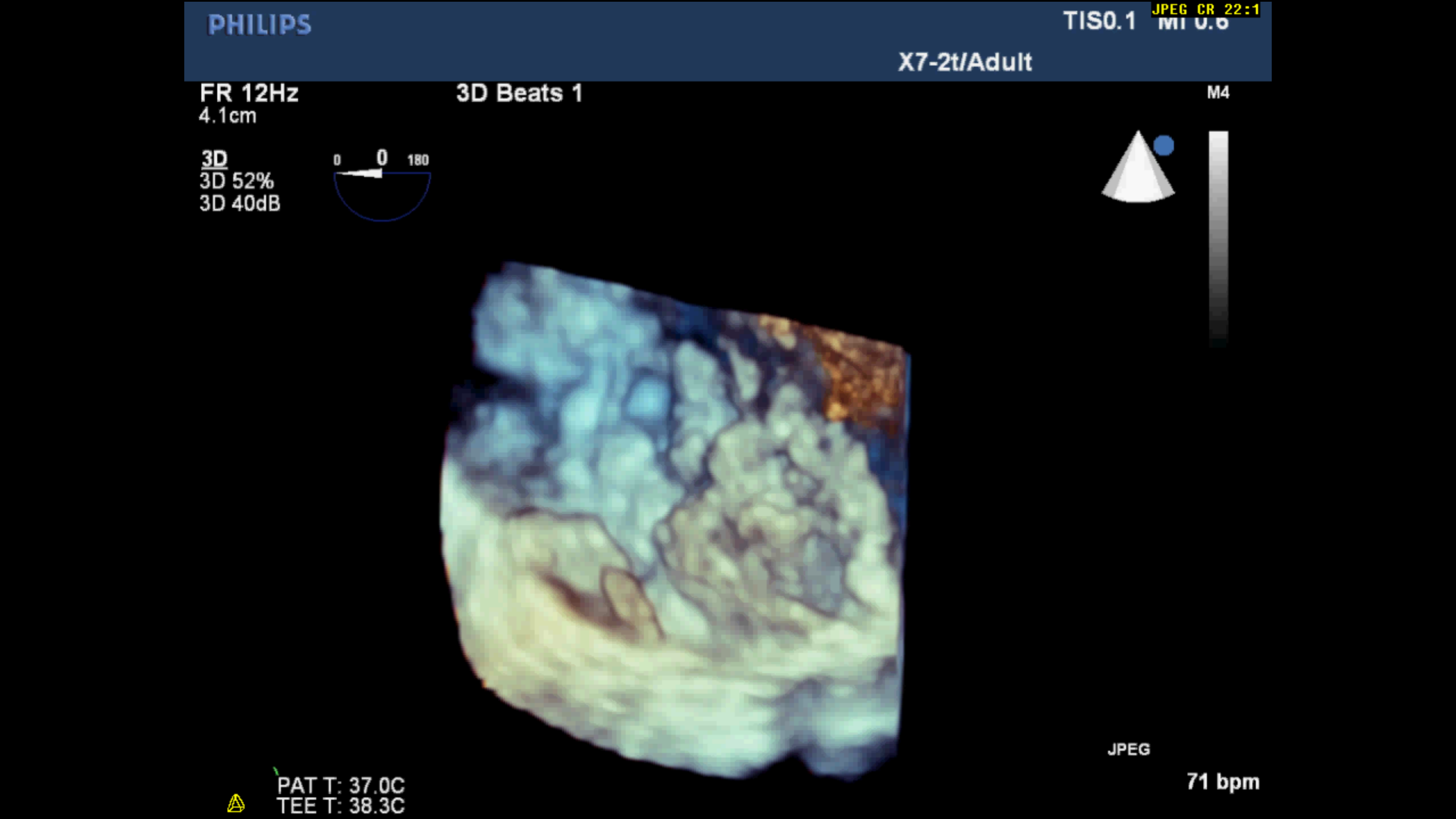
PHILIPS
JPEG CR 22:1
TIS0.1
X7-2t/Adult
FR 12Hz
4.1cm
3D Beats 1
M4
3D
3D 52%
3D 40dB
0
0
180
JPEG
71 bpm
PAT T: 37.0C
TEE T: 38.3C

Imaging of coronary atherosclerosis by Computed Tomography

Imaging of coronary atherosclerosis by Computed Tomography

- The detection of coronary artery calcium ***(CAC)*** is relatively straightforward; it is applied to detect and quantify subclinical coronary atherosclerosis even in asymptomatic individuals.
- More complex data acquisition protocols, which require higher spatial and temporal resolution, specific patient preparation, and the intravenous injection of contrast agent, allow to perform ***coronary CT angiography (CTA).***
- With CTA, the presence of luminal stenoses and, given sufficient image quality, calcified as well as non-calcified atherosclerotic plaque can be visualized.
- Initial studies have shown that certain plaque characteristics, such as **positive remodelling or very low CT attenuation, are associated with plaque vulnerability**.
- So far, the available clinical data are not sufficient to draw specific conclusions as to the risk–benefit ratio of contrast-enhanced coronary CTA for risk prediction, especially for asymptomatic individuals. Hence, CTA is currently not recommended for risk stratification purposes.
- However, the technology of coronary CTA continues to evolve at a rapid pace and clinical applications for plaque imaging and characterization may become possible in the future.

European Heart Journal (2010) 31, 1442–1448. doi:10.1093/eurheartj/ehq150.

Imaging of coronary calcification by computed tomography.
In non-enhanced scans, coronary calcium is clearly depicted because of its high computed tomography attenuation.
Here, calcium in the left main and left anterior descending coronary artery as well as diagonal branches is present (arrow).

European Heart Journal (2010) 31, 1442–1448. doi:10.1093/eurheartj/ehq150.

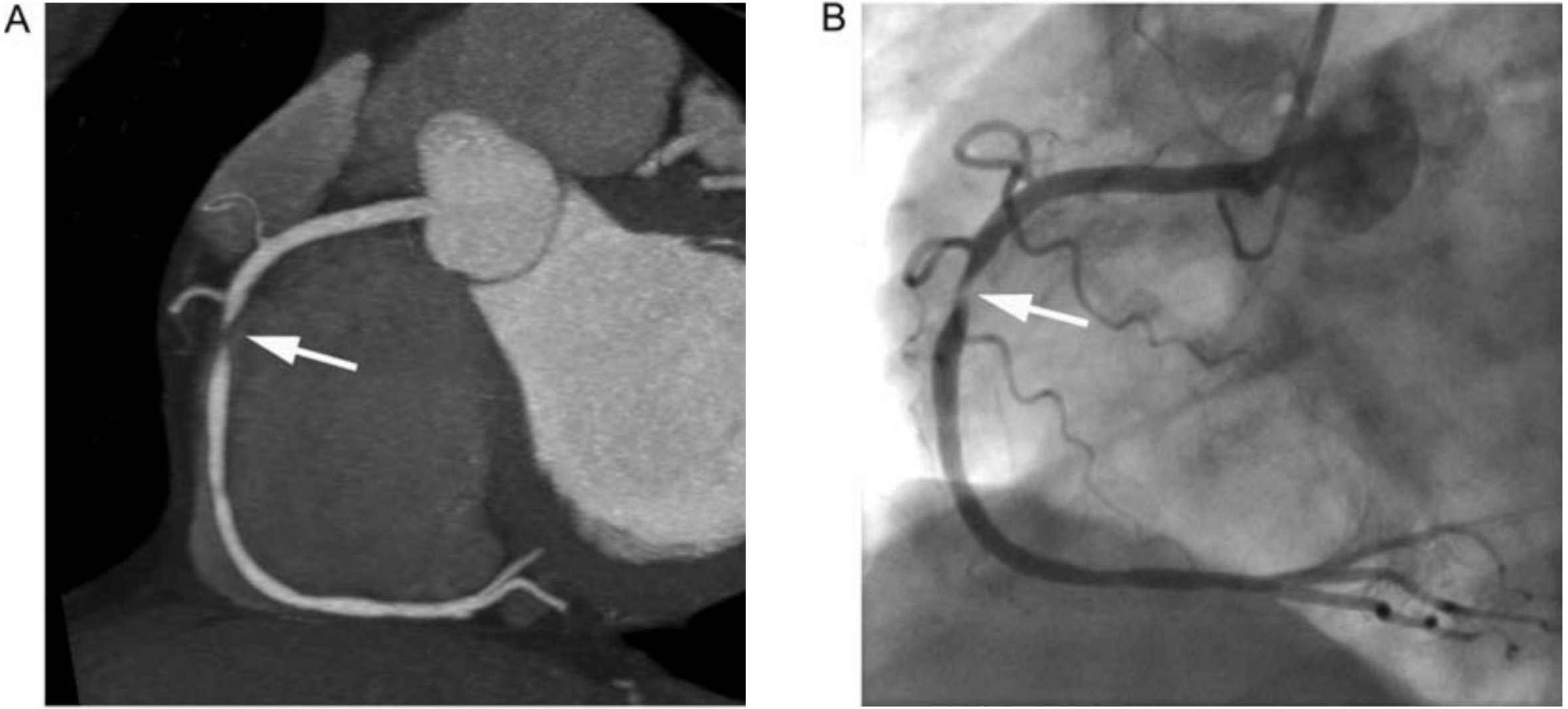

Visualization of coronary artery luminal stenosis by contrast-enhanced computed tomography angiography.
Here, a high-grade stenosis of the right coronary artery is present.
(A) Coronary computed tomography angiography (arrow = high-grade stenosis of the right coronary artery).
(B) Invasive coronary angiogram of the right coronary artery (arrow = stenosis).

European Heart Journal (2010) 31, 1442–1448. doi:10.1093/eurheartj/ehq150.

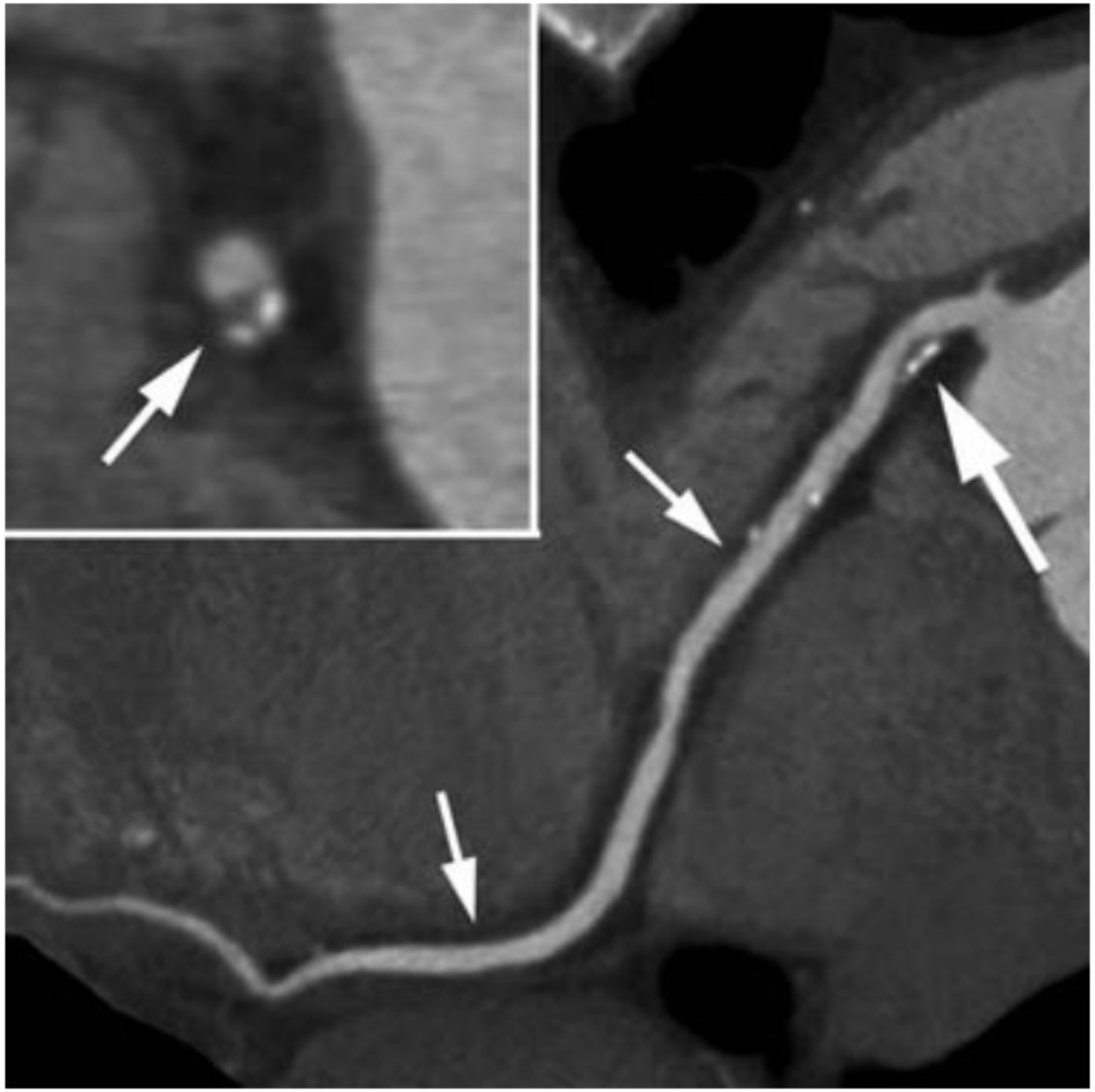

Visualization of coronary atherosclerotic plaque in contrast-enhanced computed tomography angiography. The right coronary artery is shown as a curved multiplanar reconstruction (small arrows).
A partly calcified coronary atherosclerotic plaque is present in the proximal segment of the vessel (large arrow). The insert shows a cross-sectional image of the atherosclerotic plaque in the proximal right coronary artery, the arrow points at the partly calcified plaque.

European Heart Journal (2010) 31, 1442–1448. doi:10.1093/eurheartj/ehq150.

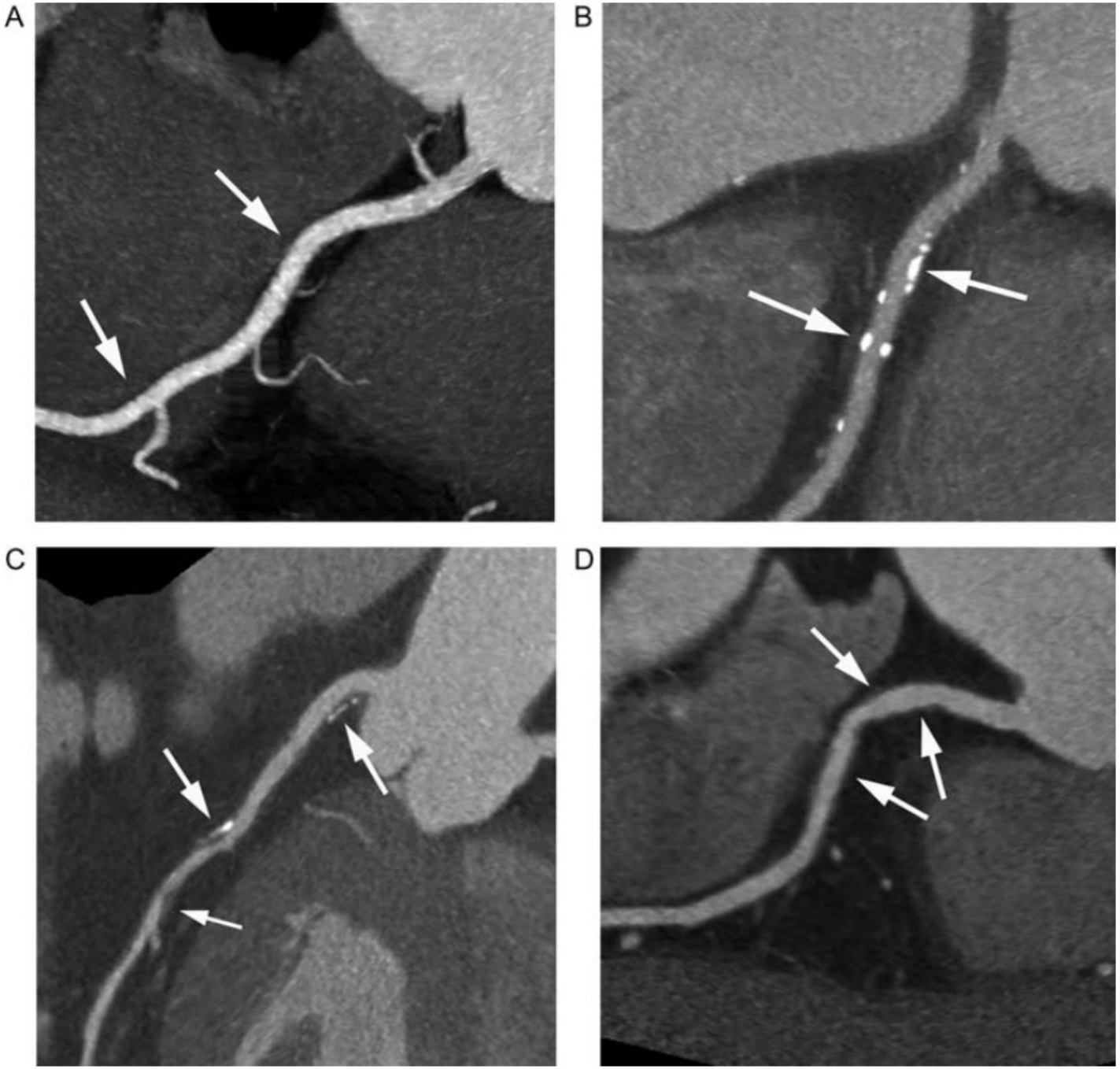

Various types of coronary atherosclerotic plaque demonstrated by coronary computed tomography angiography.
In all cases, the proximal right coronary artery is shown in the form of a ‘curved multiplanar reconstruction’.
(A) Proximal right coronary artery (arrows) without any detectable plaque.
(B) Proximal right coronary artery with calcified plaque (large arrows). Non-calcified plaque is not detectable.
(C) Proximal right coronary artery with both calcified and non-calcified plaque (sometimes referred to as ‘mixed plaque’). Two large arrows point at plaques that contain calcified and non-calcified components. A small arrow indicates a completely non-calcified plaque.
(D) Proximal right coronary artery with exclusively non-calcified plaque (arrows). Calcified plaque is not present.

European Heart Journal (2010) 31, 1442–1448. doi:10.1093/eurheartj/ehq150.

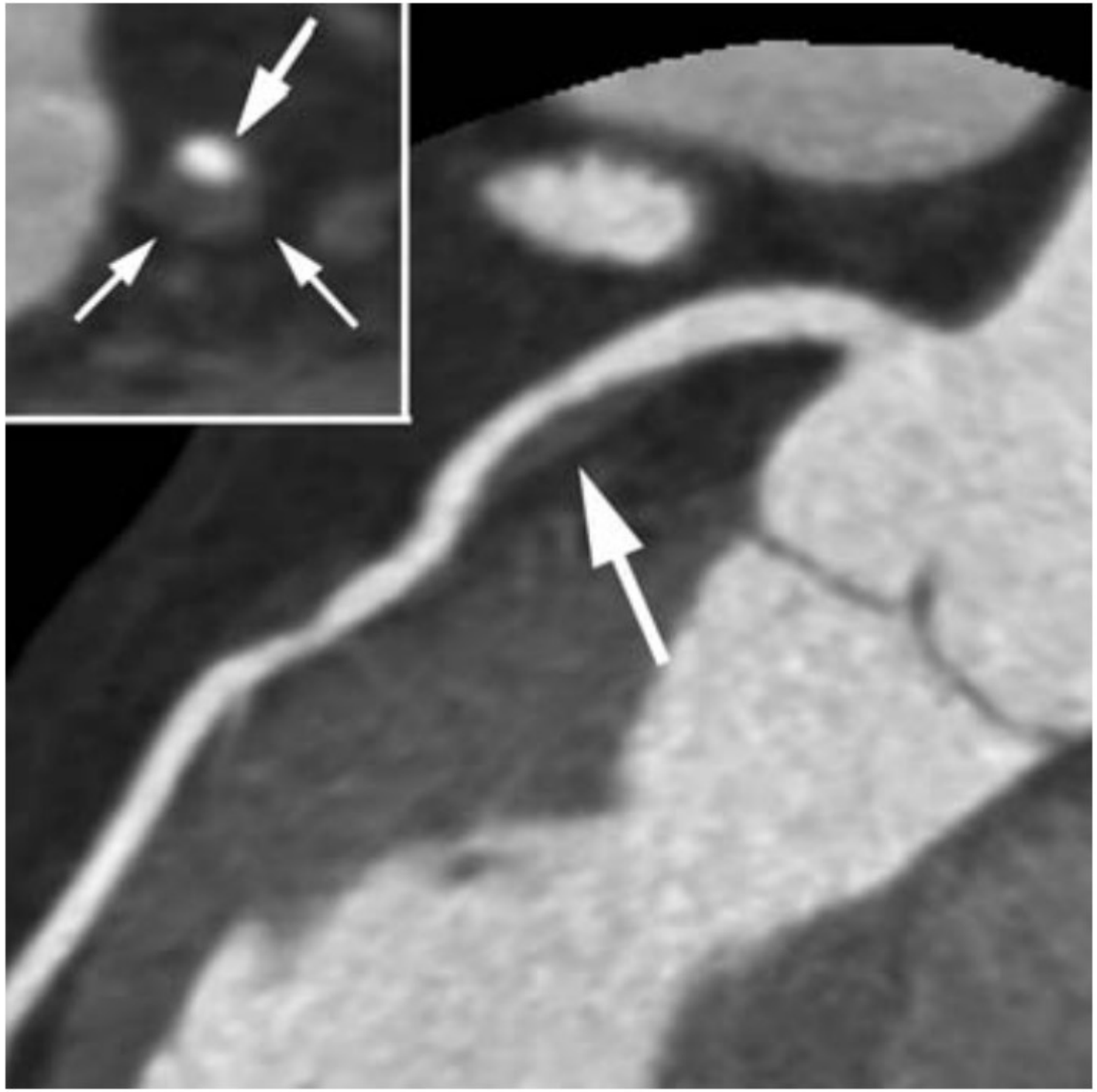

Longintudinal reconstruction of the proximal left anterior descending coronary artery.
A plaque with pronounced positive remodelling is visualized by computed tomography angiography (arrow).
The total vessel area (lumen plus plaque) is substantially larger than for normal vessel segments proximal or distal to the lesion.
The insert shows a cross-section of the plaque.
The large arrow indicates the contrast-enhanced lumen, whereas the small arrows indicate the eccentric non-calcified plaque.

Computed tomography attenuation values found in lipid-rich and fibrous plaques in various studies (HU, Hounsfield units)

Author	Reference	CT attenuation values			
		Lipid-rich plaque		Fibrous plaque	
		Mean (HU)	Range (HU)	Mean (HU)	Range (HU)
Schroeder *et al.*[79]	IVUS	14 ± 26	−42 to 47	91 ± 21	61–122
Becker *et al.*[84]	Histology	47 ± 9	—	104 ± 28	—
Carrascosa *et al.*[81]	IVUS	71 ± 32	—	116 ± 36	—
Pohle *et al.*[82]	IVUS	58 ± 43	−39 to 167	121 ± 34	60–201
Motoyama *et al.*[83]	IVUS	11 ± 12	−15 to 33	78 ± 21	32–130
Sun *et al.*[70]	IVUS	79 ± 34	7–144	90 ± 27	22–154
Petranovic *et al.*[69]	IVUS	99 ± 28	—	77 ± 39	—

It has been speculated that the identification of very low CT densities (below 30 HU) within a plaque may be associated with a higher predisposition towards rupture. Other plaque features which were demonstrated in patients who underwent CT imaging of the coronary arteries after acute coronary syndromes included a predominance of non-calcified plaque as well as pronounced positive remodelling, the assessment of which by CTA seems to correlate well with IVUS.

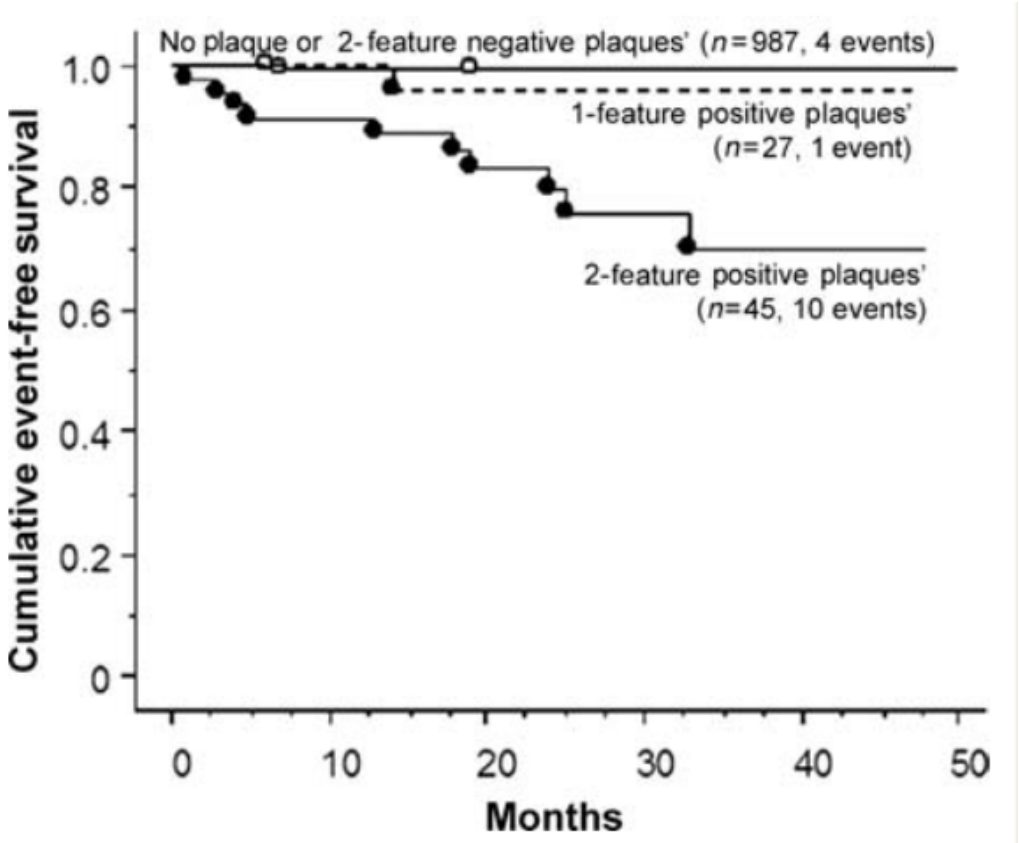

One thousand and fifty-nine patients were followed for a mean period of 27 months after a clinically indicated coronary computed tomography angiogram. Coronary atherosclerotic plaques were identified and evaluated concerning the presence of positive remodelling and low computed tomography attenuation (attenuation values ,30 HU). It could be demonstrated that the rate of acute coronary syndromes during follow-up was significantly higher in patients with plaques that demonstrated positive remodelling and low computed tomography attenuation ('2-feature positive plaques') when compared with patients with plaque of other type or without plaque.

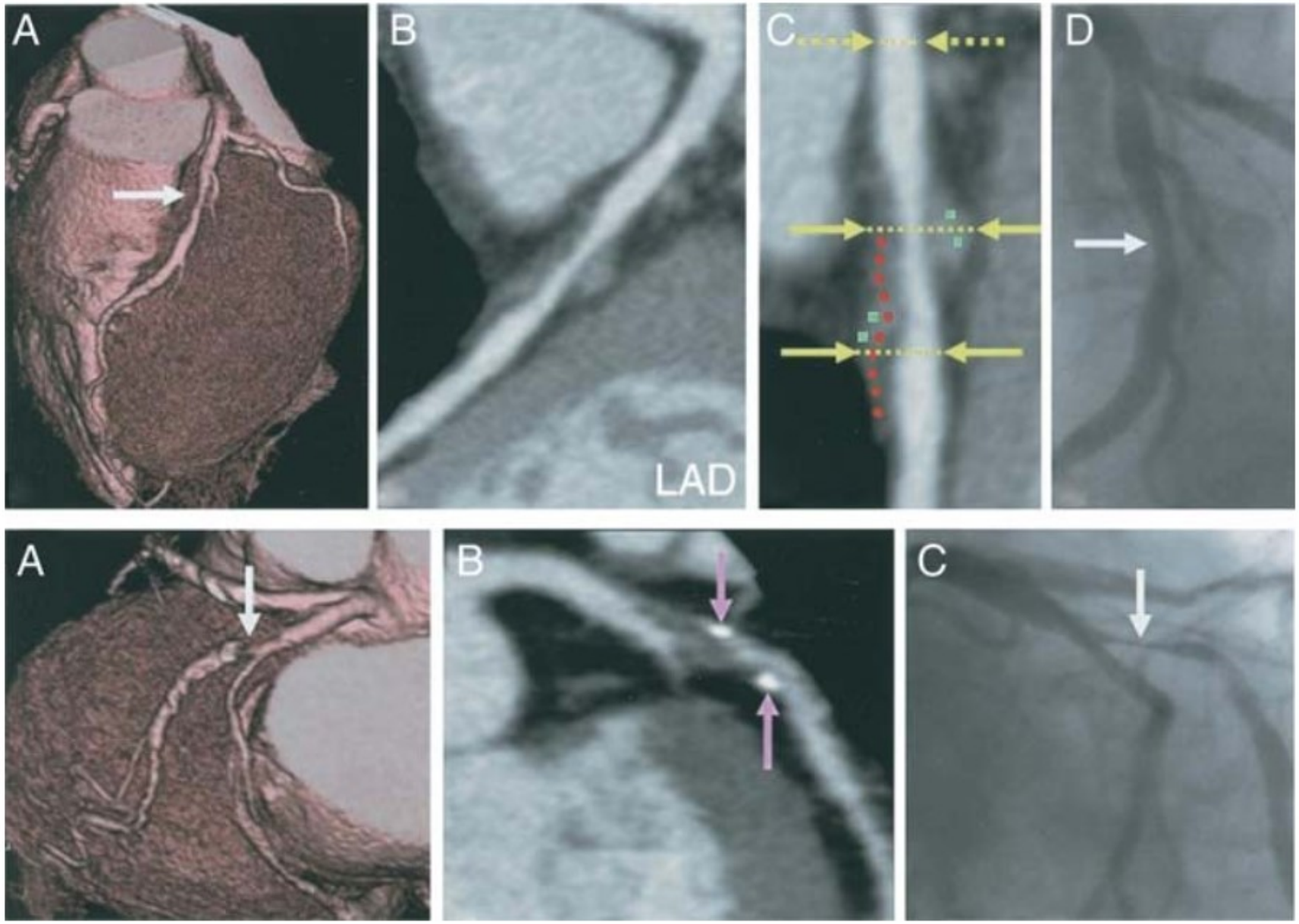

Plaque features on MDCT associated with culprit lesions in acute coronary syndromes.
Top panels: (A) Volume rendering. (B, C) Curved MPR. (D) Coronary angiogram.
Bottom panels: (A) Volume rendering. (B) Curved MPR. (C) Coronary angiogram.
White arrows show site of maximal luminal stenosis.
Yellow arrows demonstrate site of positive remodelling.
Green blocks represent non-calcified (fibrous) plaque and red blocks represents low attenuation (,30 HU) plaque.
Pink arrows show spotty calcification.

Eur Heart J Cardiovasc Imaging. 2014 Jul;15(7):730-5. doi: 10.1093/ehjci/jeu094

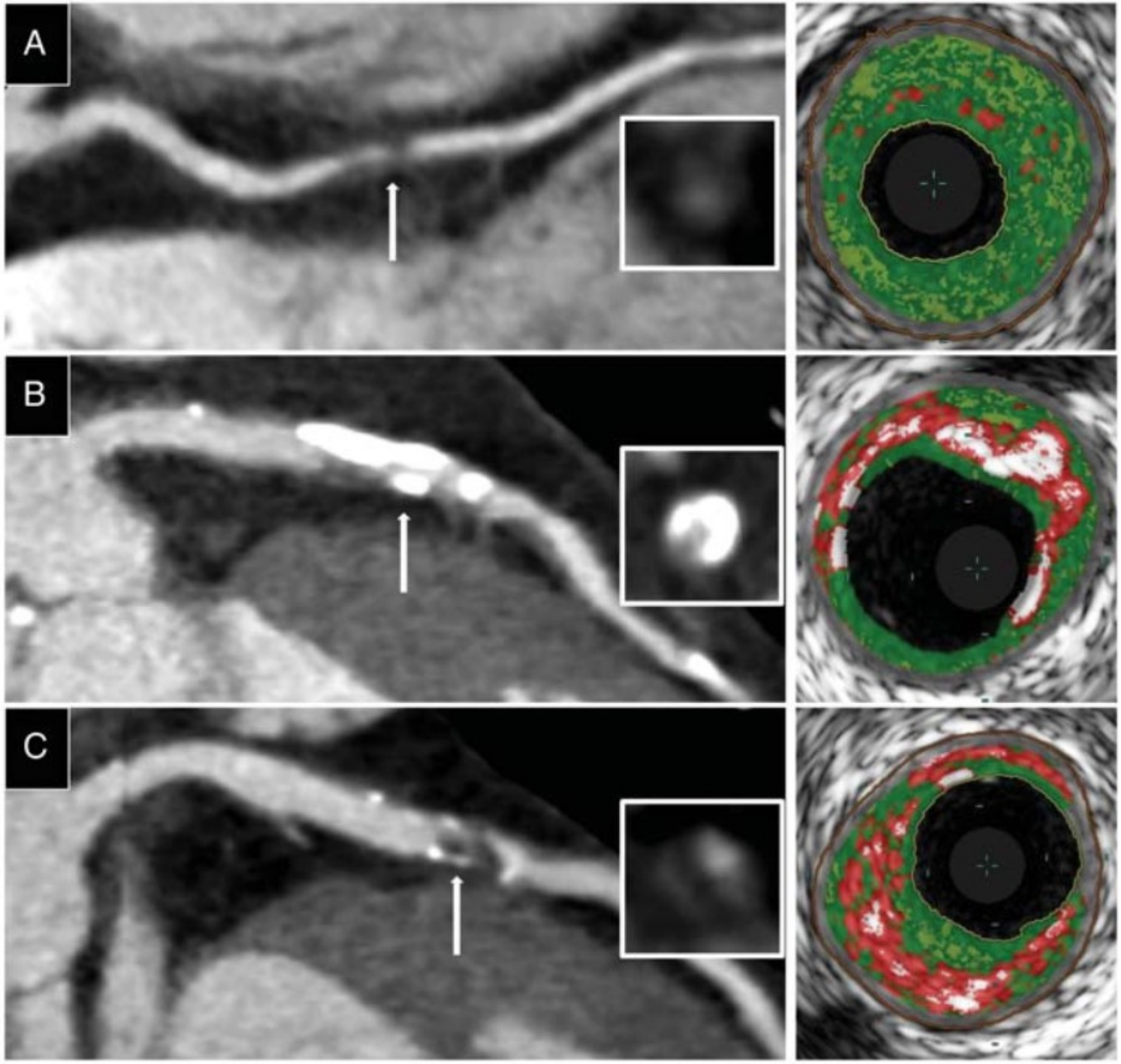

Comparison of plaque composition on MDCT and VH-IVUS. Curved MPRs of coronary arteries with transverse sections (inset) at level of the white arrows demonstrating:

(A) Non-calcified plaque with corresponding VH-IVUS image showing predominantly fibrous (green) plaque.

(B) Calcified plaque (high attenuation) with corresponding VH-IVUS image showing significant calcified (white) plaque.

(C) Low attenuation plaque and ring enhancement with corresponding VH-IVUS image showing significant necrotic core (red).

MDCT, multi-detector computed tomography; VH-IVUS, virtual histology intravascular ultrasound; MPR, multiplanar reformat.

Eur Heart J Cardiovasc Imaging. 2014 Jul;15(7):730-5. doi: 10.1093/ehjci/jeu094

Imaging of atherosclerosis by Magnetic Resonance Imaging

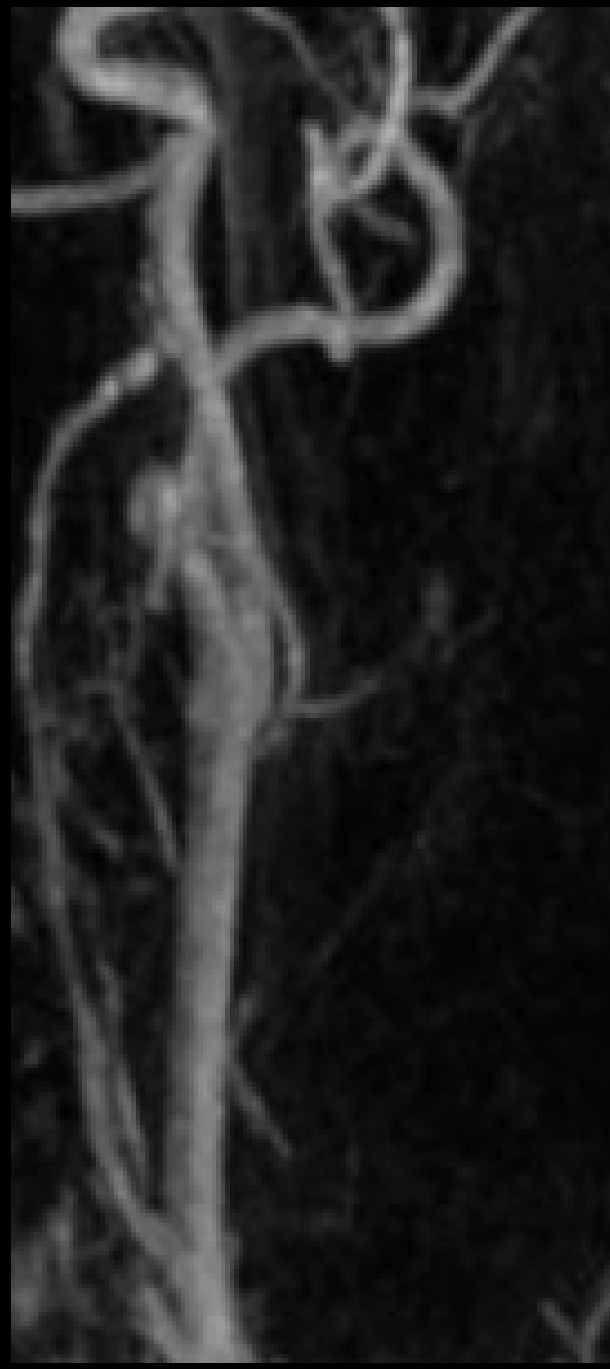

Imaging of atherosclerosis by Magnetic Resonance Imaging

- MRI allows for the characterization of plaque composition, i.e. the discrimination of **lipid core**, **fibrosis**, **calcification** and **intraplaque hemorrhage** deposits.
- Magnetic resonance imaging also allows for the detection of **arterial thrombi** and in defining thrombus age.
- Magnetic resonance imaging has been used to monitor plaque progression and regression in several animal models of atherosclerosis and in humans.
- Emerging MRI techniques capable of imaging biological processes, including inflammation, neovascularization, and mechanical forces, may aid in advancing our understanding of the atherothrombotic disease.
- MRI opens new strategies ranging from screening of high-risk patients for early detection and treatment as well as monitoring of the target lesions for pharmacological intervention.

European Heart Journal (2011) 32, 1709–1719. doi:10.1093/eurheartj/ehr068

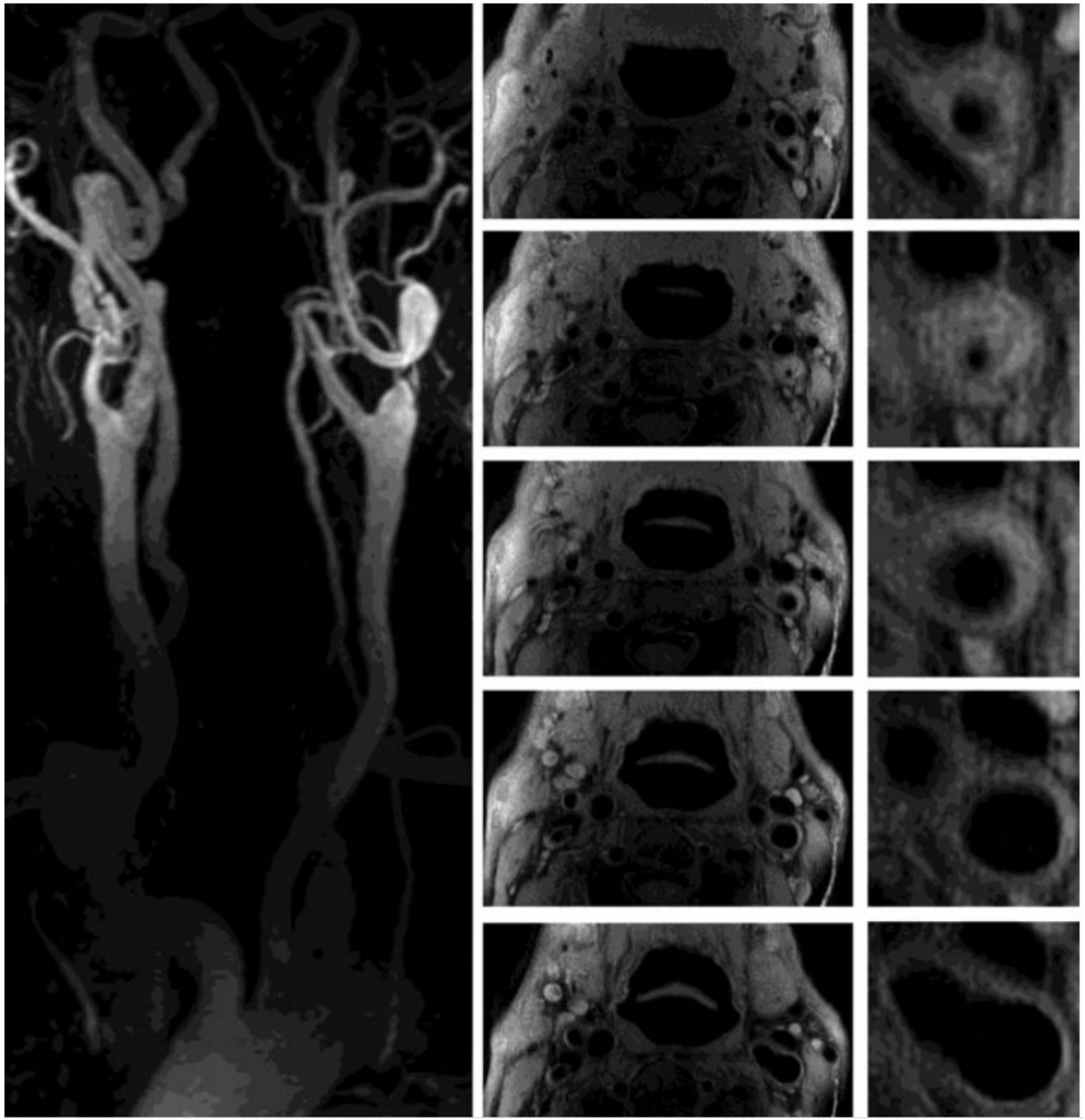

Magnetic resonance imaging of the carotid artery in a patient with arterial hypertension.

The angiography with intravenous injection of gadolinium demonstrates a subtotal stenosis of the left carotid artery followed by a 360º loop due to the elongation of the artery.

High resolution magnetic resonance imaging allows visualization of the extension of the atherosclerotic plaque and anatomical distribution in relation to the surrounding structures.

European Heart Journal (2011) 32, 1709–1719. doi:10.1093/eurheartj/ehr068

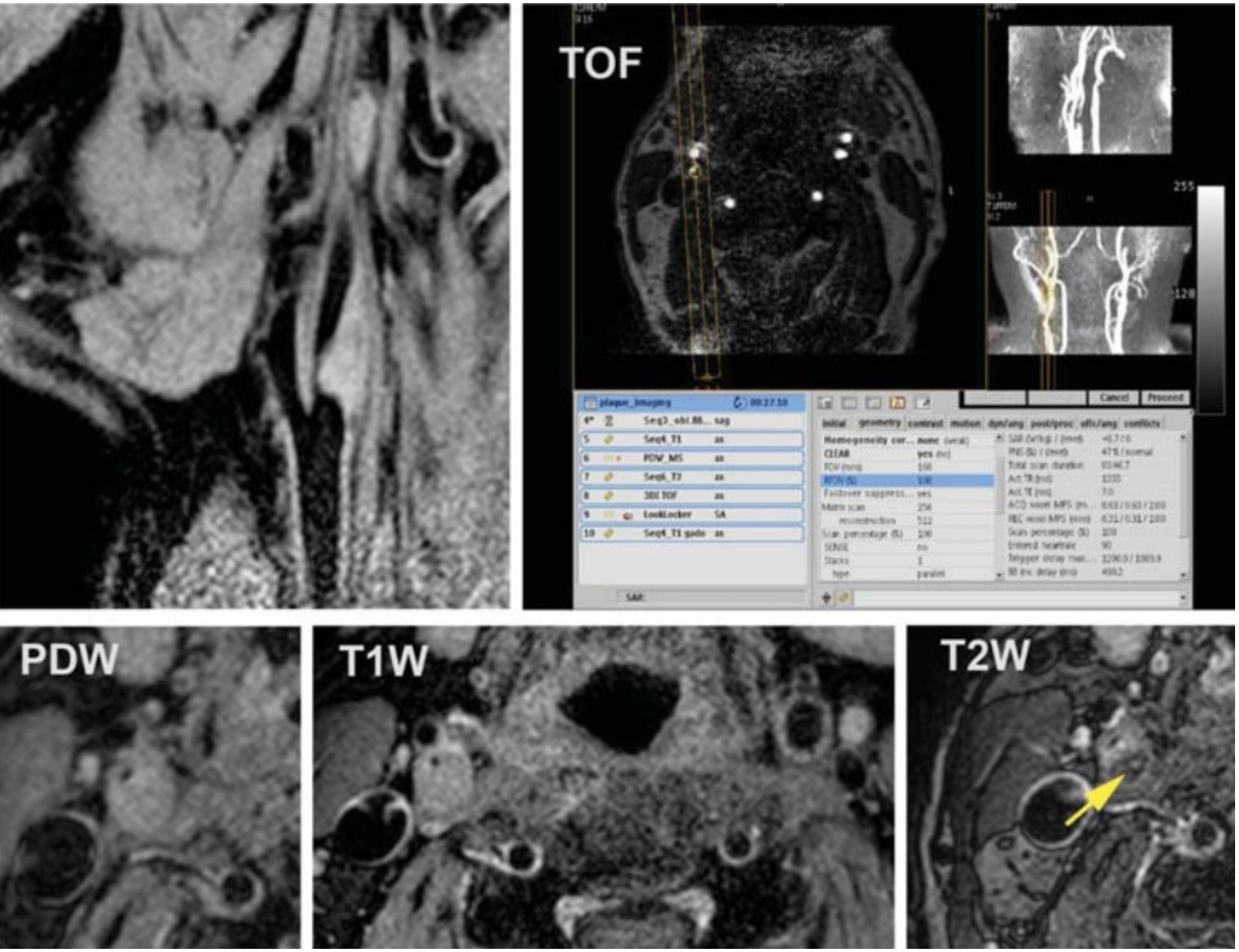

MRI examination of carotid atherosclerotic plaque in a patient with symptomatic carotid disease.
An echo sequence is used to localize the carotid bifurcation (upper panel, left) and time-of-flight (TOF) sequence allows the definition of the stenosis without needing contrast injection (upper panel, right).
Multisequence high-resolution magnetic resonance demonstrates the presence of a severely stenotic plaque with a **large lipid core** (yellow arrow in T2W image).

European Heart Journal (2011) 32, 1709–1719. doi:10.1093/eurheartj/ehr068

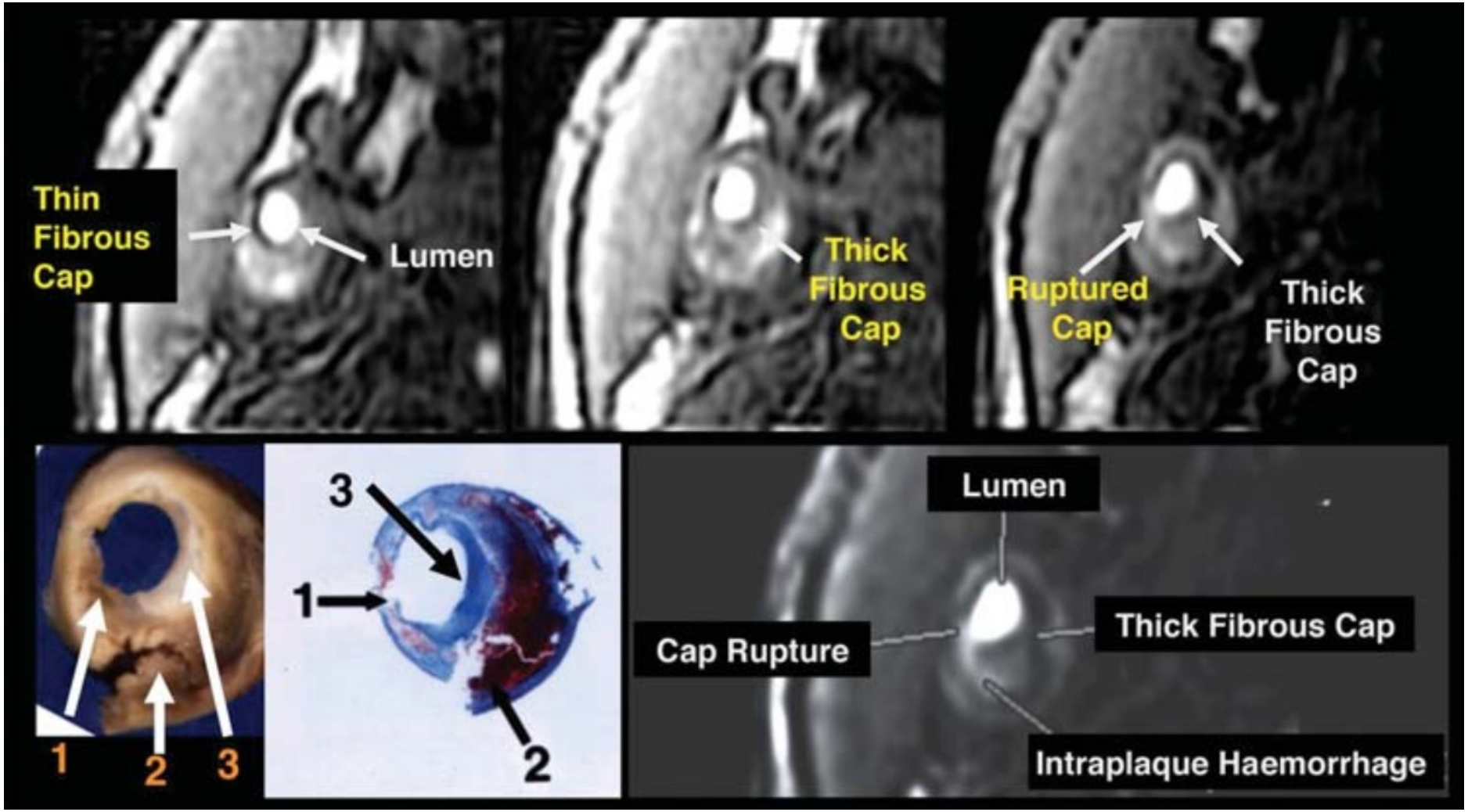

Magnetic resonance sequences normally used to perform angiography without the need of contrast agent (time-of-flight) allow the in vivo visualization of fibrous cap thickness and rupture in human atherosclerotic carotid plaque. Gross and histological sections (lower left panel) showing the area of cap rupture (arrow 1) covering the recent intraplaque haemorrhage (arrow 2) and next to a region where fibrous cap is thick (arrow 3).

European Heart Journal (2011) 32, 1709–1719. doi:10.1093/eurheartj/ehr068

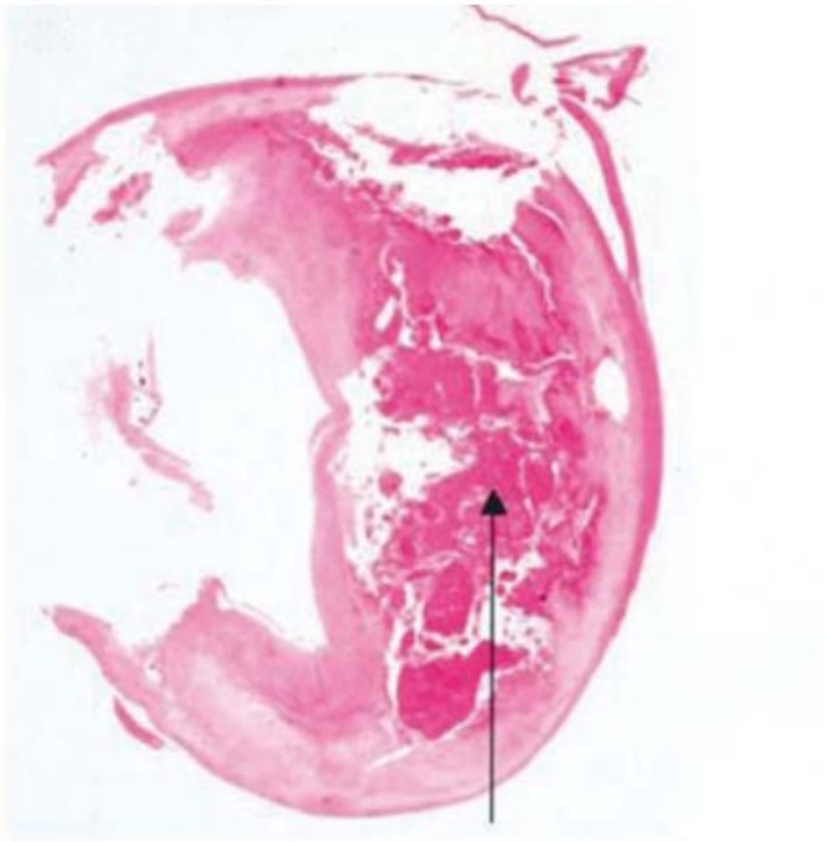

Intraplaque haemorrhage

Although not yet available for routine use, in vivo, high-resolution, multicontrast MRI remains the most promising method of non-invasively imaging plaques and characterizing the main plaque components.

Intraplaque hemorrhage and the **lipid-rich necrotic core** are the best indicators of lesion severity currently visualized by high-resolution MRI. However, MRI methods capable of imaging other important aspects of atherosclerotic disease in vivo, including inflammation, neovascularization, and mechanical forces, are emerging and may aid in advancing our understanding of the atherothrombotic disease.

Specific designed sequences for the visualization of thrombi allow detection of **intraplaque haemorrhage** (arrow) in stroke patients.

European Heart Journal (2011) 32, 1709–1719. doi:10.1093/eurheartj/ehr068

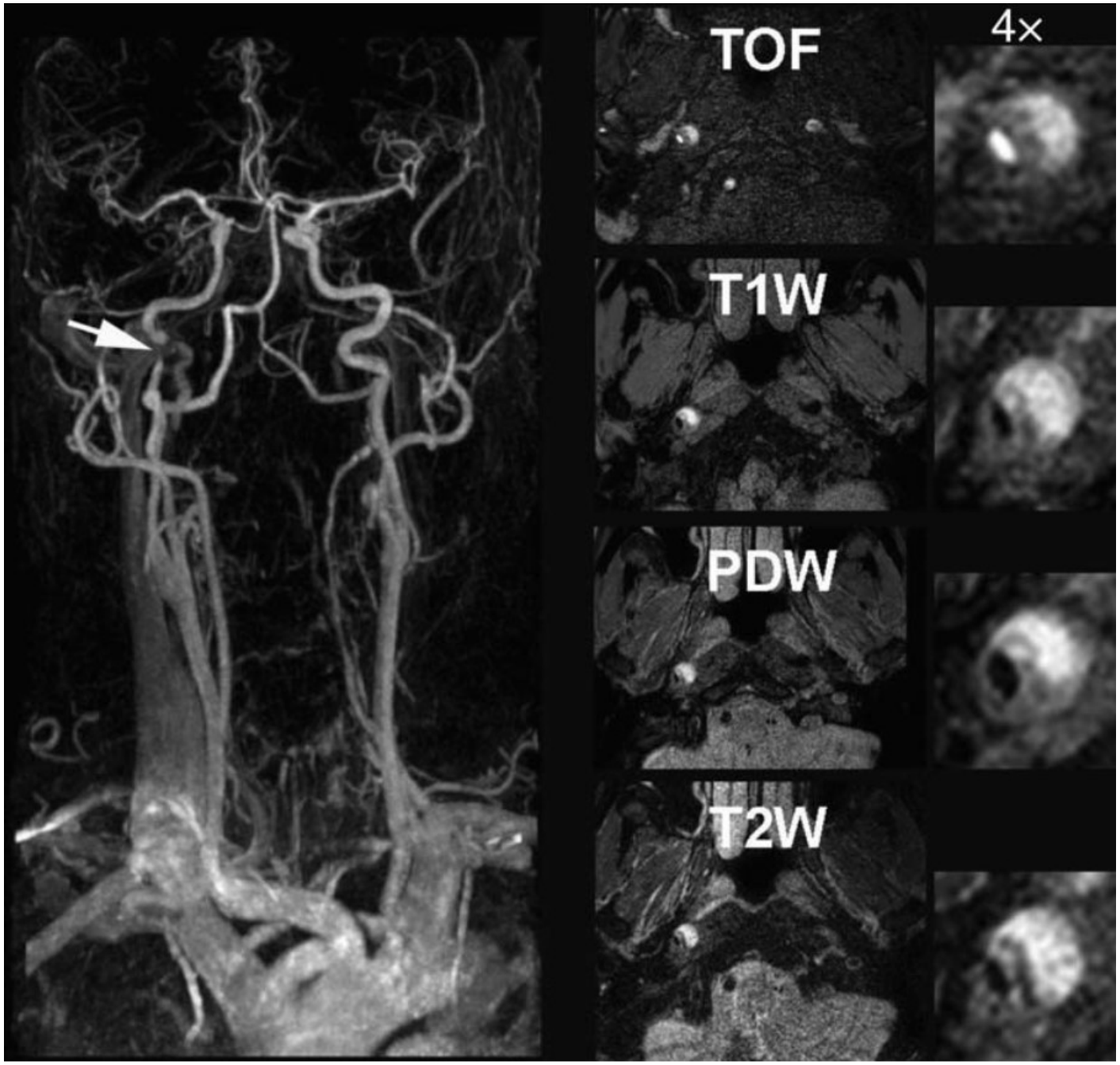

Magnetic resonance angiography demonstrating a subtotal stenosis of the right internal carotid artery (arrow) in a patient with acute stroke.
High-resolution multicontrast imaging demonstrates a ***disrupted plaque with intraplaque haemorrhage*** as a cause of the subtotal obstruction (middle panels).
Details of the cross-sectional multicontrast magnetic resonance images (four-fold enlargement) are provided in the right panels.

European Heart Journal (2011) 32, 1709–1719. doi:10.1093/eurheartj/ehr068

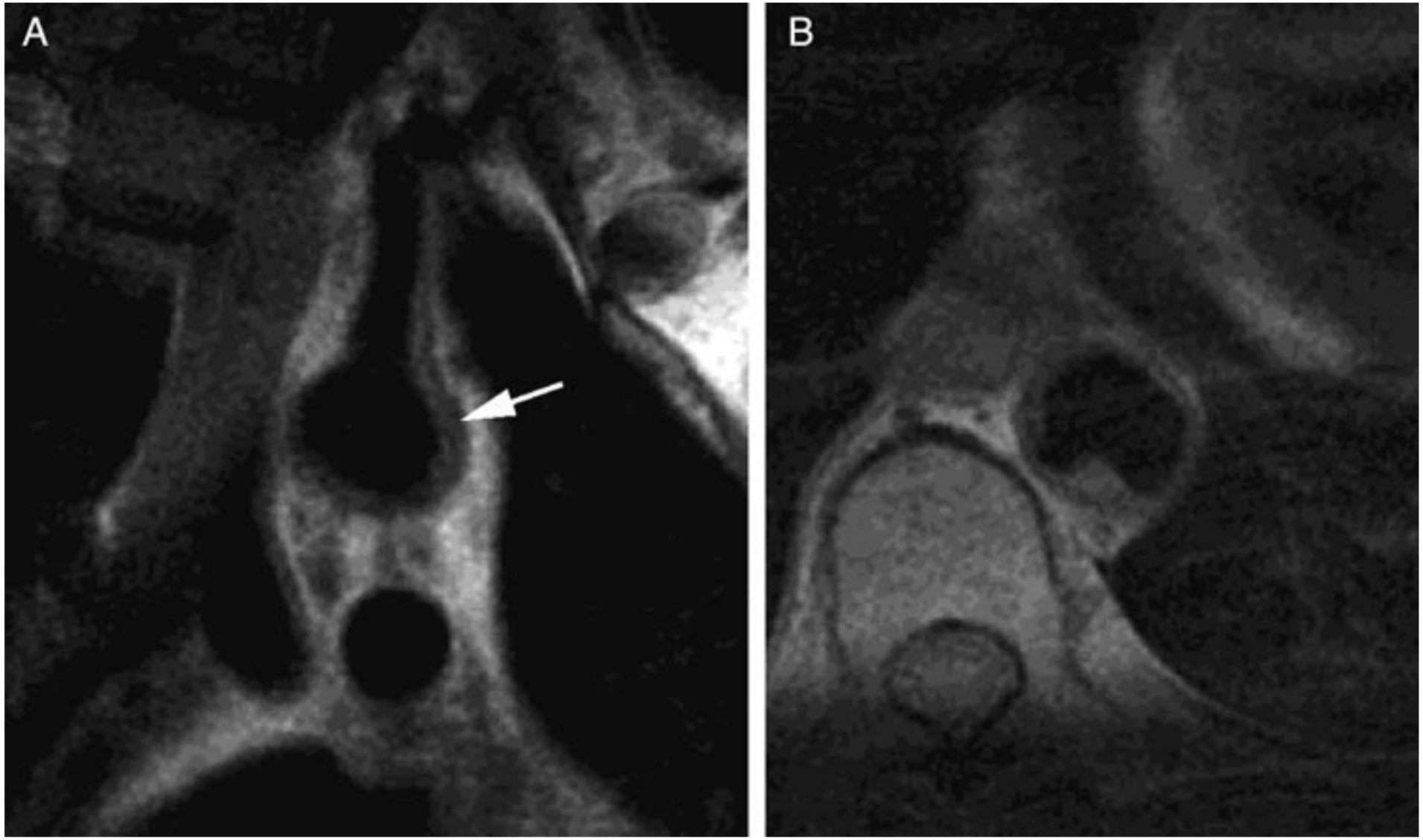

Magnetic resonance imaging high-resolution T2W oblique imaging **of the aortic arch demonstrating an atherosclerotic plaque particularly evident in the posterior wall** (arrow) extending in the left subclavian artery (A).
(B) A protruding 4 mm thick plaque at the level of the distal thoracic aorta

European Heart Journal (2011) 32, 1709–1719. doi:10.1093/eurheartj/ehr068

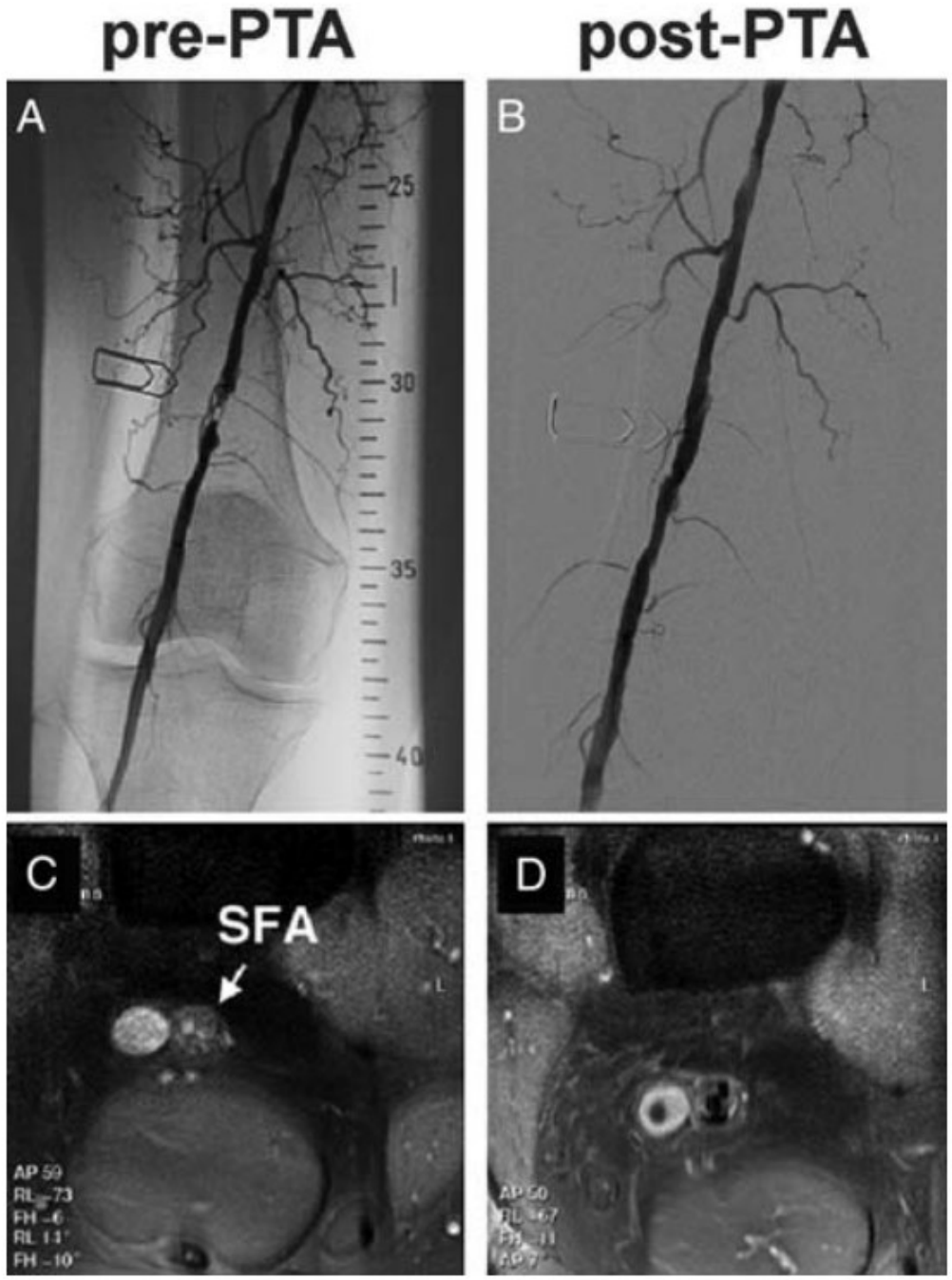

Effect of percutaneous transluminal angioplasty on severe femoral stenosis.
Angiography (upper panel) and high-resolution magnetic resonance imaging (lower panel) before and after percutaneous transluminal angioplasty.
SFA, superficial femoral artery.

European Heart Journal (2011) 32, 1709–1719. doi:10.1093/eurheartj/ehr068

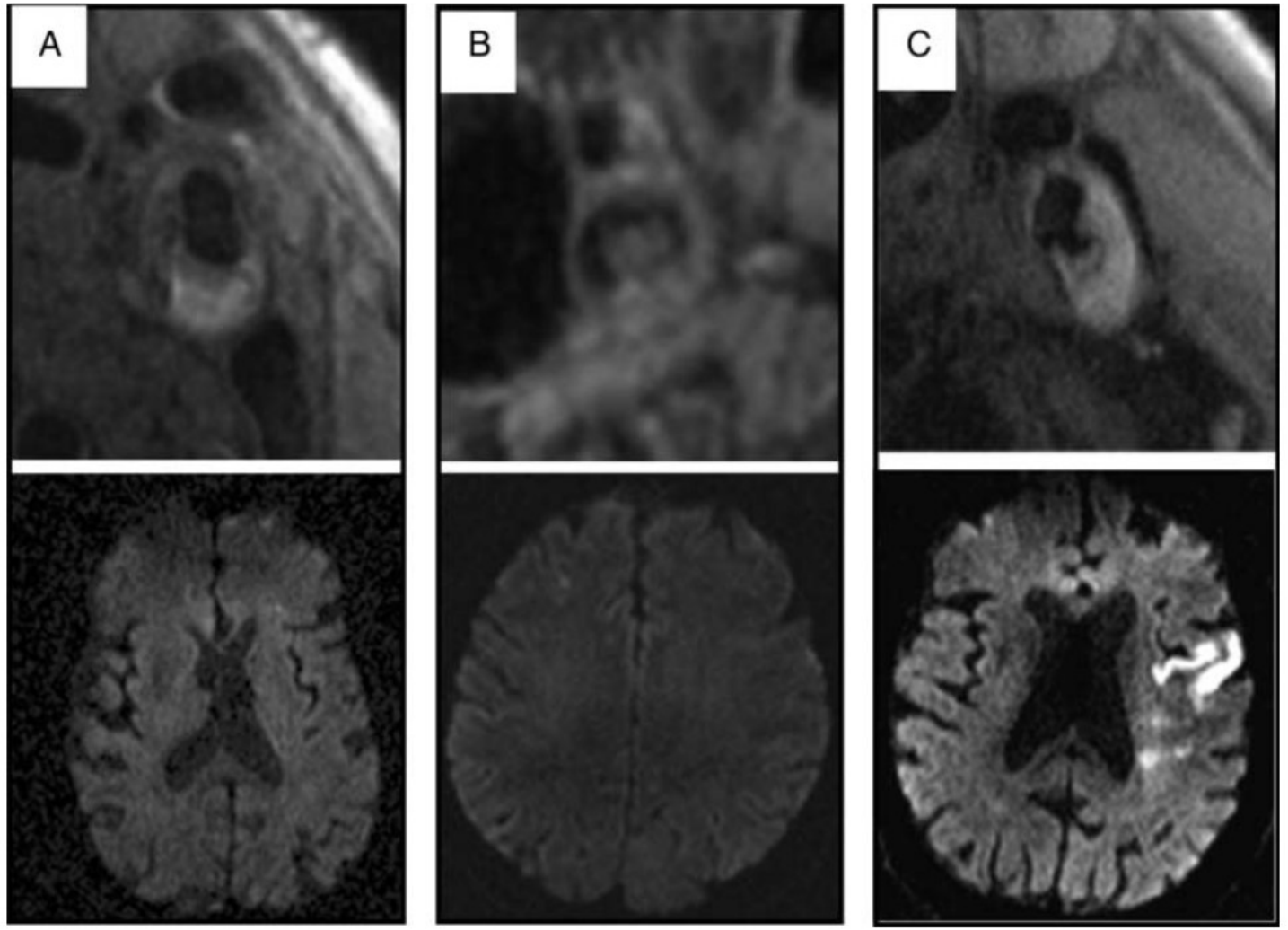

Examples of plaque changes and downstream injury (T1 images top, diffusion-weighted imaging images bottom).
(A) Upper panel shows **an intraplaque hemorrhage** associated with minimal diffusion-weighted imaging injury (lower left) in the left anterior lobe.
(B) Centre, a **large thrombus** is seen in the lumen of the right internal carotid artery, which was associated with only minimal damage in the right anterior lobe.
(C) Right, **clear surface disruption** is seen, which in this case was associated with a large infarct in the left cerebral hemispheres.

Eur Heart J Cardiovasc Imaging. 2014 Jul;15(7):730-5. doi: 10.1093/ehjci/jeu094

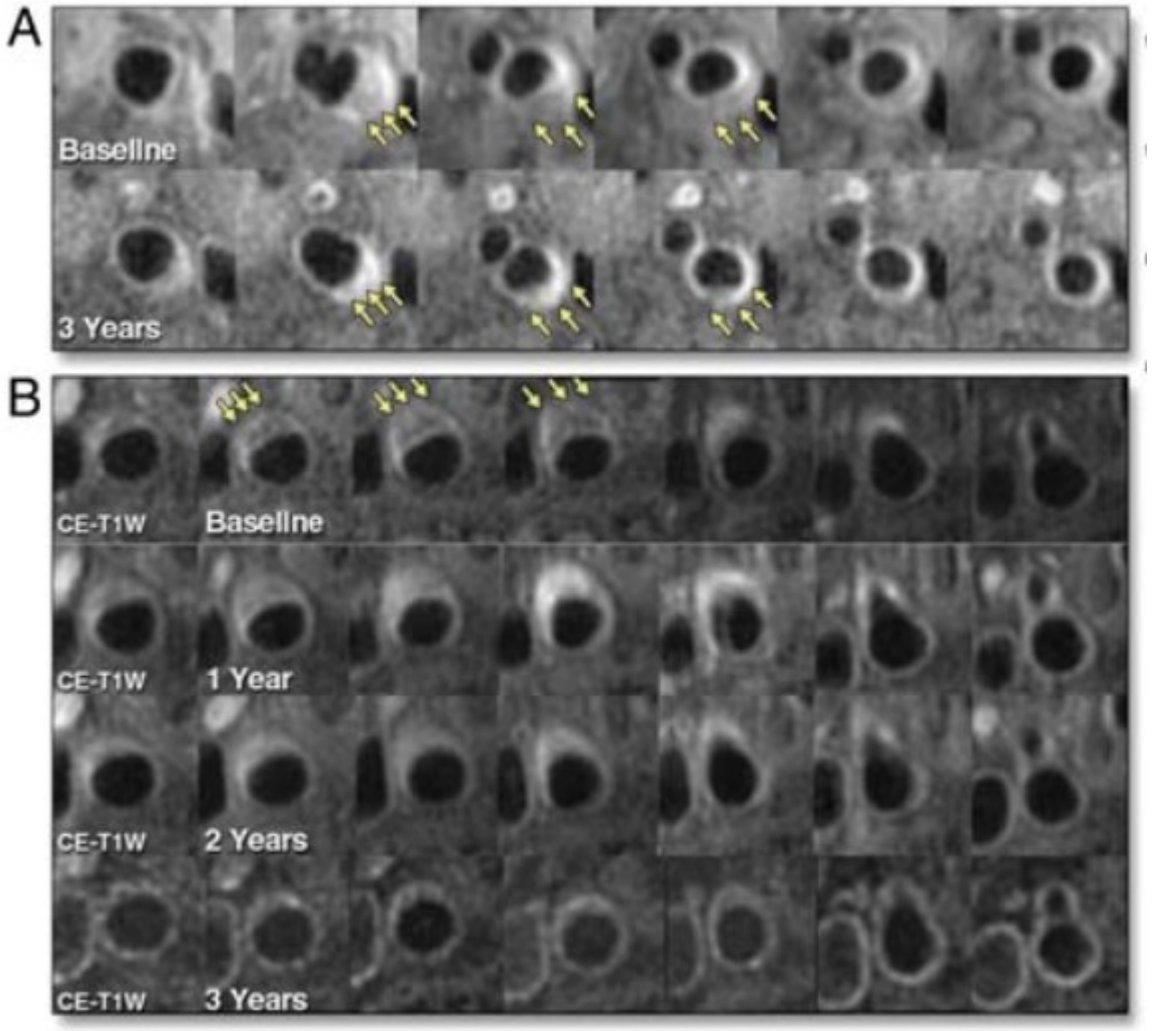

Changes in carotid plaque lipid content and tissue composition with atorvastatin.

(A) An example of significant lipid content reduction (yellow arrows) and plaque regression at 3 years compared with baseline in the left carotid artery. Overall, 11% of study subjects had completed plaque lipid depletion over 3 years.

(B) Magnetic resonance imaging example of the plaque lipid depletion time course. Regression in lipid-rich necrotic core size was notable between the baseline, 1-year, and 2-year magnetic resonance imaging scans. Regression in plaque volume seemed to follow plaque lipid depletion and was most pronounced from years 1 to 3. CE, contrast enhanced; T1W, T1-weighted.

Eur Heart J Cardiovasc Imaging. 2014 Jul;15(7):730-5. doi: 10.1093/ehjci/jeu094

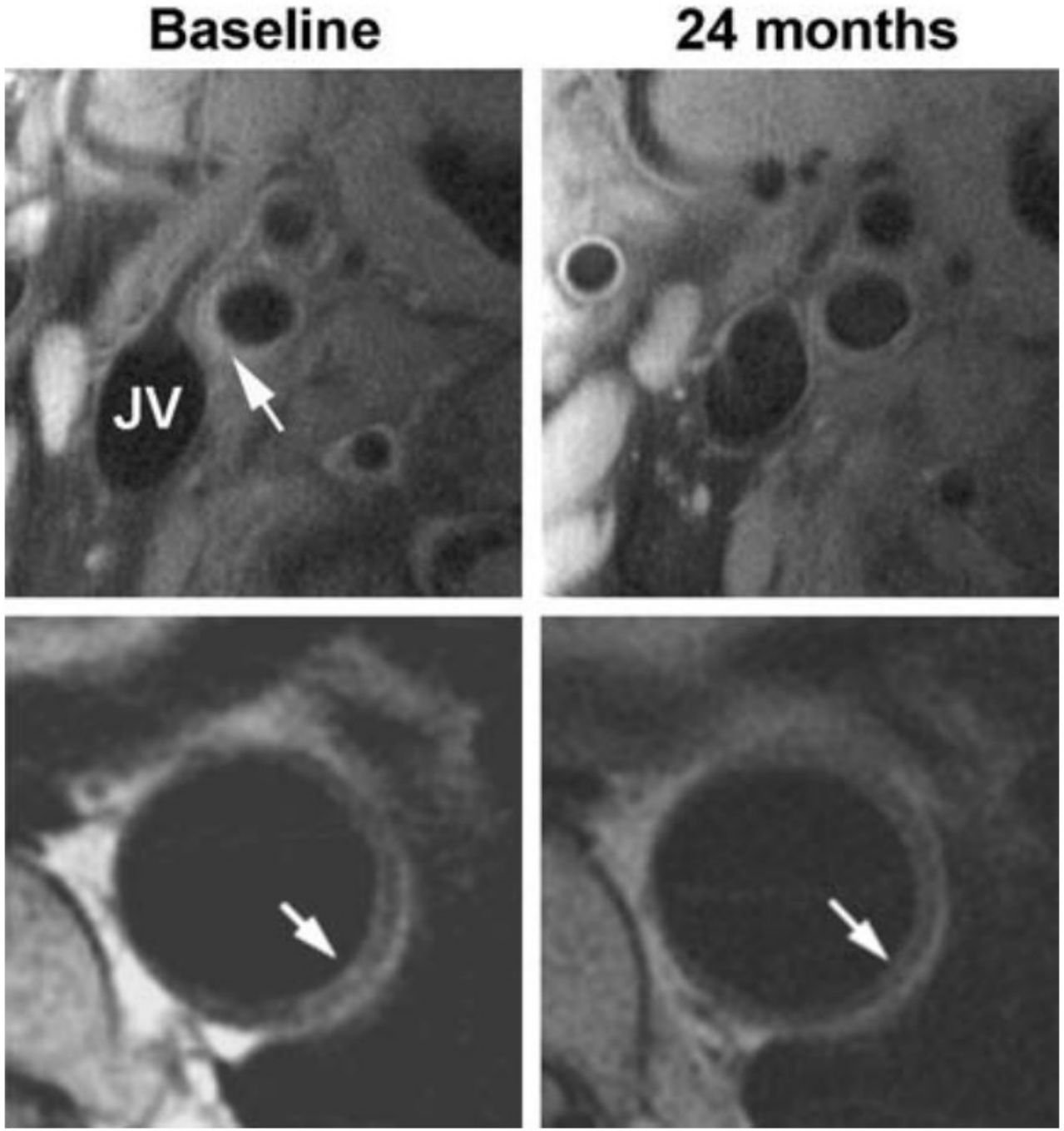

Matched magnetic resonance images of the right carotid bifurcation (upper panels) and the descending aorta (lower panels) in a hypercholesterolaemic patient at baseline and after 24 months of simvastatin therapy.

A regression of the plaque (indicated by arrows) with small enlargement of the lumen is evident.

European Heart Journal (2011) 32, 1709–1719. doi:10.1093/eurheartj/ehr068

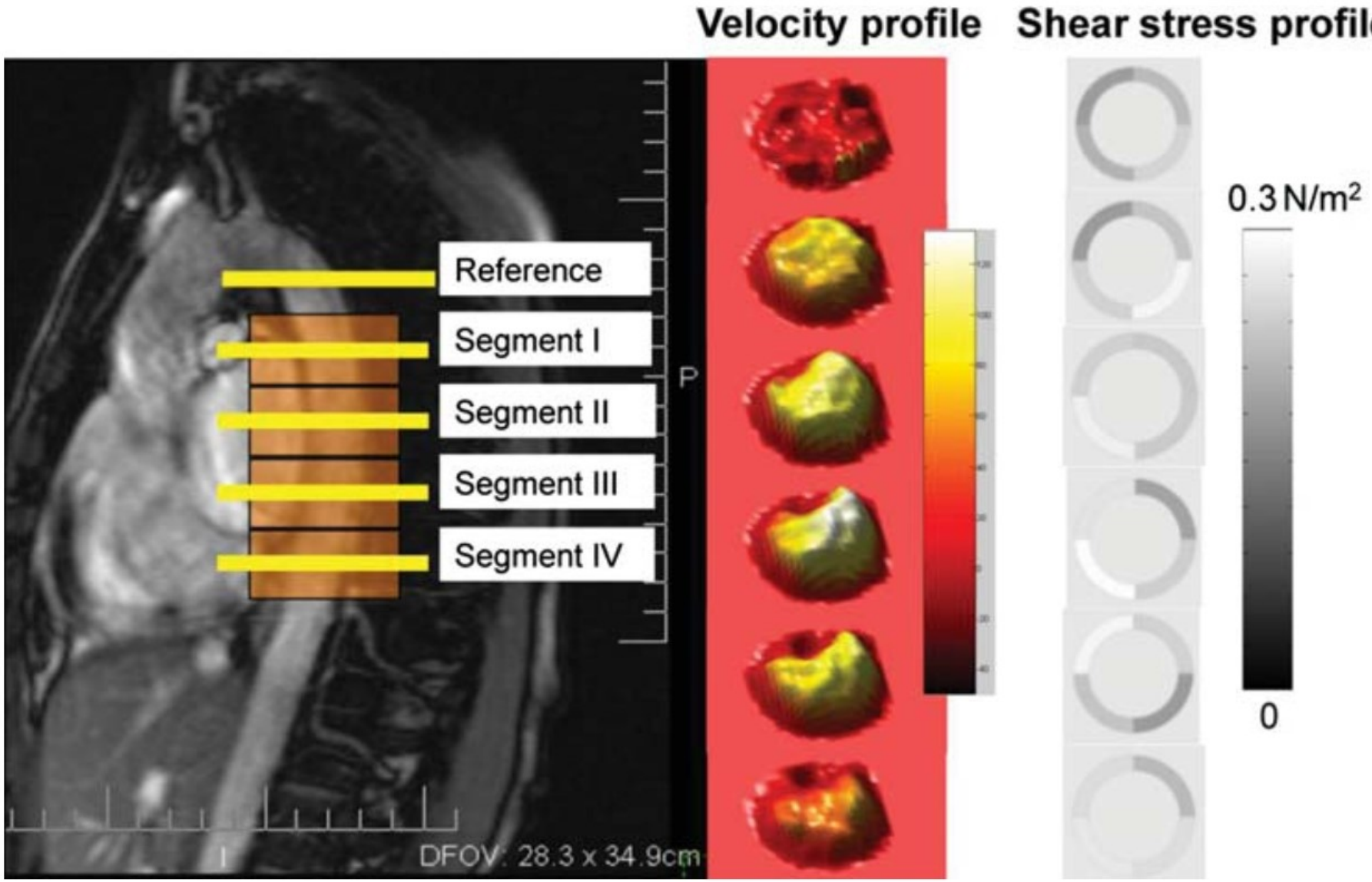

Velocity profiles at different levels of the descending aorta (left panel) can be measured by magnetic resonance imaging and used to derive shear stress. The middle panel show the velocity spectral analysis for the different segment and the right panel indicates the related shear stress condition.

European Heart Journal (2011) 32, 1709–1719. doi:10.1093/eurheartj/ehr068

Imaging of atherosclerosis by nuclear imaging

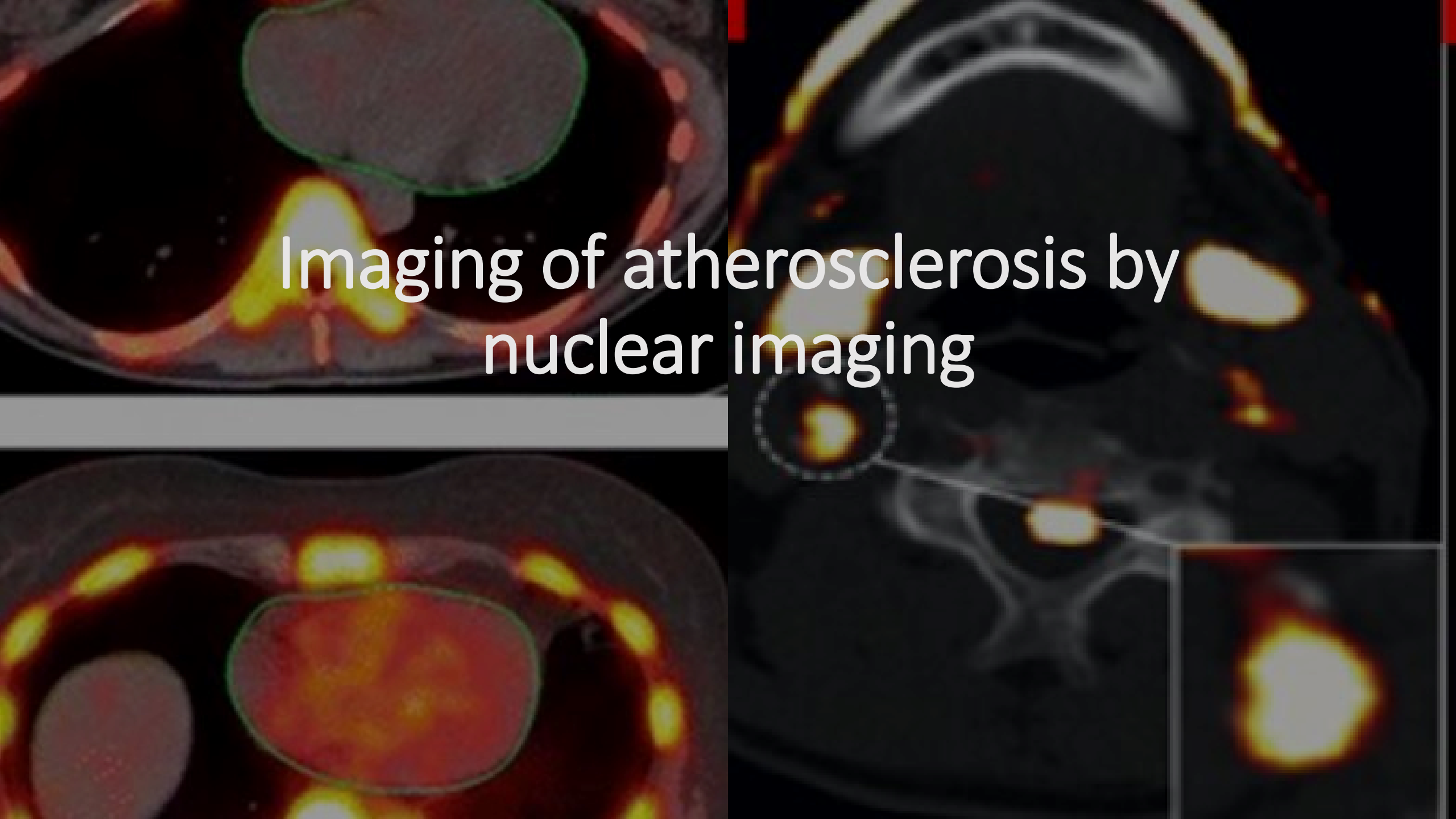

Rupture-prone coronary artery plaques, also known as **"vulnerable" or "unstable" or "high-risk" plaques**, usually ***do not cause significant stenosis*** and are not detectable by ischemia detecting tests (stress echo, stress MRI, SPECT)

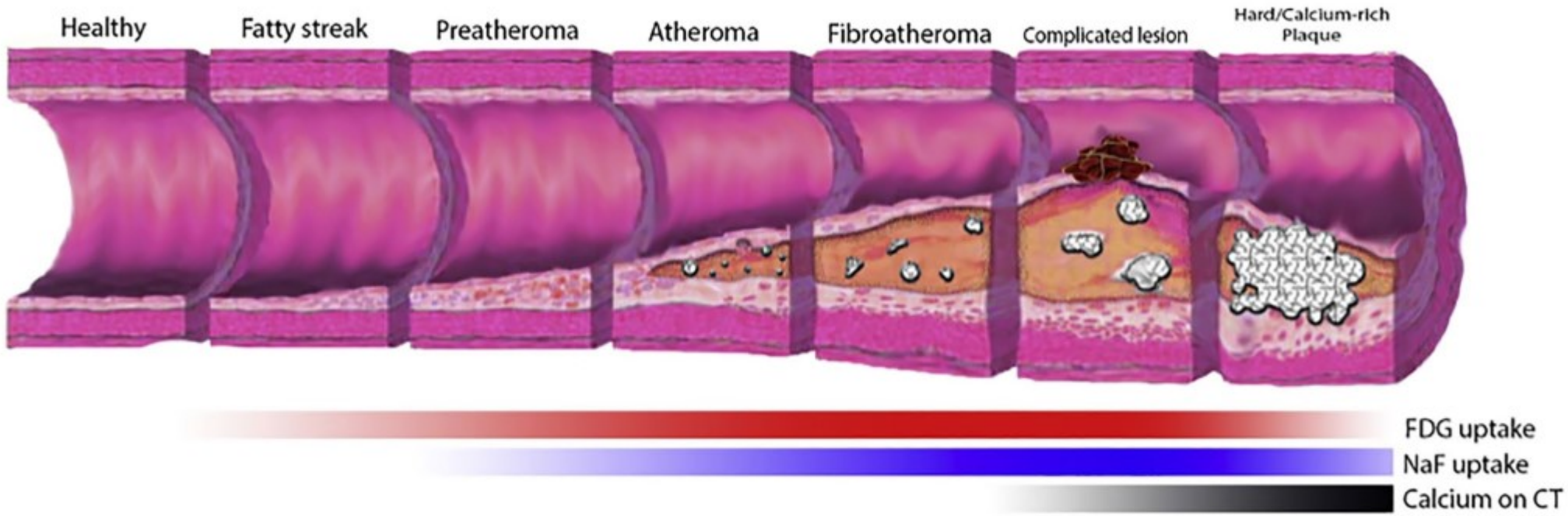

Progression of a calcium-rich atheroma with the temporal distribution of abnormalities present on ^{18}F-FDG-PET, ^{18}F-NaF-PET, and CT. As a specific marker of active microcalcification, ^{18}F-NaFPET has great promise in the domain of monitoring atherogenic activity even in early stages of disease.

Clinical and Translational Imaging (2022) 10:259–272https://doi.org/10.1007/s40336-022-00483-y

PET imaging of vulnerable coronary artery plaques

- ^{18}F-fluorodeoxyglucose (^{18}F-FDG), the first radiotracer used for its wide availability, has several limitations for the detection and quantification of coronary artery plaque inflammation.
- ^{18}F-sodium fluoride (^{18}F-NaF), a marker of vascular microcalcification, seems to be the most promising radiotracer for vulnerable coronary artery plaque imaging.
- ^{68}Ga-DOTATATE and ^{68}Ga-pentixafor have also shown interesting results on coronary plaque inflammation in humans.

While there are limitations in the use of 18F-FDG for the detection of atherosclerosis in coronary arteries due to physiological uptake in myocardium and high luminal blood pool activity of 18F-FDG, 18F-NaF PET is less affected and can be utilized to analyze the coronary arteries in addition to the peripheral vasculature.

Clinical and Translational Imaging (2019) 7:267–284. https://doi.org/10.1007/s40336-019-00334-3

The hypothesized trends of ^{18}F-FDG uptake, ^{18}F-NaF uptake, and CT calcification in the arterial wall with aging. Uptake of ^{18}F-NaF appears to be more persistent compared to that of ^{18}F-FDG, which increases and decreases with damage to the arterial wall.

Once macrocalcifications have become sufficiently stable in later years of life, ^{18}F-NaF uptake may decrease while there is stronger evidence of CT calcification

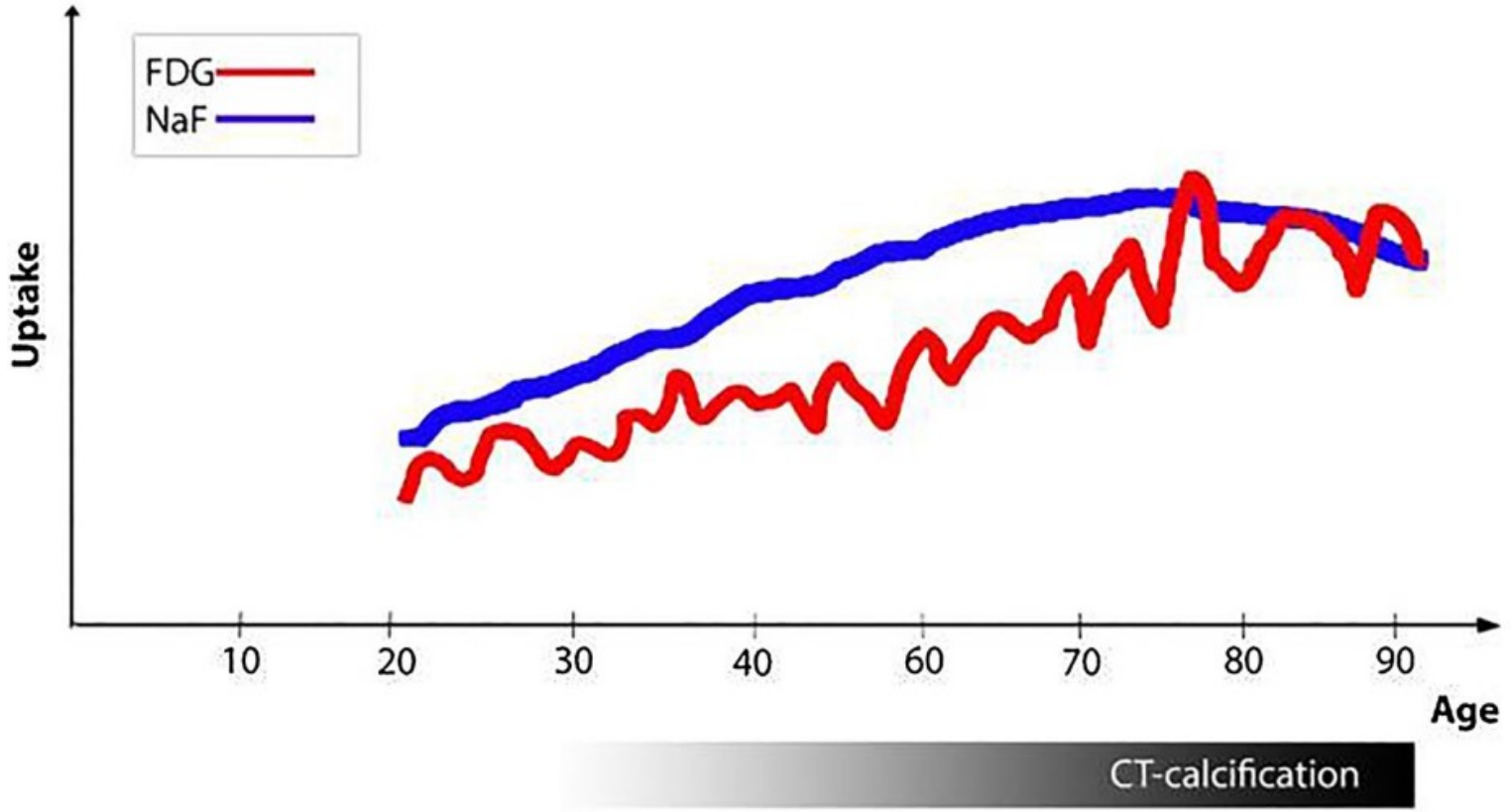

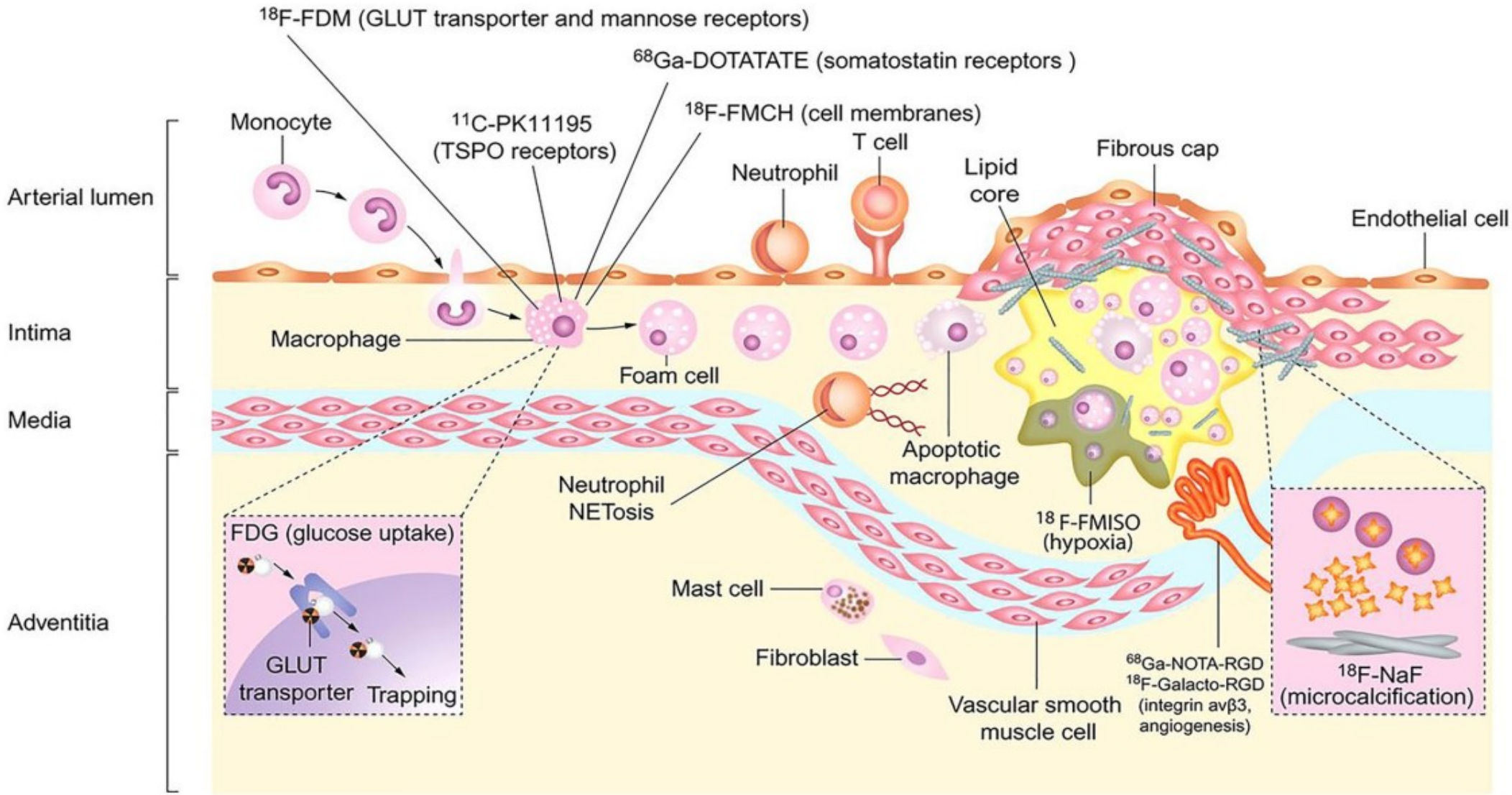

Cellular targets for PET imaging of atherosclerosis. **Macrophage activity** is responsible for increased 18F-FDG uptake as a reflection of increased glycolysis. ^{18}F fluorodeoxymannose, ^{68}GaDOTATATE, ^{11}C-PK11195, and ^{18}F-FMCH uptake is also mediated by macrophages**.** **Cellular hypoxia** is targeted by ^{18}F-FMISO, while ^{68}Ga-NOTA-RGD and ^{18}F-Galacto-RGD show areas of **neoangiogenesis**. **Microcalcification** is uniquely revealed by ^{18}F-NaF activity.

Clinical and Translational Imaging (2022) 10:259–272https://doi.org/10.1007/s40336-022-00483-y

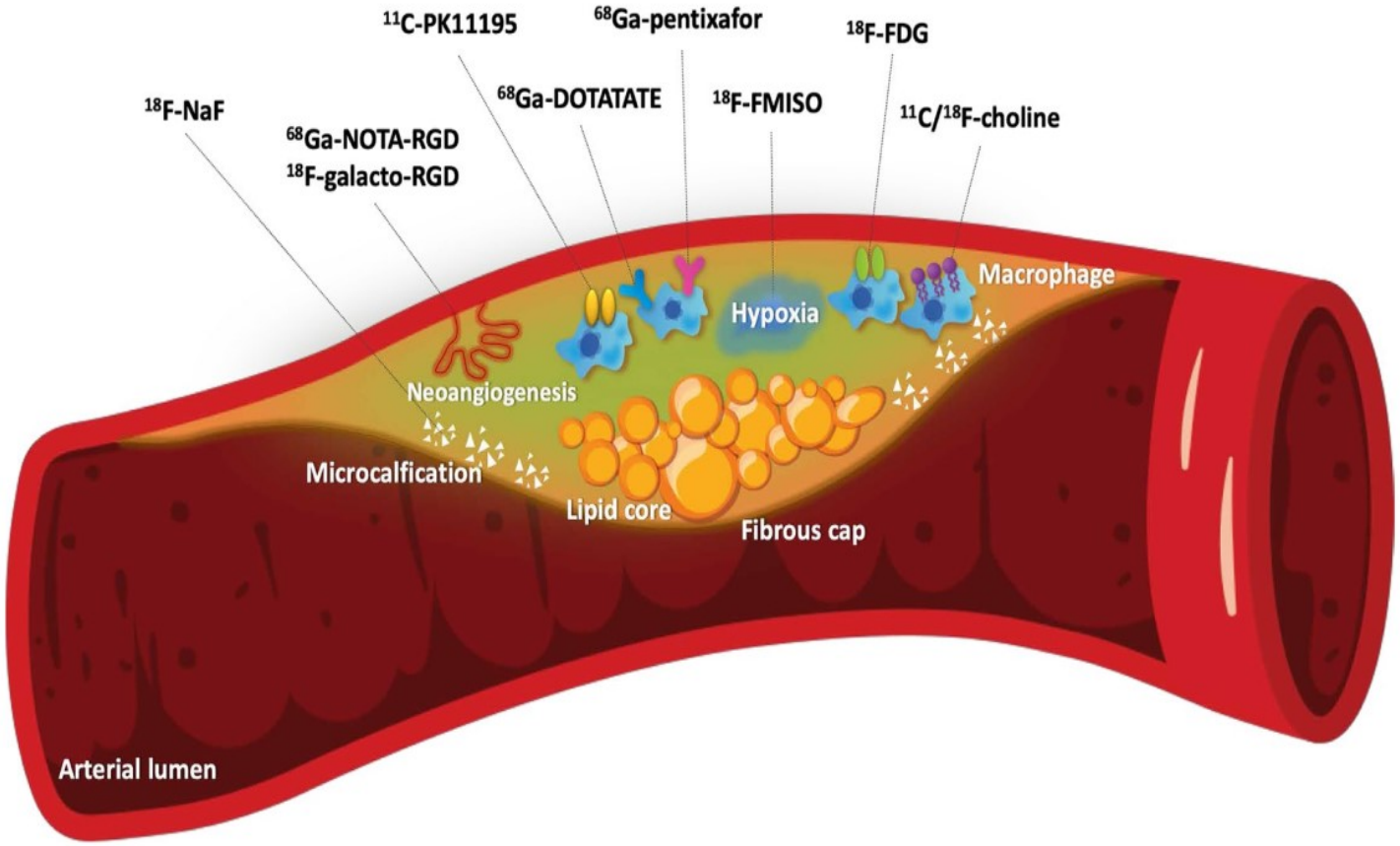

Schematic representation of molecular imaging targets in vulnerable atherosclerotic plaques. Atherosclerosis process is a complex and dynamic process that involves activated macrophages that take up **$_{18}$F-fluorodeoxyglucose ($_{18}$F-FDG)** by glucose transporters.

Somatostatin receptors are also expressed on activated macrophages and are the target for **$_{68}$Ga-DOTATATE.**

Macrophage-mediated inflammation can also be detected by radiotracers targeting translocator protein receptors (**$_{11}$C-PK11195)**, chemokine receptors (**$_{68}$Ga-pentixafor**) and membrane phospholipids (**$_{11}$C- or $_{18}$F-choline**).

Other radiotracers are able to detect microcalcification (**$_{18}$F-sodium fluoride [$_{18}$F-NaF**]), cellular hypoxia (**$_{18}$F-misonidazole [$_{18}$F-MISO**]) and neoangiogenesis ($\alpha_v\beta_3$ integrin affine agents: **$_{68}$Ga-NOTA-RGD**, **$_{18}$F-galacto-RGD**)

Clinical and Translational Imaging (2019) 7:267–284. https://doi.org/10.1007/s40336-019-00334-3

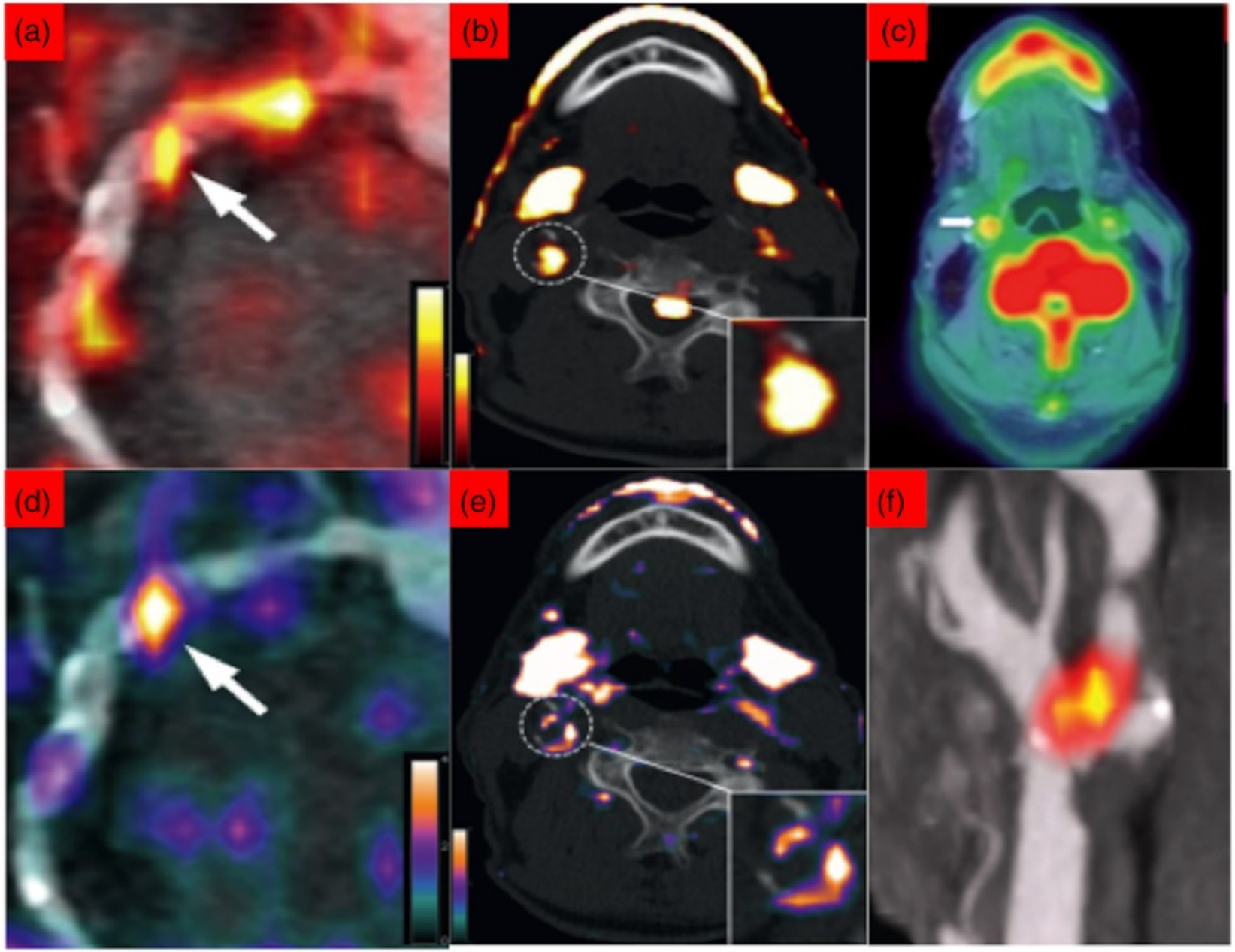

PET imaging of inflammation and microcalcification in atherosclerosis.
(a) Coronary artery inflammation as visualised by ^{18}F-FDG/CT.
(b) Carotid artery inflammation as visualised by ^{18}F-FDG/CT.
(c) ^{18}F-NaF PET/CT image of symptomatic right carotid artery.
(d) Coronary artery inflammation visualised by ^{68}Ga-DOTATATE.
(e) Carotid artery inflammation visualised by ^{68}Ga-DOTATATE.
(f) ^{18}F-NaF PET/CT image of symptomatic coronary artery.

Main characteristics of radiotracers used in vulnerable coronary artery plaque imaging

Radiotracer	Target	Strengths	Limitations
^{18}F-FDG	Macrophages Glucose transporters	Widely available Low cost	Physiological uptake by the myocardium Patient preparation Dietary restrictions I.v. heparin Less specificity for inflammation
^{68}Ga-DOTATATE	Macrophages Somatostatin subtype 2 receptor (SSR2)	Greater specificity for inflammation than ^{18}F-FDG No patient preparation No uptake by the myocardium Favourable dosimetry	Generator production Increased hepatic uptake may limit right coronary artery assessment Limited data in coronary artery plaque imaging in humans
^{18}F-NaF	Calcified area Fluoride ion exchange with hydroxyl ions in hydroxyapatite crystal	High specificity for vascular microcalcification No patient preparation No uptake by the myocardium Available and easily produced Abundance of literature data	Uptake of calcified aortic root and valvular structures may limit the assessment of proximal tract of coronary arteries
^{18}F-/^{11}C-choline	Macrophages Choline transporters	High affinity to membrane phospholipids No patient preparation No uptake by the myocardium	Less availability Need for on-site cyclotron for ^{11}C-choline Short half-life (20 min) for ^{11}C-choline Increased hepatic uptake may limit right coronary artery assessment No published data on coronary artery plaque imaging in humans
^{11}C-PK11195	Macrophages Ligand of 18 kDa translocator protein (TSPO)	Greater specificity for inflammation than ^{18}F-FDG No patient preparation Favourable dosimetry	Need for on-site cyclotron Short half-life (20 min) No published data on coronary artery plaque imaging in humans
^{18}F-FMISO	Hypoxic area	Complementary information to inflammation and calcification processes No patient preparation	Small target No experience in coronary artery plaque imaging in humans
^{68}Ga-pentixafor	Macrophages C–X–C chemokine receptor 4 (CXCR4)	High affinity to inflammatory cells No patient preparation No uptake by the myocardium Favourable dosimetry	Generator production Less availability in the world Initial experience in coronary artery plaque imaging in humans

Clinical and Translational Imaging (2019) 7:267–284. https://doi.org/10.1007/s40336-019-00334-3

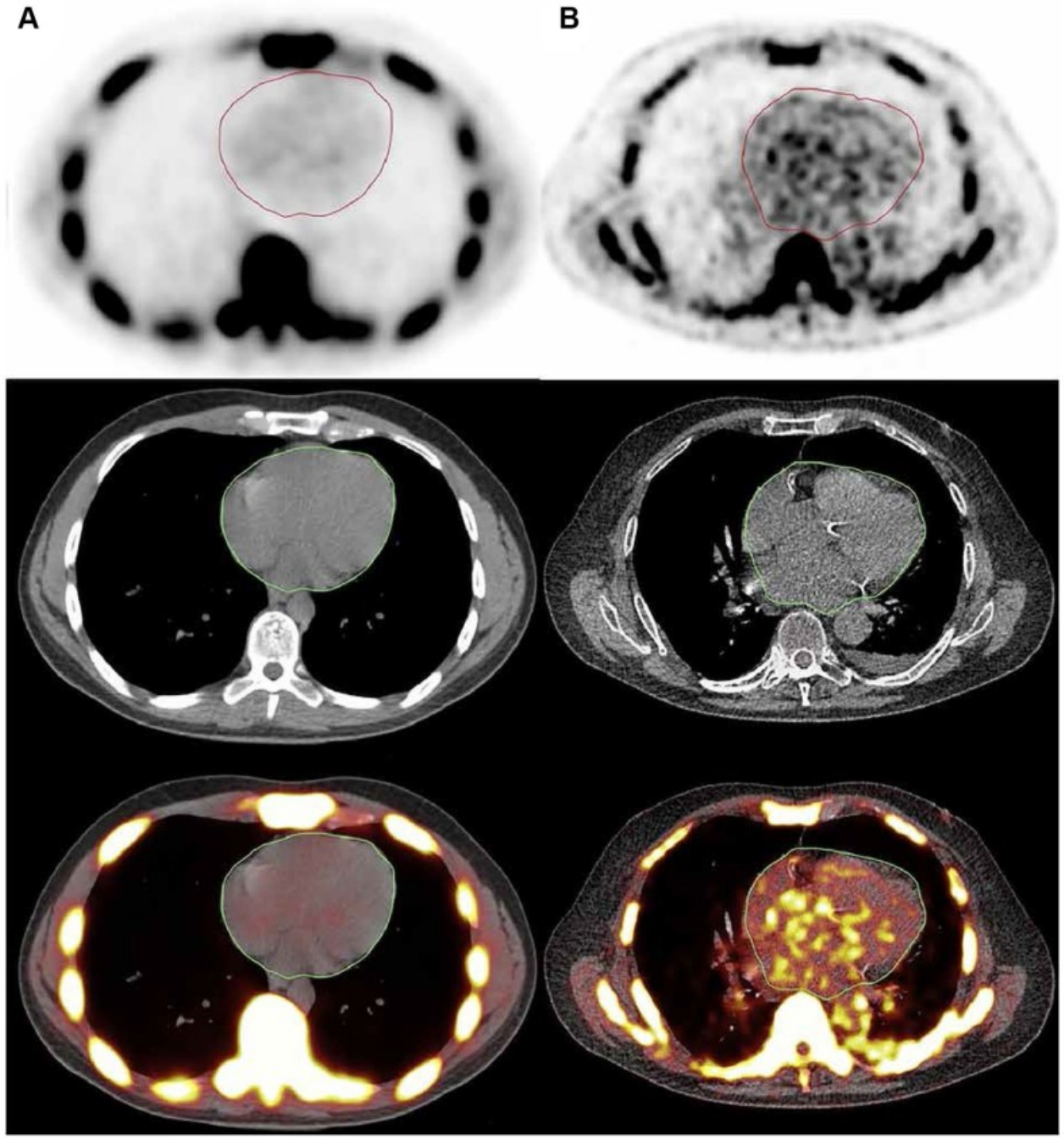

Global cardiac quantification.
This figure shows the methodology to globally assess the coronary artery calcification with $_{18}$F-sodium fluoride ($_{18}$F-NaF) PET/CT.

a. Image of a 25-year-old man and
b. image of a 75-year-old man.

Regions of interest were manually assigned to include the entire heart; mean SUV values for the young and old subjects were 0.42 and 1.29, respectively.
This approach provides a more accurate assessment of the disease burden and overcomes the limitations of partial volume correction and movement.

Clinical and Translational Imaging (2019) 7:267–284. https://doi.org/10.1007/s40336-019-00334-3

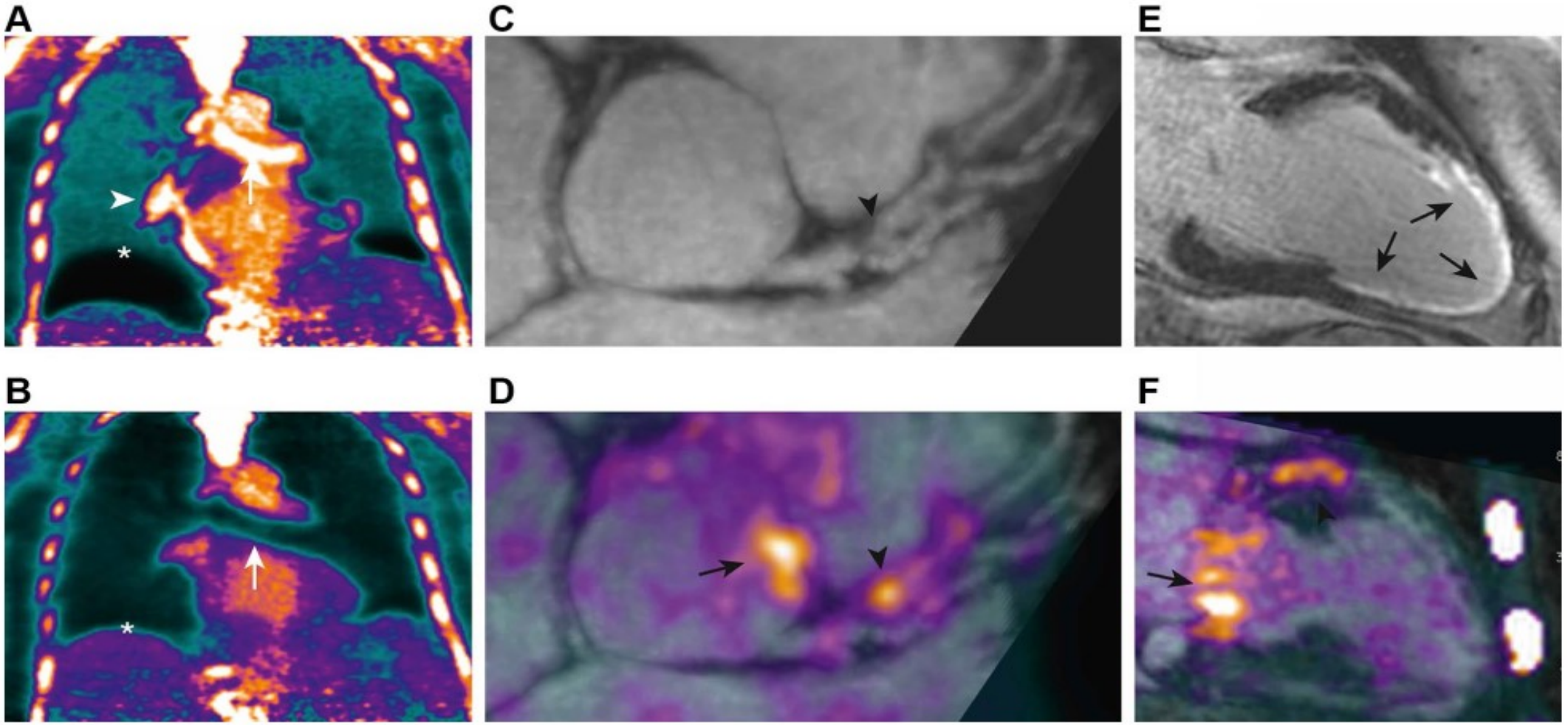

PET/MRI imaging of coronary atherosclerosis. Patient with breathlessness underwent $_{18}$F-sodium fluoride ($_{18}$F-NaF) PET/MRI imaging. **a** Standard breath-held attenuation correction leads to artefacts at the diaphragm (asterisk), heart–lung boundary (white arrowhead), and bronchus (white arrow). **b** These artefacts were corrected with a free-breathing MR sequence for attenuation correction, **c**, **d**, **f** allowing an area of increased $_{18}$F-NaF uptake to be visualized overlying **an obstructive plaque (black arrowhead) in the left anterior descending artery.** Additional uptake was observed in the aortic wall and mitral valve annulus (black arrows). **e** Transmural late gadolinium enhancement was observed in the perfusion territory of this lesion, suggesting recent plaque rupture and myocardial infarction.

Clinical and Translational Imaging (2019) 7:267–284. https://doi.org/10.1007/s40336-019-00334-3

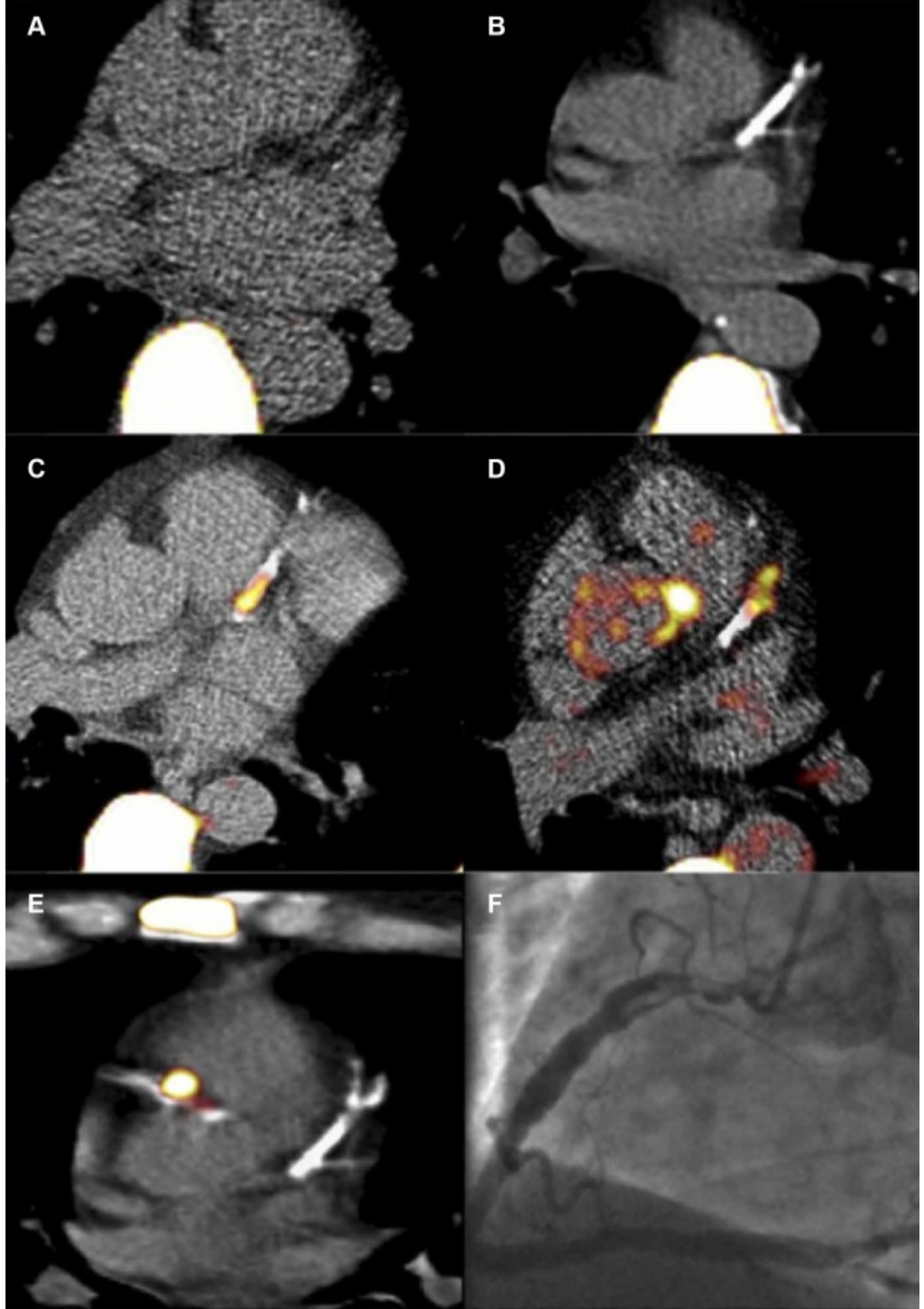

Fused PET/CT images of 18F-NaF activity in the coronary arteries.

a. Patient in the control group with no coronary calcium and no coronary 18F-sodium fluoride (18F-NaF) uptake. Note the intense uptake in the vertebrae.

b. Patient with extensive calcification in the left anterior descending artery (LAD) but no 18F-NaF uptake.

c. Intense focal 18F-NaF uptake is observed in the proximal LAD overlying existing coronary calcium in this region.

d. Increased and focal 18F-NaF uptake is observed in the mid-LAD adjacent to an area of existing coronary calcification.

e. Patient who suffered a recent inferior non-ST-segment elevation myocardial infarction showing intense focal uptake of the proximal right coronary artery with sparing of the LAD. The proximal right coronary artery was felt to be the culprit artery on the basis of the electrocardiogram and appearances on coronary angiography

f. which demonstrated a complex ulcerated plaque with in situ thrombus.

Clinical and Translational Imaging (2019) 7:267–284. https://doi.org/10.1007/s40336-019-00334-3

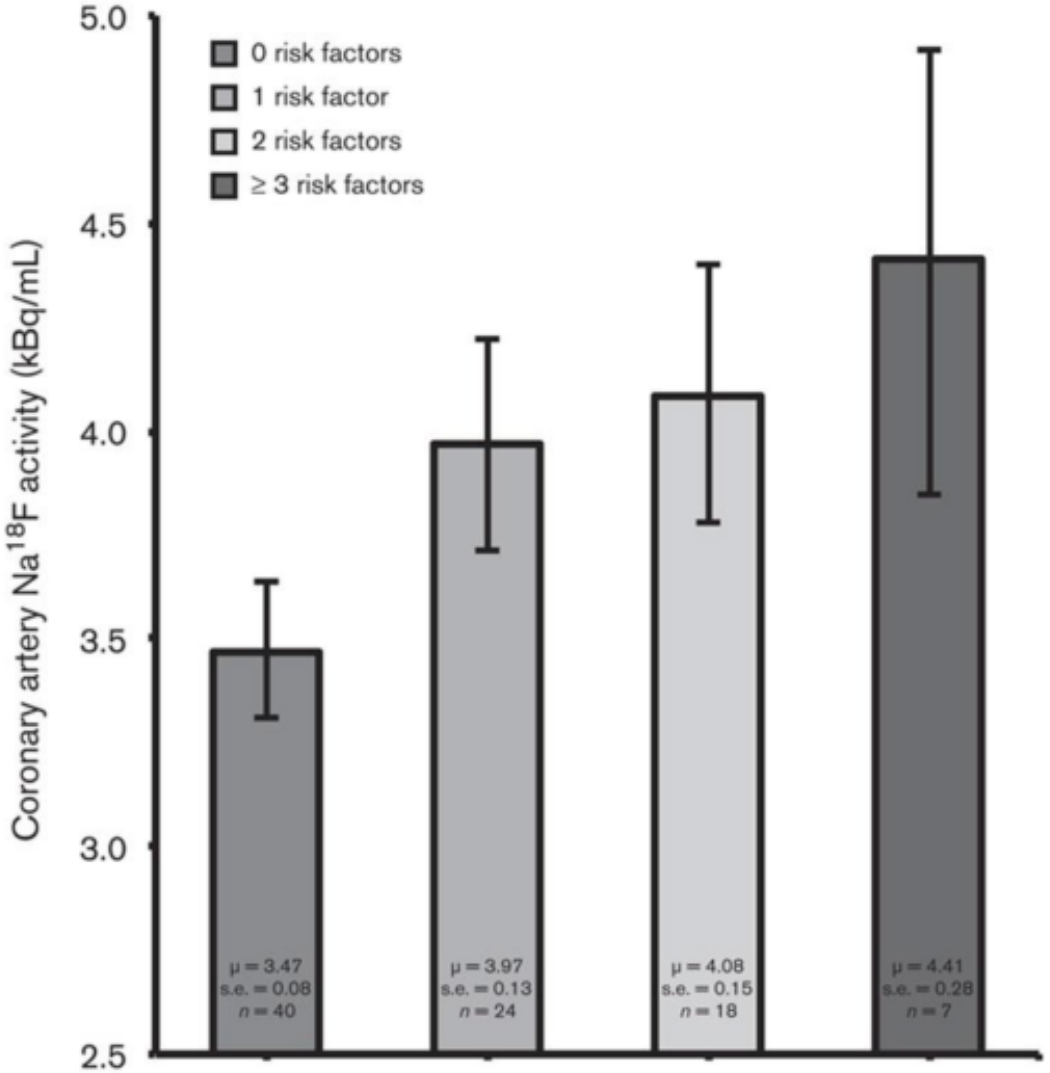

NaF uptake in relation to cardiovascular risk factors.
Bar graph showing coronary artery NaF uptake (kBq/ml), adjusted for blood NaF activity, injected NaF dose and PET/CT technology, in relation to the number of cardiovascular risk factors (i.e., BMI, systolic blood pressure, serum triglyceride concentration, and serum low-density lipoprotein-cholesterol concentration) present.
Coronary NaF uptake increased linearly according to the number of risk factors present ($P < 0.001$ for a linear trend).
Coronary NaF uptake was significantly lower in the absence of risk factors compared with the presence of one or more risk factors (3.47 vs. 3.97, 4.08, and 4.41 kBq/ml, respectively; $P < 0.001$).
Error bars represent the 95% confidence interval of the mean.

Front. Physiol. 11:511391.doi: 10.3389/fphys.2020.511391

The main pathophysiological mechanism used for atherosclerotic plaque imaging at each stage.

Stage of a Plaque	Target Pathophysiological Process	RP
Thickening of intima, intimal xanthoma, or "fatty streak"	Lipoprotein accumulation	^{99m}Tc, ^{111}In, ^{68}Ga-labeled LDL ^{89}Zr-labeled HDL
	Lipoprotein oxidation	^{131}I and ^{125}I-labeled antibodies to OSE ^{89}Zr-LA25
	Monocyte adhesion and infiltration	VCAM-1: ^{18}F-4V; ^{99m}Tc- or ^{18}F labeled cAbVCAM1-5 P-selectin: ^{64}Cu-antibodies, ^{68}Ga-fucoidan
Macrophage migration and "foam cell" formation, macrophage activation	Native cells migration	^{111}In-oxine, ^{99m}Tc-exmetazime blood cell labelling
	Increased macrophage glucose uptake and metabolism	^{18}F-FDG *
	Increased membrane production	^{18}F-choline *
	Scavenger receptor	^{99m}Tc-specific mab to LOX-1
	Somatostatin receptor	^{68}Ga-DOTA-TATE * ^{111}In-DOTA-JR11
	Mannose receptors	^{68}Ga-mannose-specific mab ^{99m}Tc-tilmanocept * ^{18}F-FDM ^{68}Ga-NOTA-MSA
	Folate receptor	^{99m}Tc-EC20 (etarfolatide) ^{18}F-fluorofolic acid
	TSPO	^{11}C-PK11195 ^{18}F-GE-180 ^{11}C-PBR28
	Chemokine receptor	^{64}Cu-DOTA-vMIP-II ^{68}Ga-pentixaphor
	LFA-1	^{111}In-DOTA-butylamino-NorBIRT (DANBIRT)
	Nicotinic acetylcholine receptor	^{18}F-ASEM
	Increased phagocytosis	^{64}Cu-trimodal nanoparticles ^{18}F-iron oxide nanoparticles
Plaque formation	Interleukin-2 receptor	^{99m}Tc-HYNIC-IL-2
	Neoangiogenesis	^{18}F-galacto-RGD ^{18}F-Alphatide II ^{68}Ga-NOTA-PRGD2 ^{18}F-flotegatide ^{99m}Tc-maracyclatide ^{99m}Tc-IDA-D—[c(RGDfK)]2
	Hypoxia	^{18}F-FMISO * ^{18}F-HX4
	Macrophage apoptosis	^{99m}Tc- and ^{68}Ga-labeled annexin V
	Proteases	^{99m}Tc-RP805 (MPI), ^{111}In-RP782
Plaque progression and deterioration	Calcification	^{18}F-sodium fluoride *
	Thrombosis	^{99m}Tc-labeled mab to tissue thromboplastin ^{111}In-labeled platelets

RP—radiopharmaceutical, LDL—low-density lipoproteins, HDL—high-density lipoproteins, OSE—oxidation specific epitopes, VCAM—vascular cell adhesion molecule, mab—monoclonal antibody, LOX-1—lectin-like receptor for oxidized low-density lipoproteins, FDG—fluorodeoxyglucose, FDM—fluoro-D-mannose, NOTA-MSA— human serum albumin enriched with mannose, TSPO—18 kDa translocation protein, LFA-1—the lymphocytefunction associated antigen-1, RGD—arginine-glycine-aspartic acid. (*) RPs denoted with an asterisk are readily achievable for clinical practice.

J. Imaging 2022, 8, 261. https://doi.org/10.3390/jimaging8100261

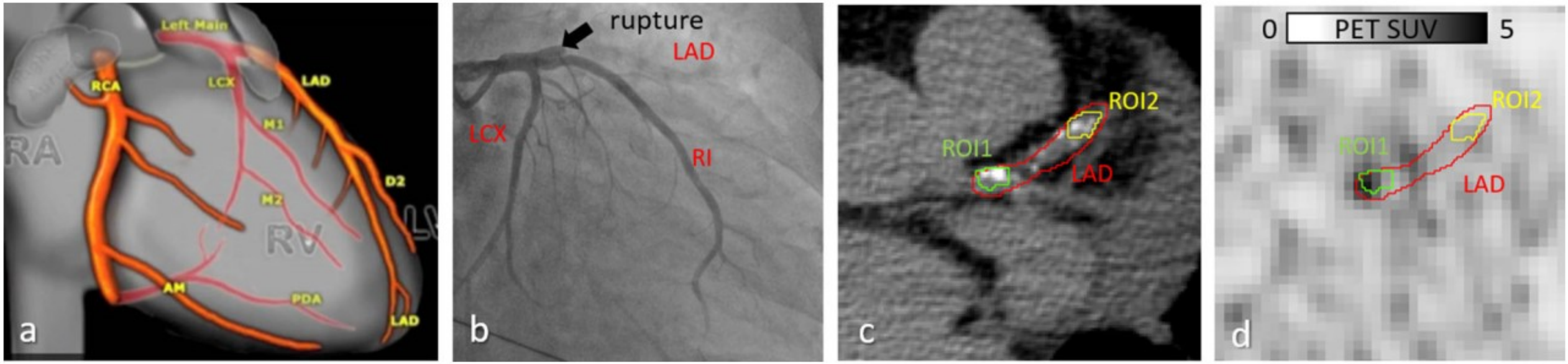

Example of ^{18}F-NaF PET–CT detection of a ruptured plaque.

A. Definition of the coronary arteries, by ‘‘Robin Smithuis and Tineke Wilems, the Radiology Assistant.’’

B. Angiogram examination showing plaque rupture and acute occlusion at proximal LAD. (RI represents a large Ramus Intermedius)

C. CT calcium scoring images in the axial view where the LAD and 2 ROIs have been segmented.

D. Corresponding PET image with the reported segmentations; images were scaled with SUV in range [0-5].

ROI^{1} corresponds to the ruptured plaque.

J Nucl Cardiol. 2018 Dec;25(6):2001-2011. doi: 10.1007/s12350-017-0918-8.

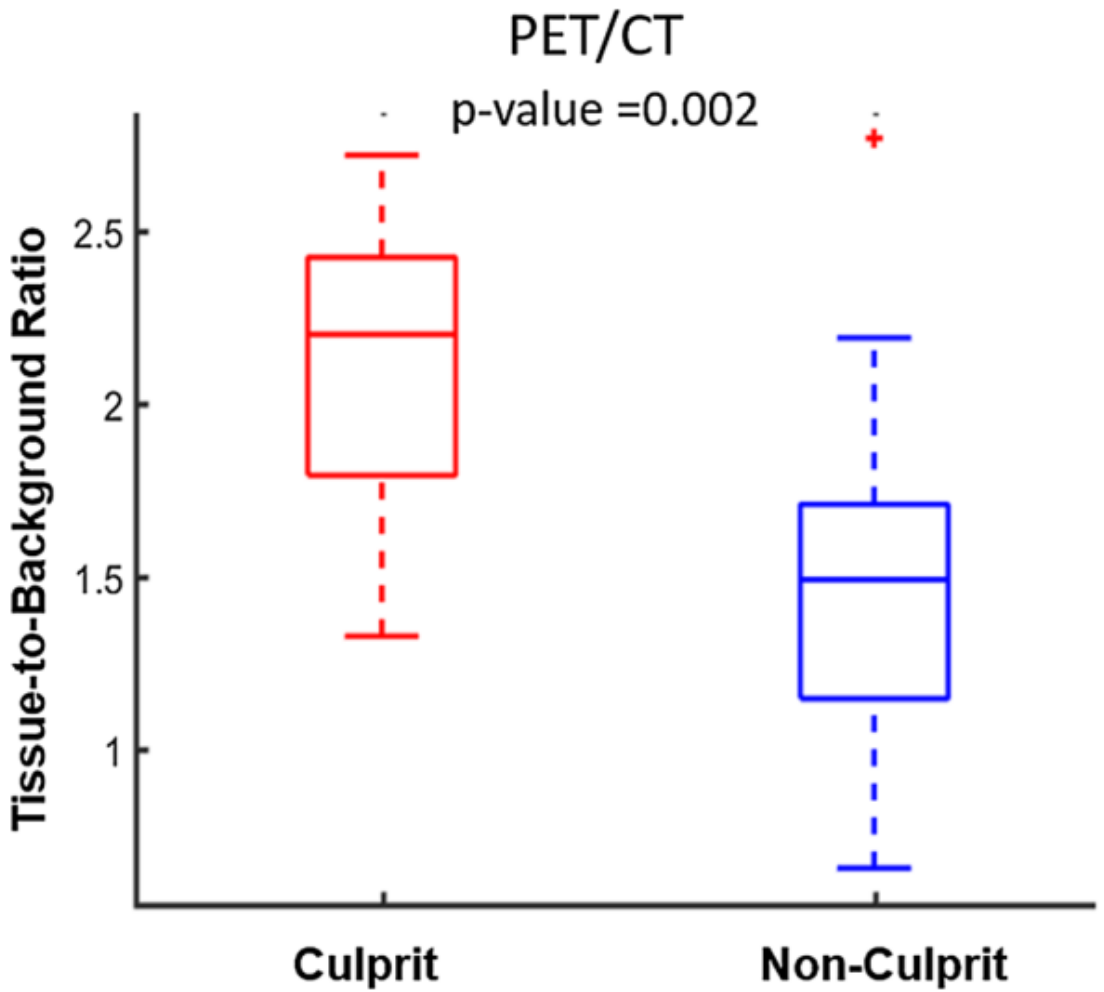

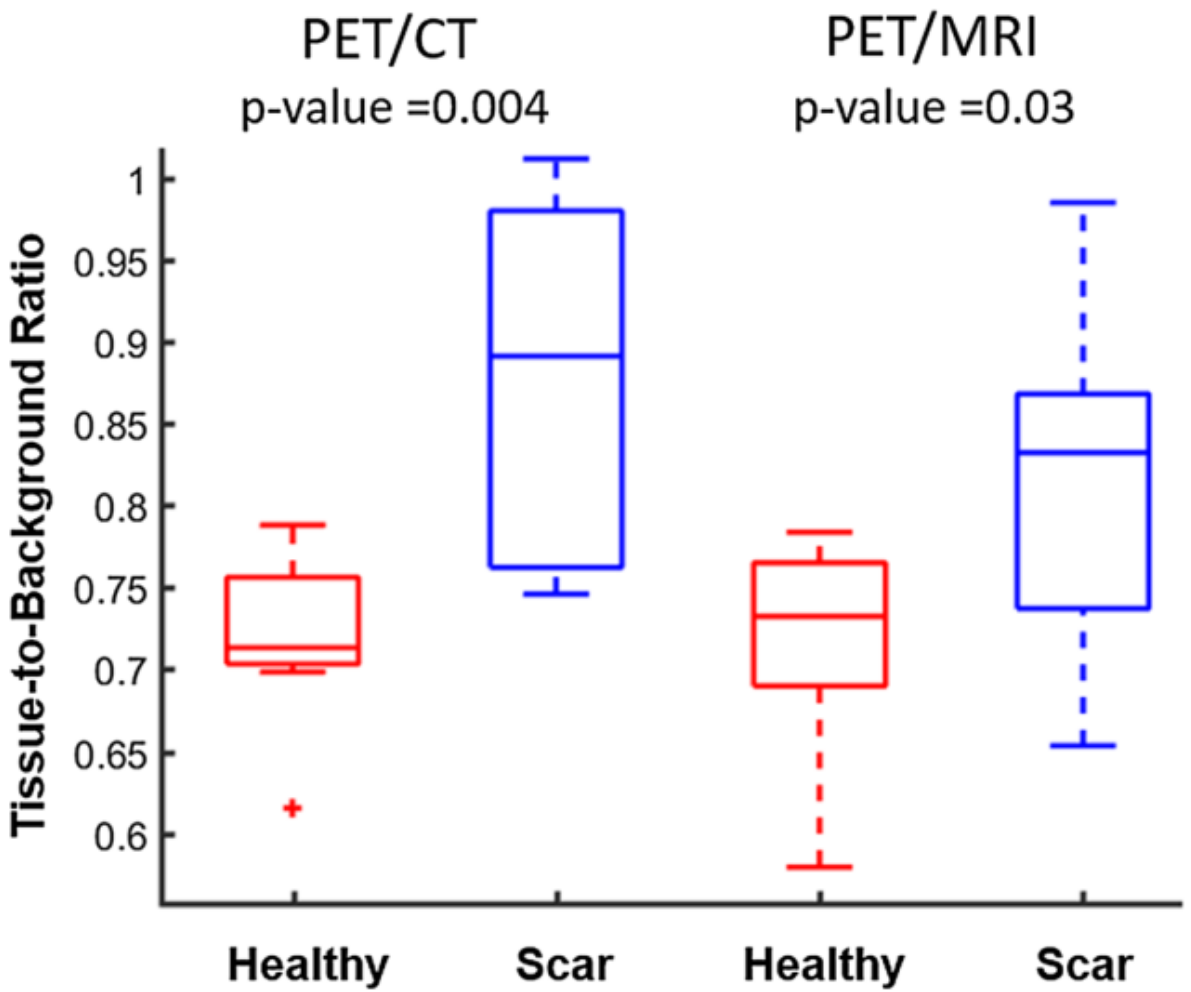

J Nucl Cardiol. 2018 Dec;25(6):2001-2011. doi: 10.1007/s12350-017-0918-8.

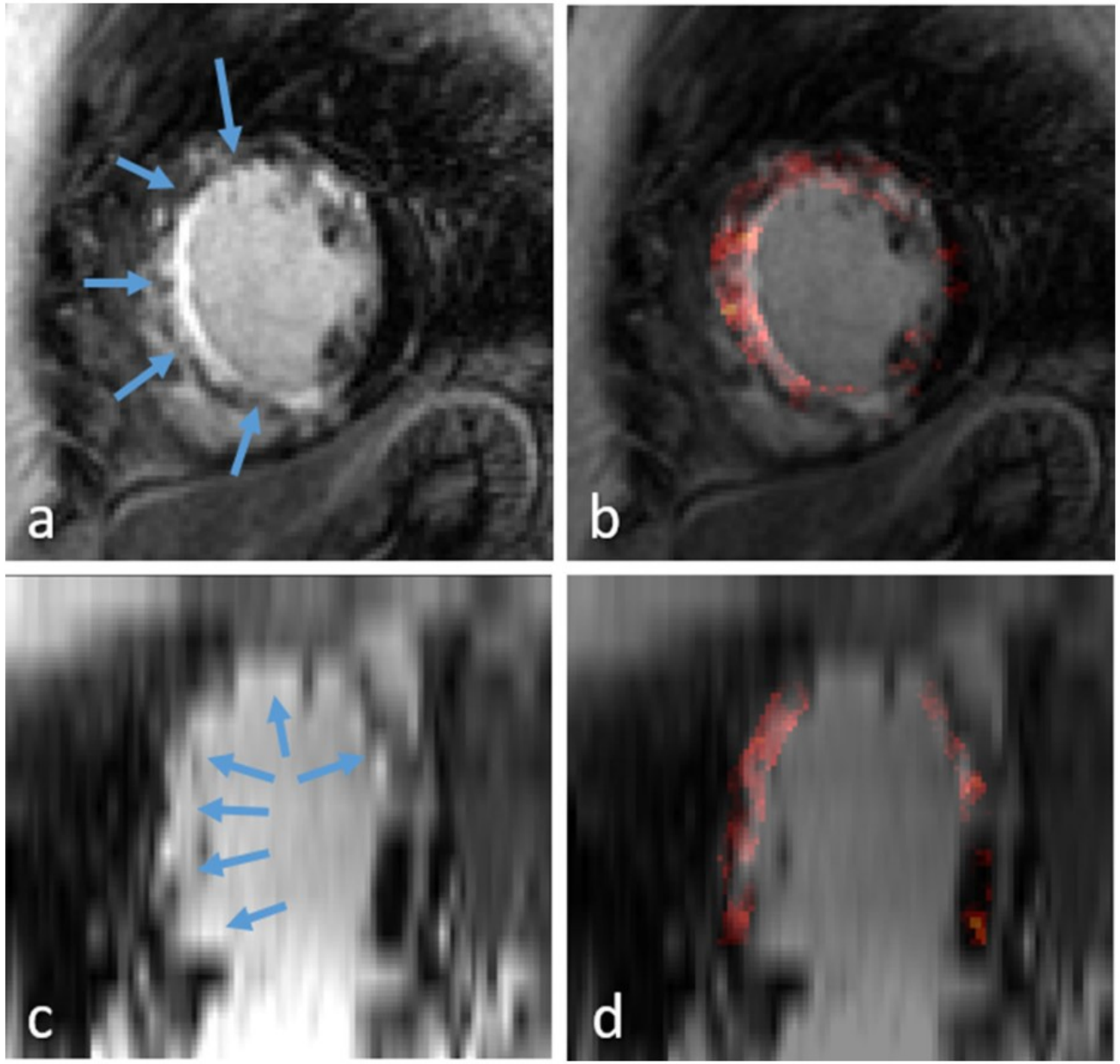

Example of LGE image showing extensive infarct tissue (arrows) in short-axis (A) and 2-chamber (C) views. 18F-NaF PET uptake was overlaid on the myocardium muscle on images (B) and (D), respectively, showing increased uptake in the infarct tissue compared to healthy myocardium.

The use of $_{18}$F-NaF PET/CT imaging to detect high risk coronary lesions in patients with STEMI is confirmed in a small Asian population. The comparison of $_{18}$F-NaF uptake in myocardial scar tissue with remote healthy myocardium shows, for the first time in humans, that $_{18}$F-NaF **also binds to myocardial scar tissue.**

These data serve as proof-of-principle that first, **pathobiological processes involving microcalcification may be common to both atherosclerotic plaque disruption and myocardial infarction** and second, $_{18}$F-NaF PET/CT could be potentially applied to **simultaneous coronary and myocardial imaging applications to quantify both vulnerable plaque burden and myocardial scar tissue**.

J Nucl Cardiol. 2018 Dec;25(6):2001-2011.
doi: 10.1007/s12350-017-0918-8.

Comparison between structural and molecular imaging

	Structural imaging	Molecular imaging
Advantages	Offers greater information about the structure and morphology of the plaque, as well as the risk factors for ruptures Higher-resolution aids in the diagnosis of low-density, non-calcified plaques	Detects microscopic changes early in the disease's course when progression can be suppressed Can detect metabolic activity within plaque to differentiate between active and indolent plaque
Disadvantages	Visualizes the macroscopic alterations that occur late in the disease's course, when the effects are frequently permanent Inability to distinguish between metabolically active and indolent atherosclerotic lesions	Small plaque may not be detectable due to limited spatial resolution Cardiac and respiratory movements decrease the quality of images

Clinical and Translational Imaging (2022) 10:259–272https://doi.org/10.1007/s40336-022-00483-y

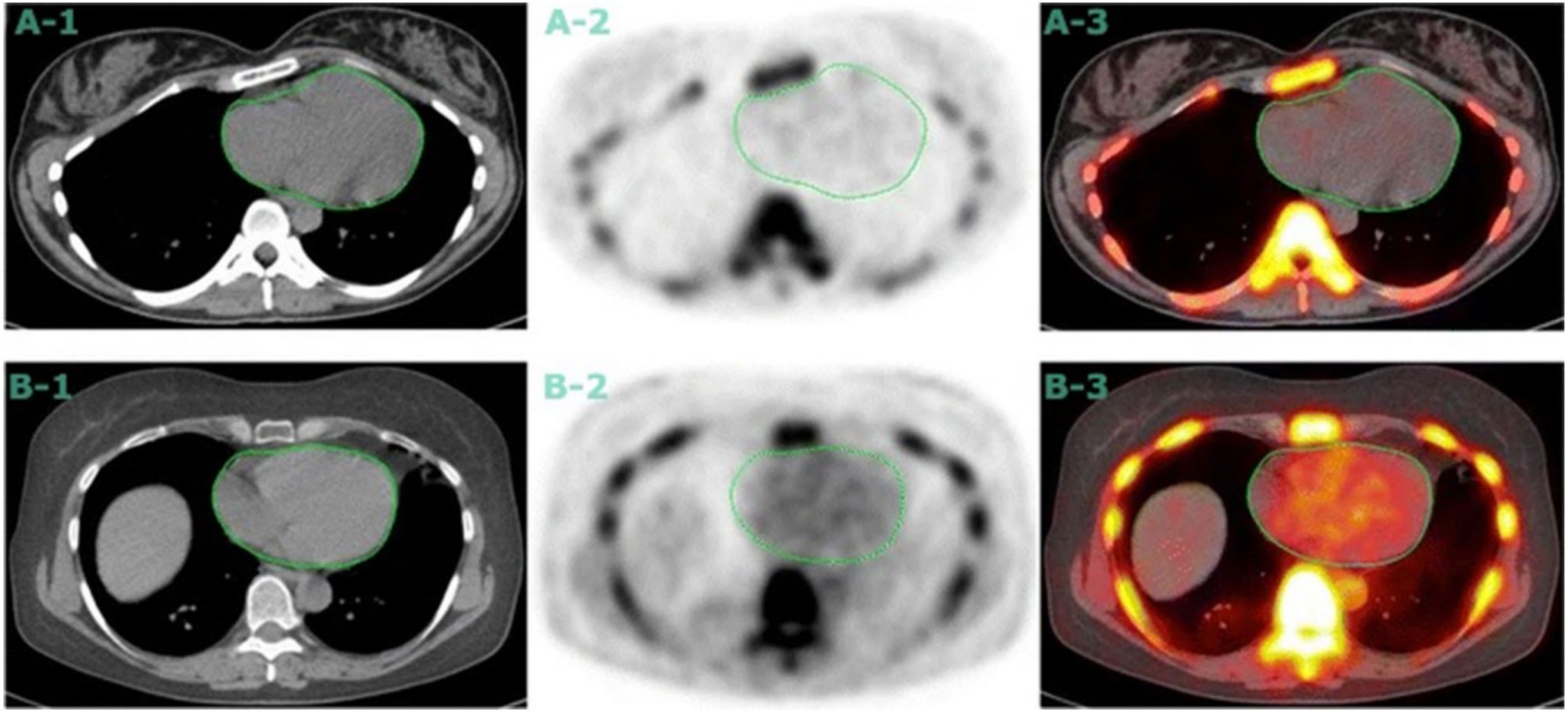

Axial CT scan (A-1 and B-1), Axial PET scan (A-2 and B-2), and axial fused scan (A-3 and B-3) of two clinically normal subjects (A, 25-year-old) and (B, 61-year-old) with delineating heart. ^{18}FNaF PET/CT images demonstrating differential coronary ^{18}F-NaF uptake in A in comparison with B. The matching CT scan shows no structural calcification at the areas of NaF uptake in subject (B), and the PET and CT results are significantly different. Coronary calcification as assessed by CT does not portray the full extent of the disease, as evidenced by its discrepancy with 18F-NaF PET/CT findings. Evidence of molecular changes in the absence of irreversible macrocalcification may allow for early interventions that can change the course of the disease.

Clinical and Translational Imaging (2022) 10:259–272https://doi.org/10.1007/s40336-022-00483-y

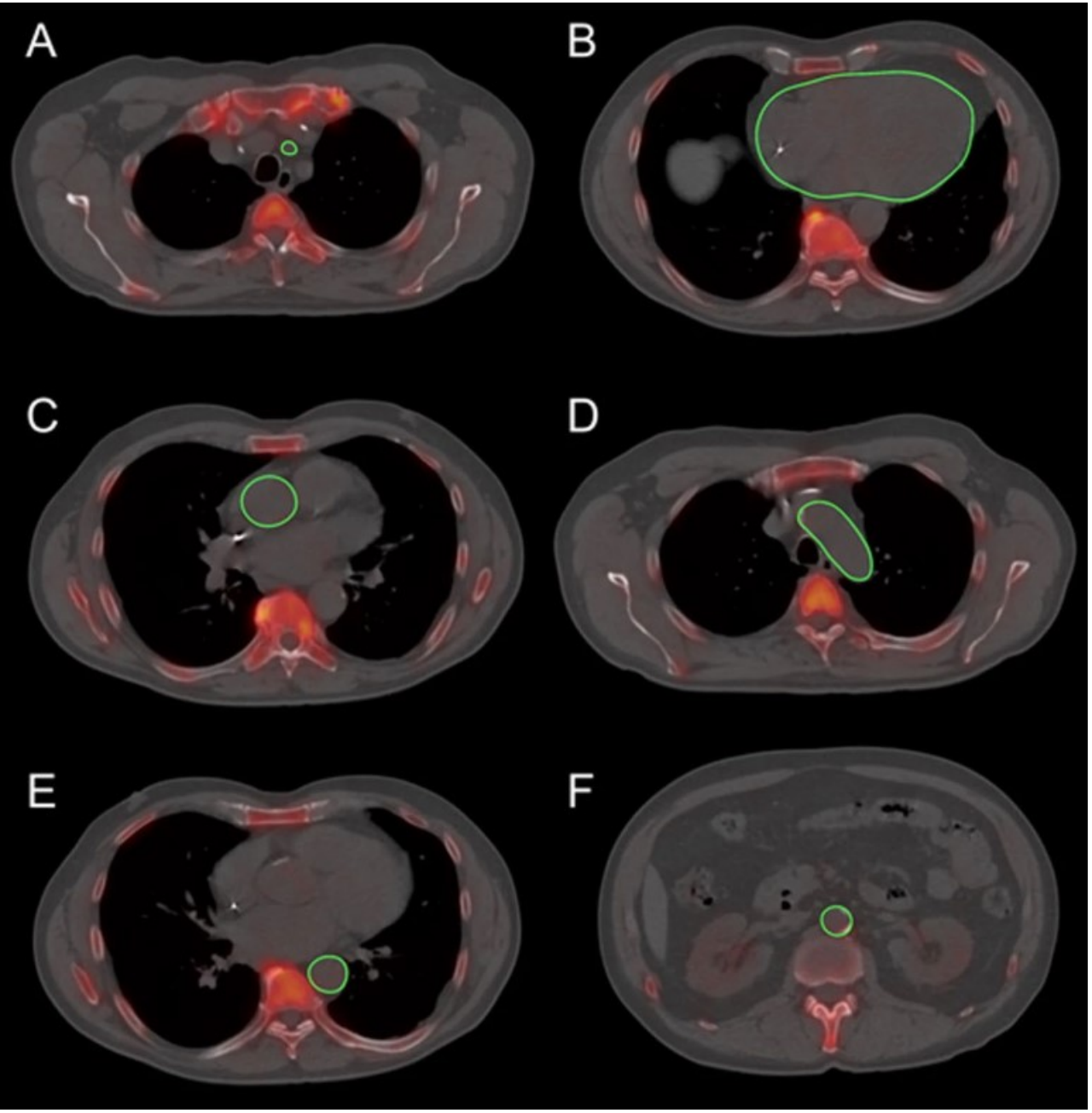

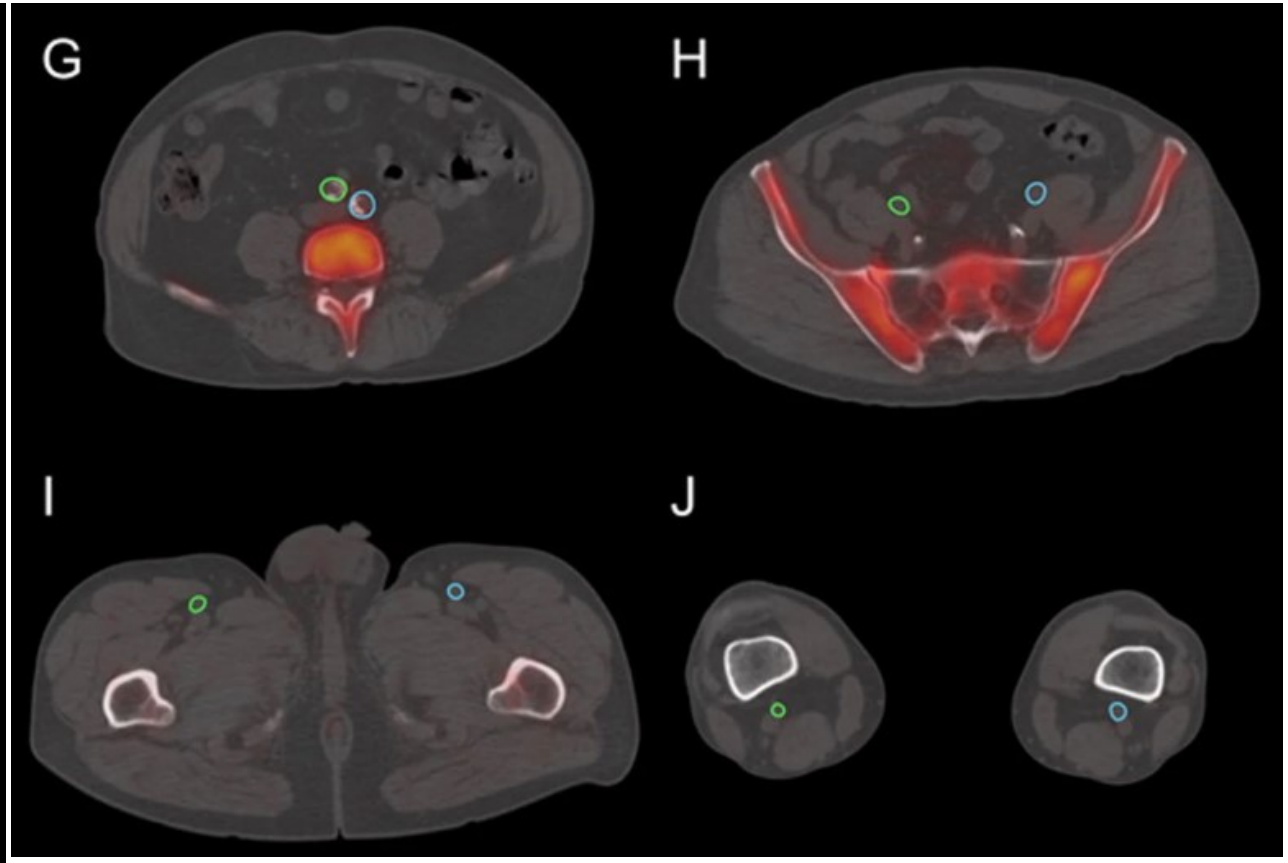

Global assessment of 18F-NaF uptake in various arterial vessels in a 67-year-old man. Regions of interest measured activity in the left carotid artery (A), coronary arteries (B), ascending aorta (C), aortic arch (D), descending aorta (E), abdominal aorta (F), bilateral common iliac arteries (G), external iliac arteries (H), femoral arteries (I), and popliteal arteries (J) to **calculate the Alavi-Carlsen global molecular calcium score**, which in this patient was determined to be 16.08.

Clinical and Translational Imaging (2022) 10:259–272https://doi.org/10.1007/s40336-022-00483-y

INVASIVE ASSESSMENT OF ATHEROSCLEROSIS

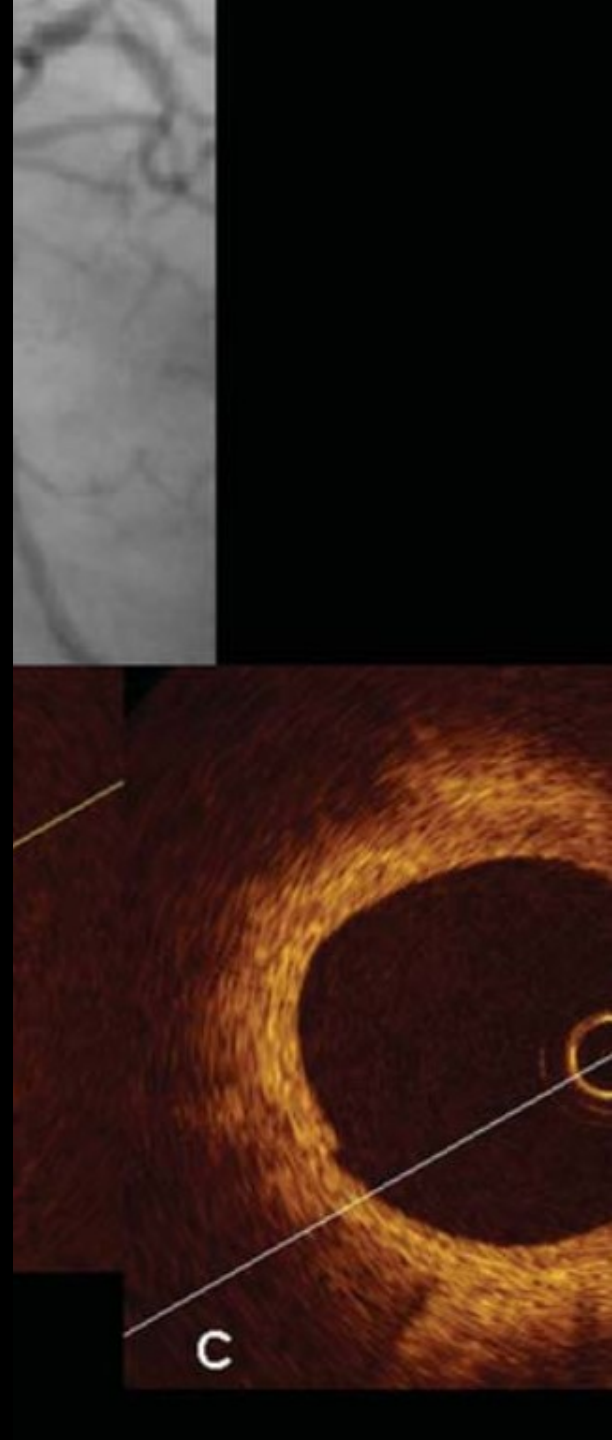

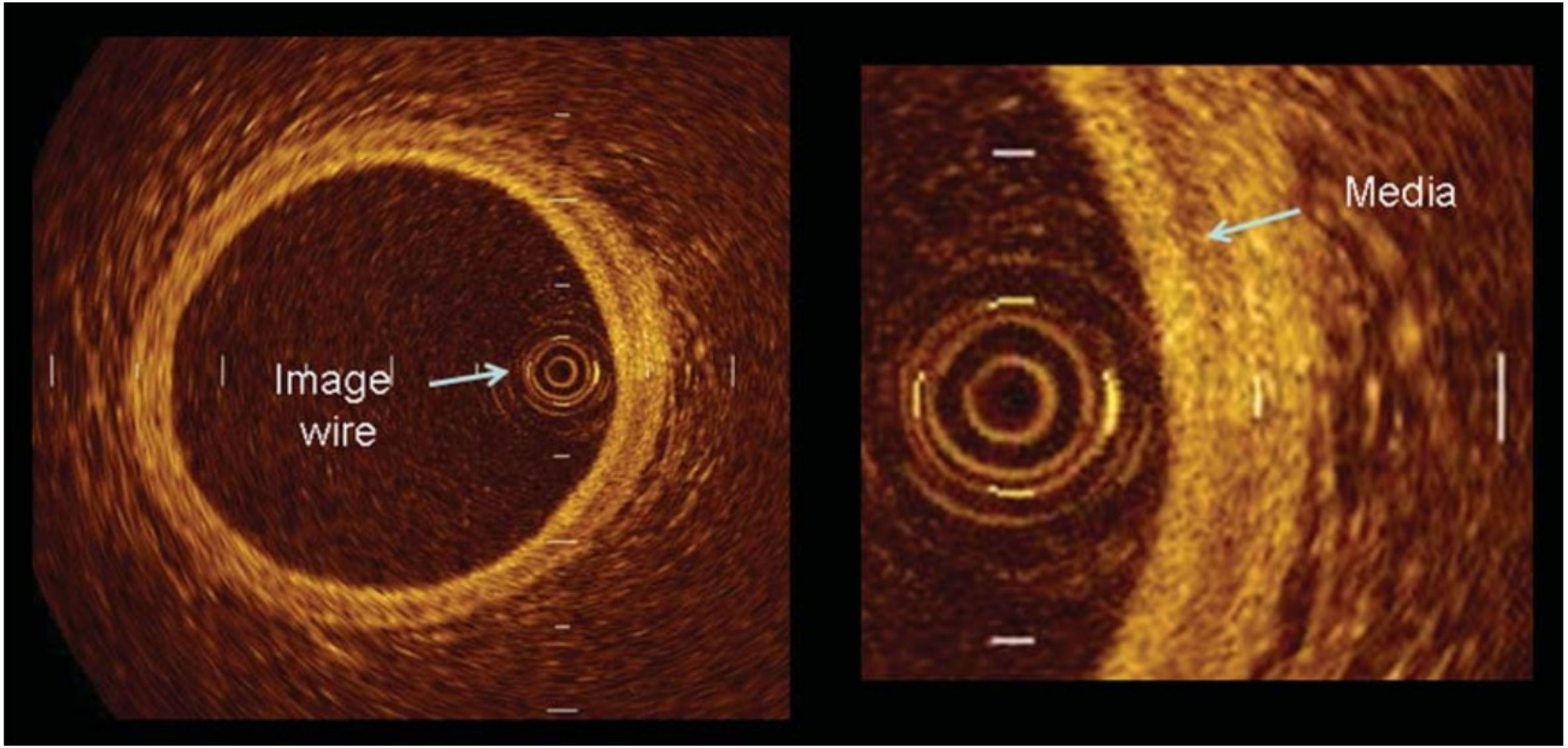

Optical coherence tomography shows the three layer appearance of normal vessel wall, with the muscular media being revealed as a low signal layer comprised between internal and external lamina.

European Heart Journal (2010) 31, 401–415 doi:10.1093/eurheartj/ehp433.

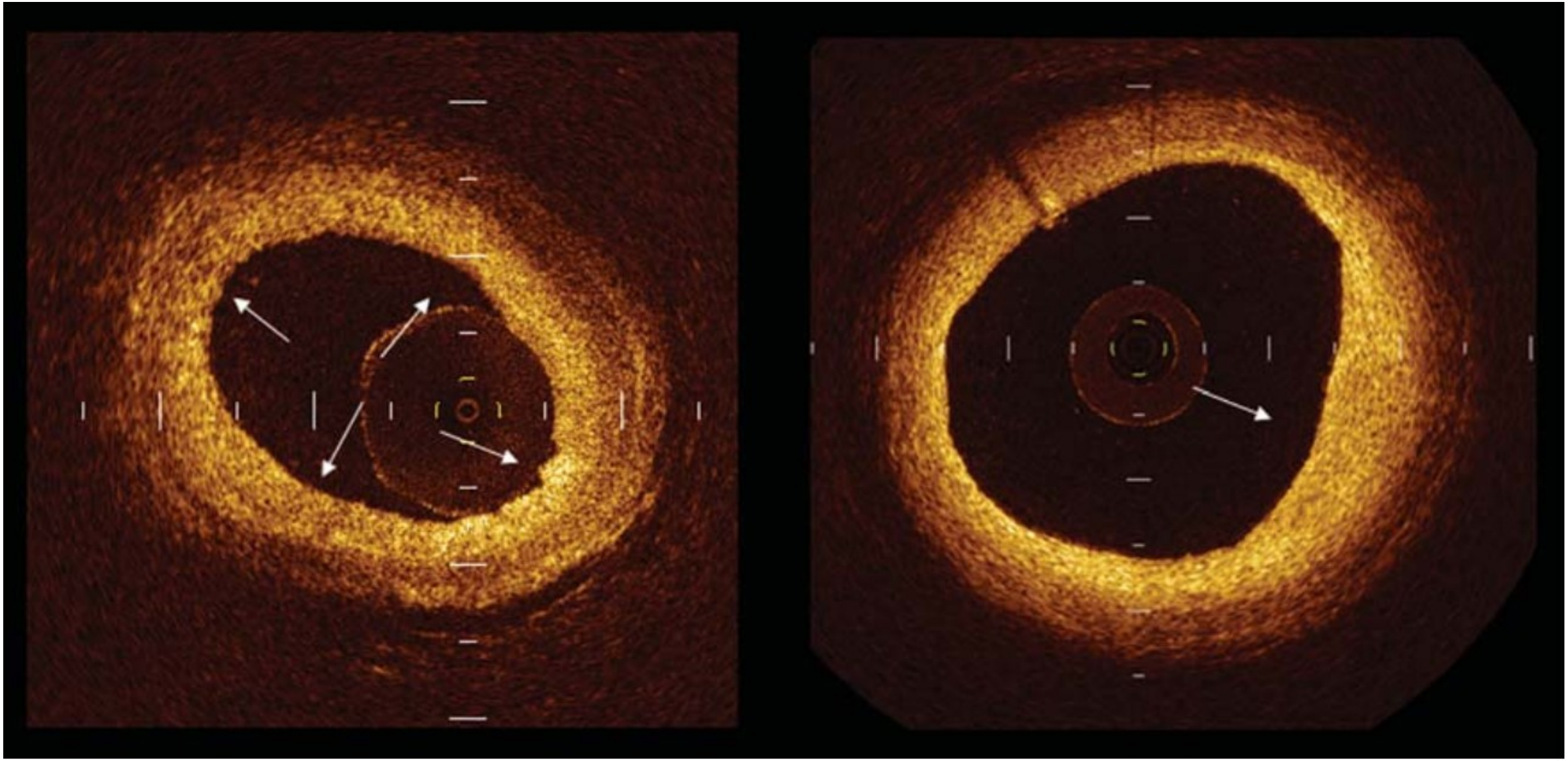

Example of intimal thickening revealed by optical coherence tomography as a bright homogeneous layer. The left panel shows a **diffuse intimal thickening**, the right panel a localized one (arrow).

European Heart Journal (2010) 31, 401–415 doi:10.1093/eurheartj/ehp433.

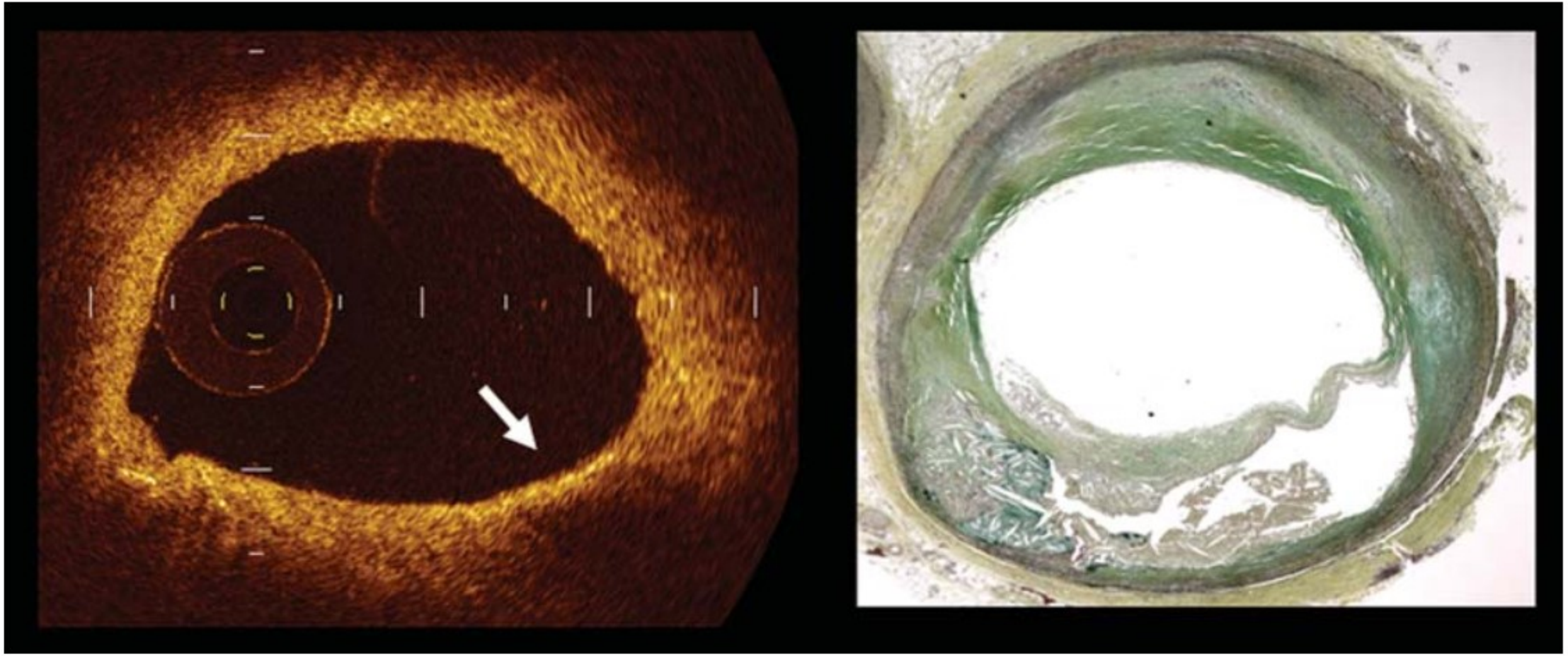

Left panel shows an optical coherence tomography example **of cluster of foam cells,** located in the fibrous cap and revealed as a band with high reflectivity (arrow). Right panel shows the corresponding histology.

European Heart Journal (2010) 31, 401–415 doi:10.1093/eurheartj/ehp433.

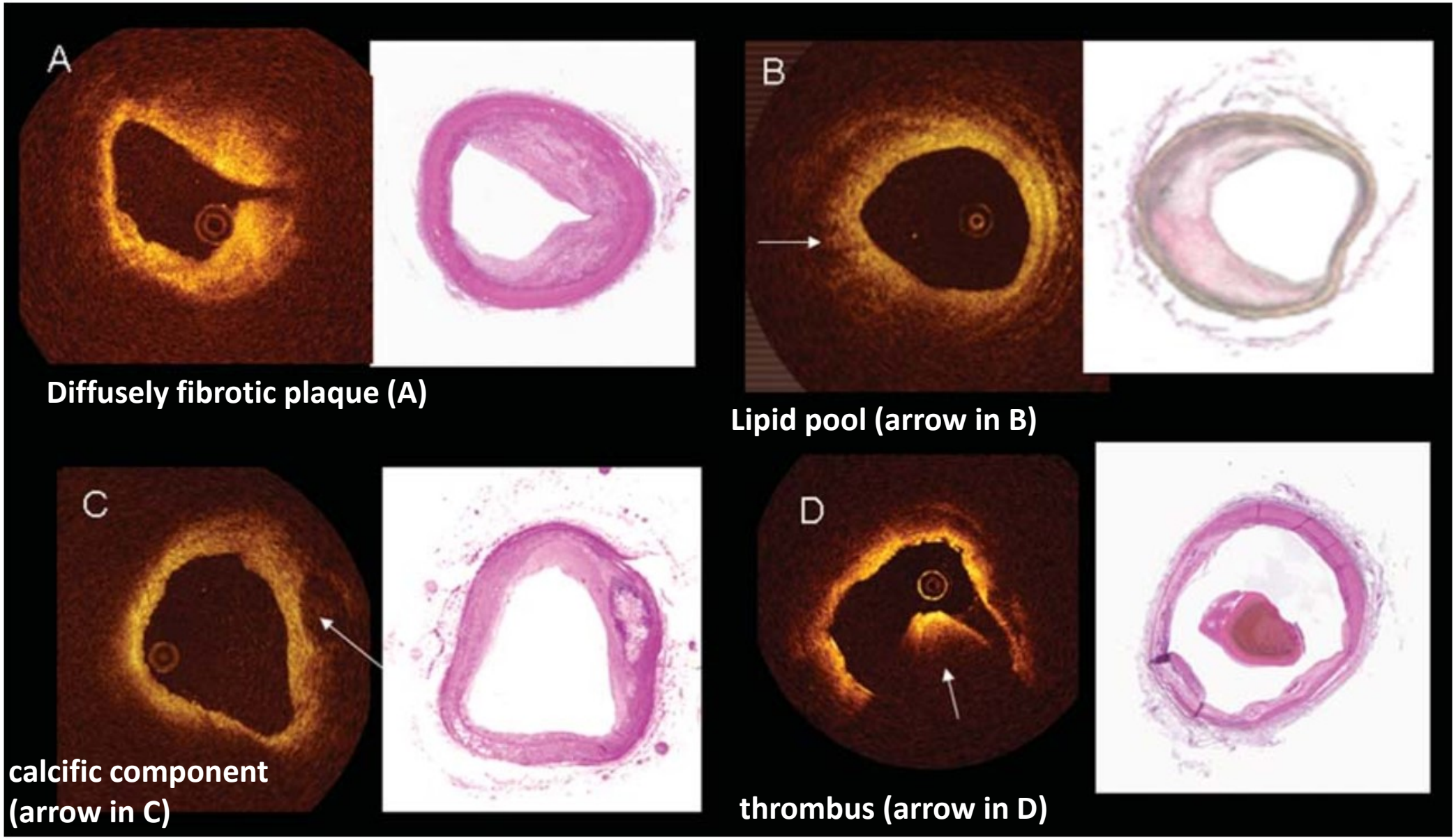

Optical coherence tomography examples of plaque composition (left panels) and corresponding histology (right panel).

European Heart Journal (2010) 31, 401–415 doi:10.1093/eurheartj/ehp433.

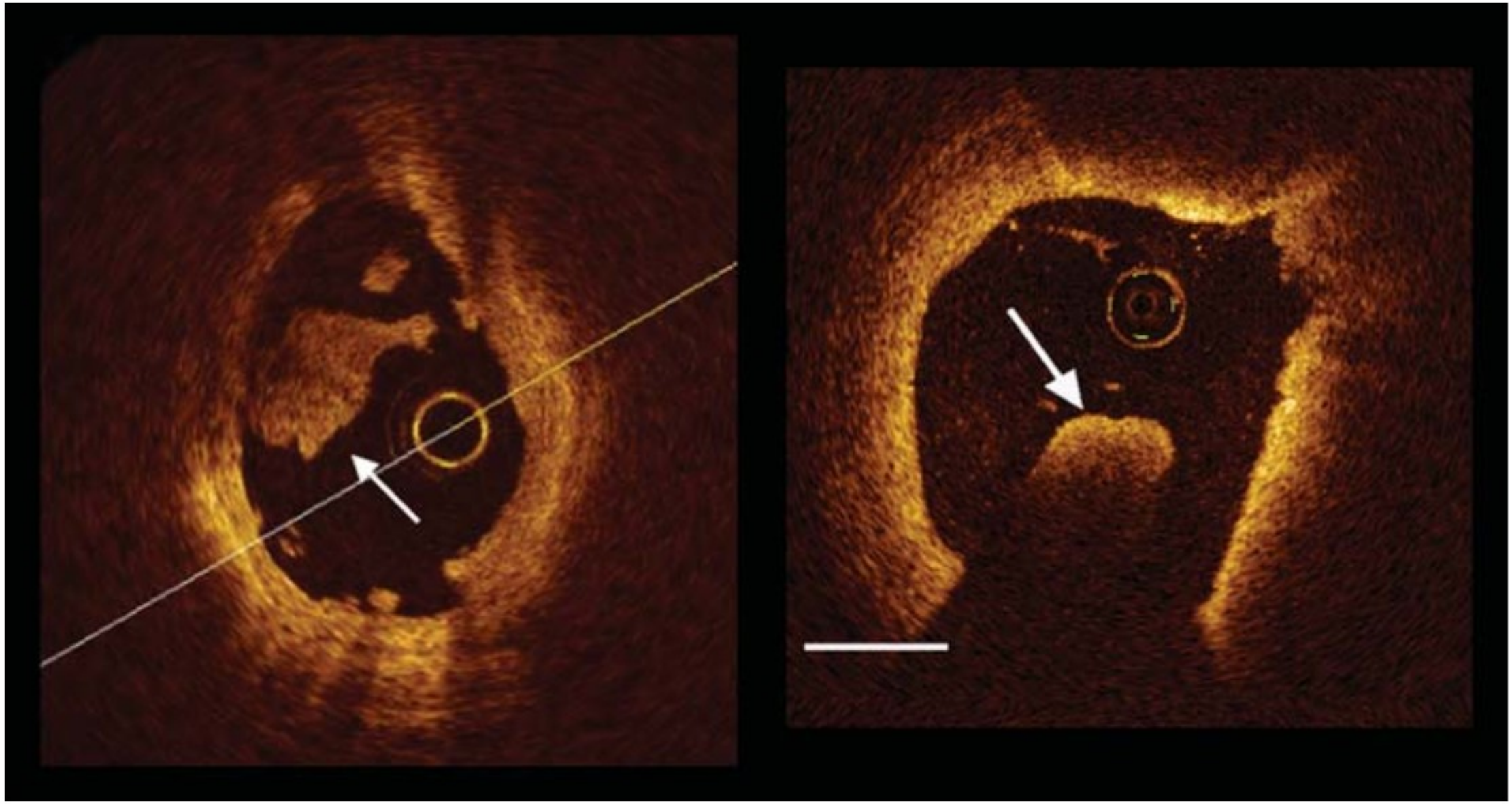

Example of white and red thrombus. **White thrombus is platelet rich and exhibits a low signal attenuation** (arrow in the left panel), while **red thrombus, due to presence of red blood cells components, causes a marked signal attenuation** (arrow in the right panel).

European Heart Journal (2010) 31, 401–415 doi:10.1093/eurheartj/ehp433.

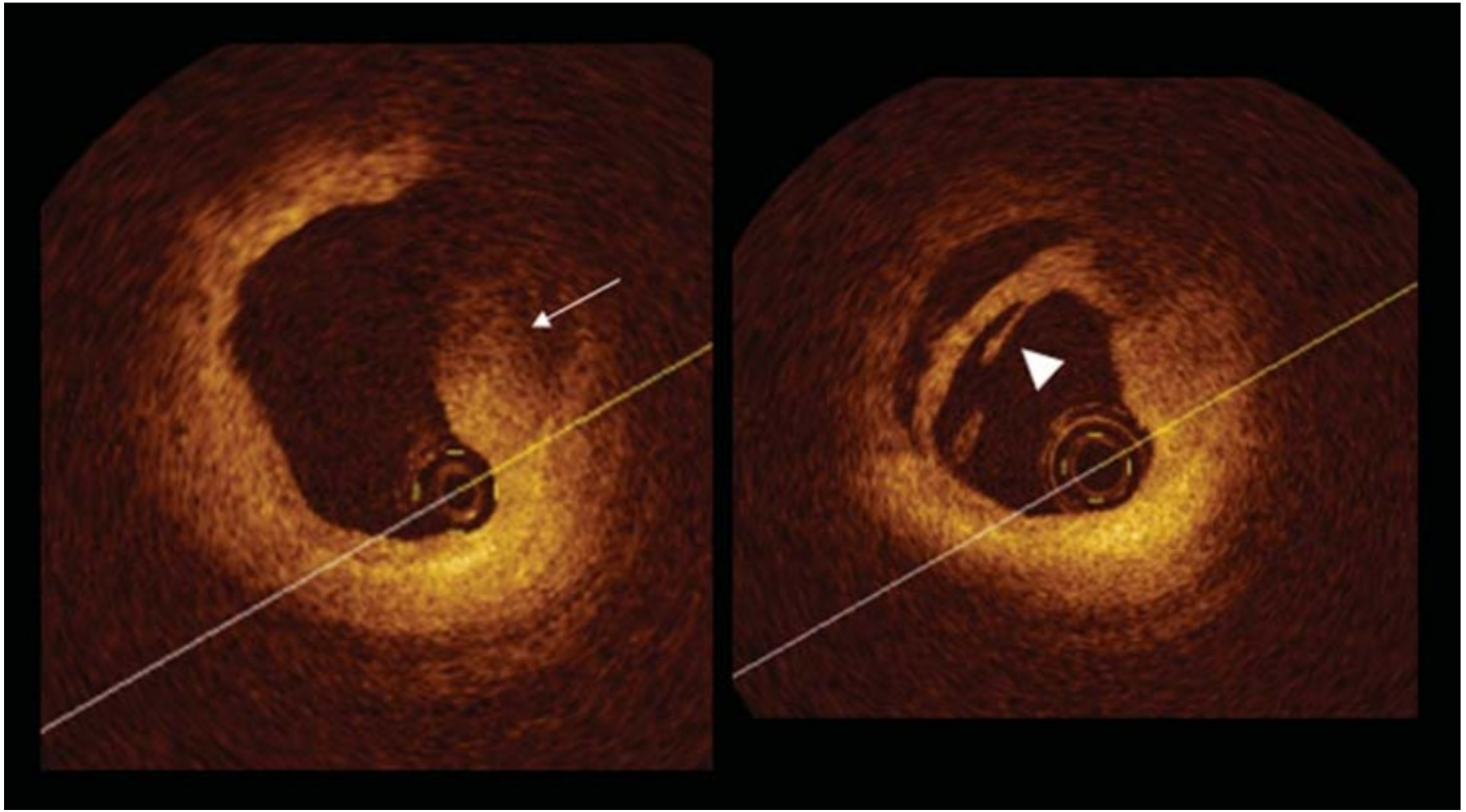

Atherosclerotic plaque with **superficial lipid pool located at 1–3 o'clock** (left panel). The right panel shows the plaque ***rupture at the site of plaque shoulder, with a clear rim of dissection*** (arrow head).

European Heart Journal (2010) 31, 401–415 doi:10.1093/eurheartj/ehp433.

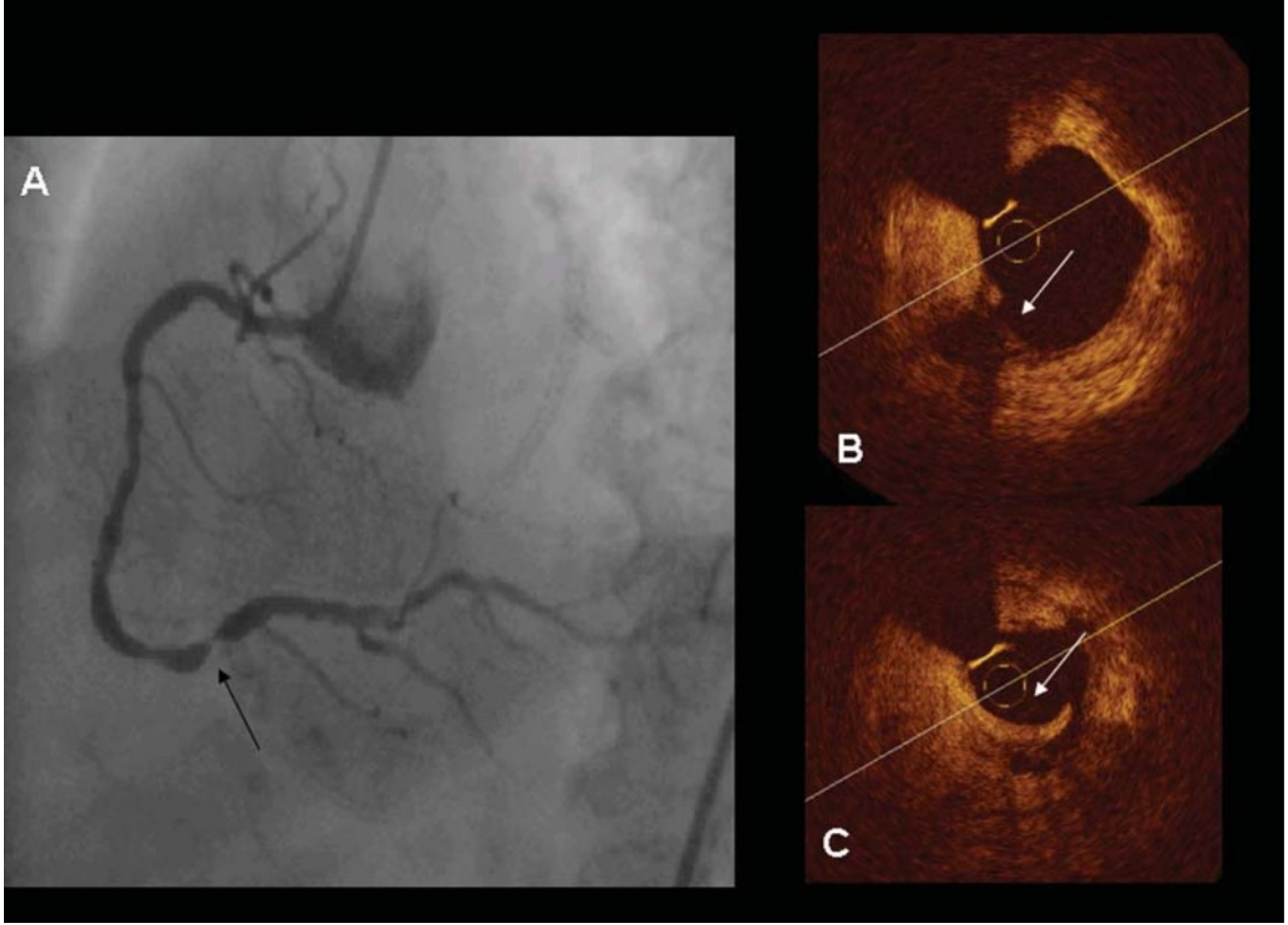

Example of culprit lesion in the right coronary artery (arrow in A). (B) shows a superficial ruptured lipid pool (arrow), while (C) reveals an intracoronary thrombosis (arrow).
Arrowheads indicate image wire artefacts.

European Heart Journal (2010) 31, 401–415 doi:10.1093/eurheartj/ehp433.

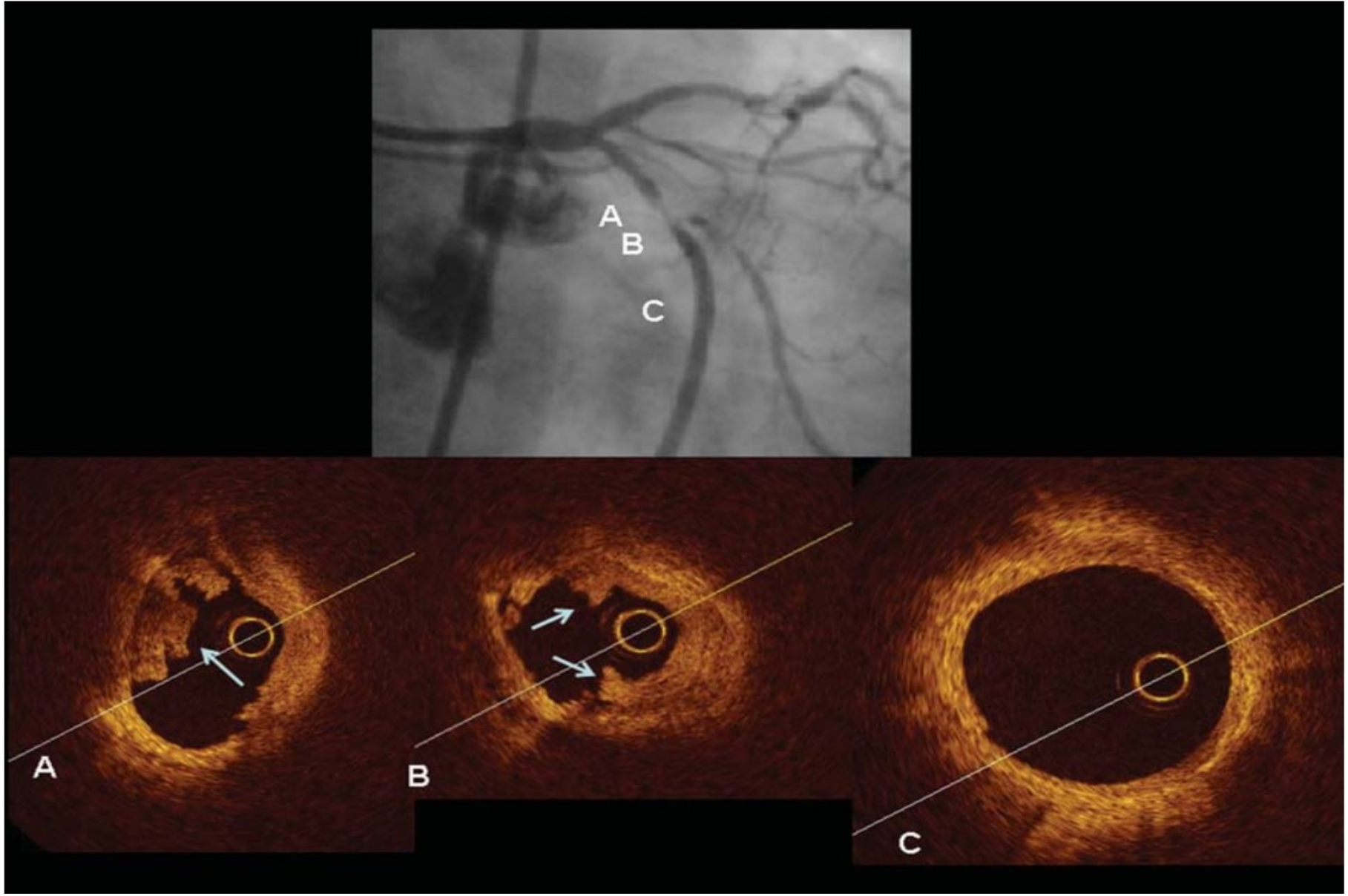

Culprit lesion in the left circumflex in a patient with unstable angina. Minimal dimensions of the optical coherence tomography probe enable an accurate visualization and quantification of lumen area (0.6 mm^2 in site B). Arrows show intracoronary thrombi at sites B and A, obtained 0.5 mm proximal to site B. In site C the proximal reference cross-section is displayed.

European Heart Journal (2010) 31, 401–415 doi:10.1093/eurheartj/ehp433.

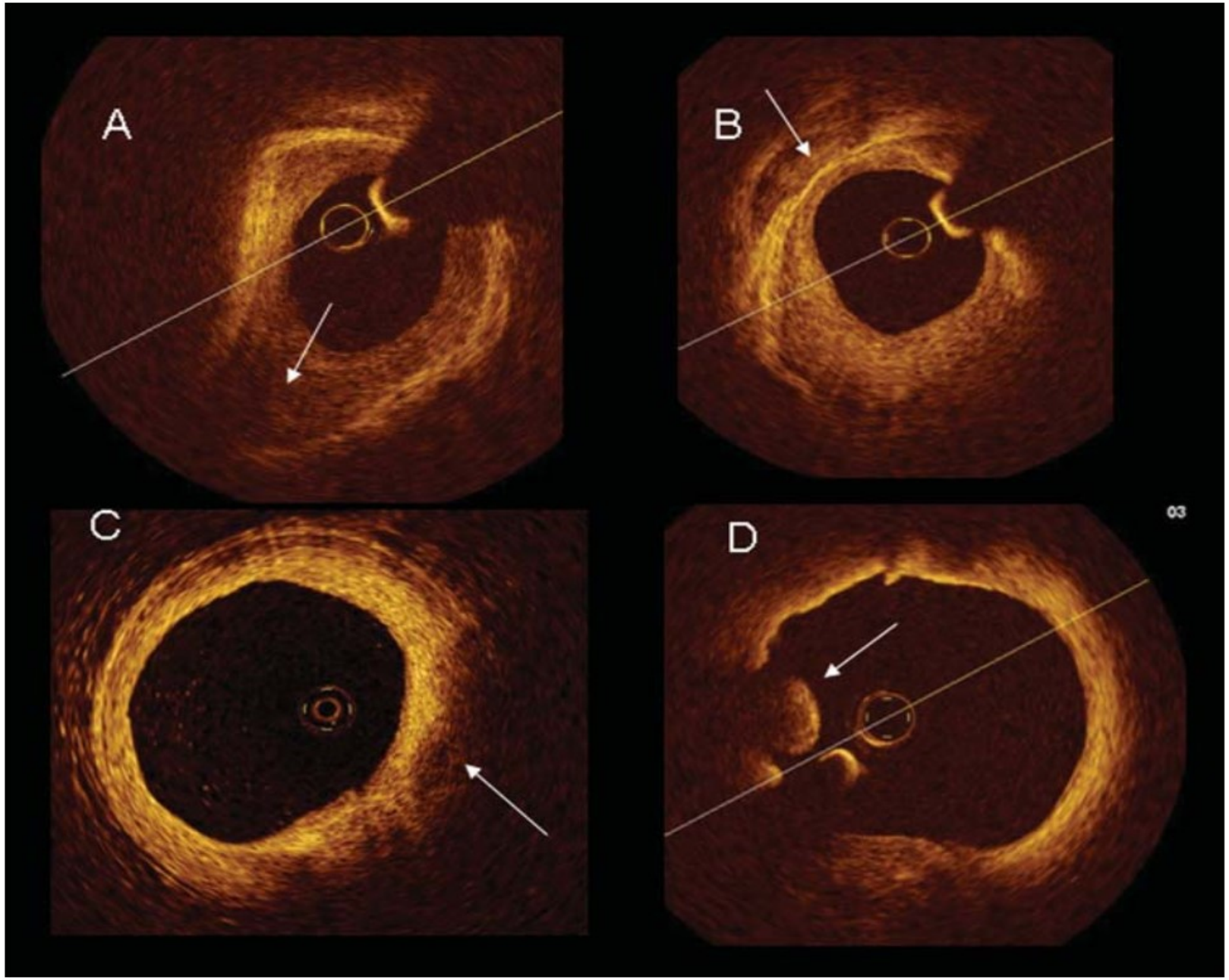

Optical coherence tomography penetration is due to plaque composition.

Penetration is maximal for fibrotic tissue (A), and progressively less for calcific (B), lipid (C), and thrombus (D).

European Heart Journal (2010) 31, 401–415 doi:10.1093/eurheartj/ehp433.

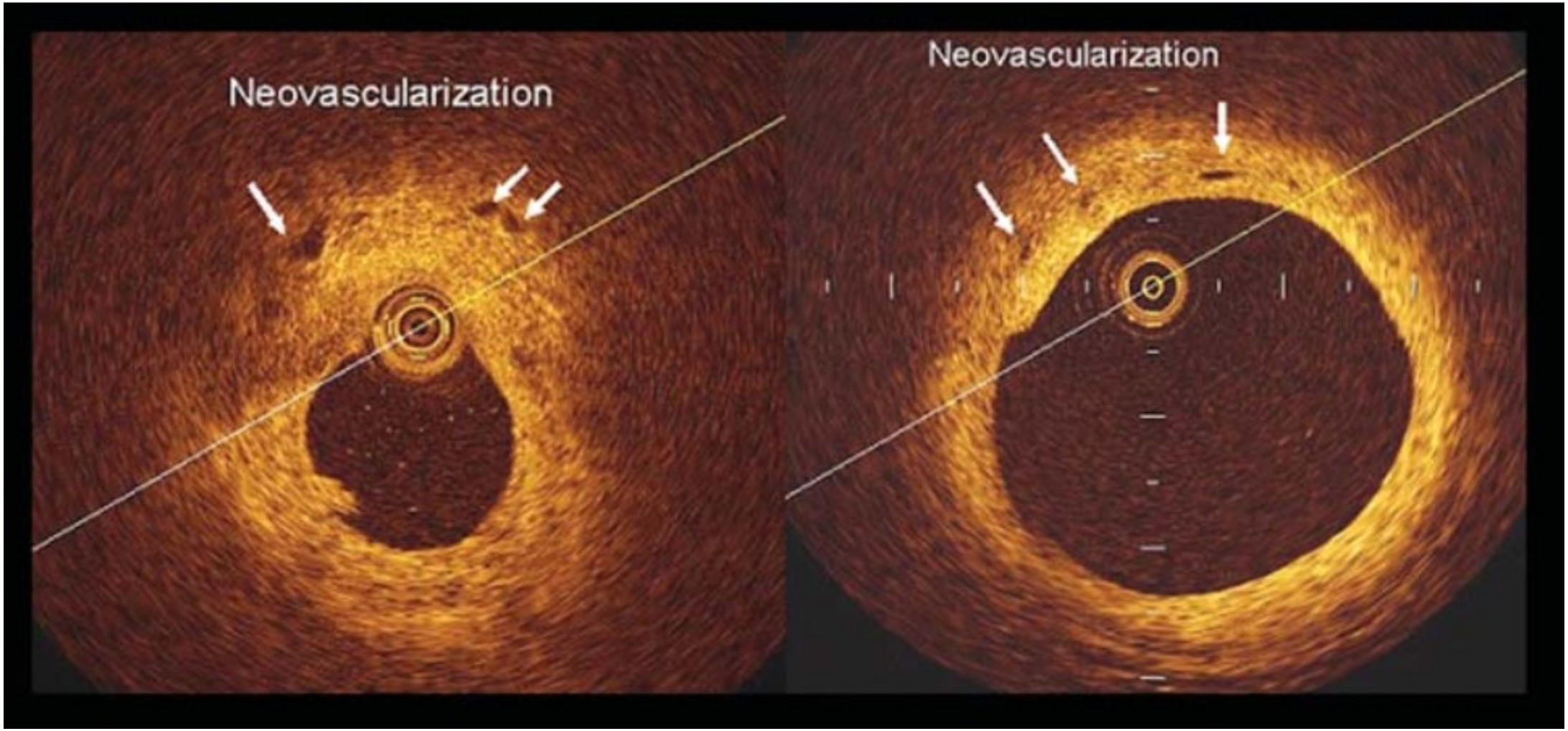

Presence of thin black holes at optical coherence tomography study, located in the outer plaque, near the adventitia (left panel) and in the inner plaque (right panel). These holes have a diameter of 50–100 mm and are likely due to plaque angioneogenesis.

European Heart Journal (2010) 31, 401–415 doi:10.1093/eurheartj/ehp433.

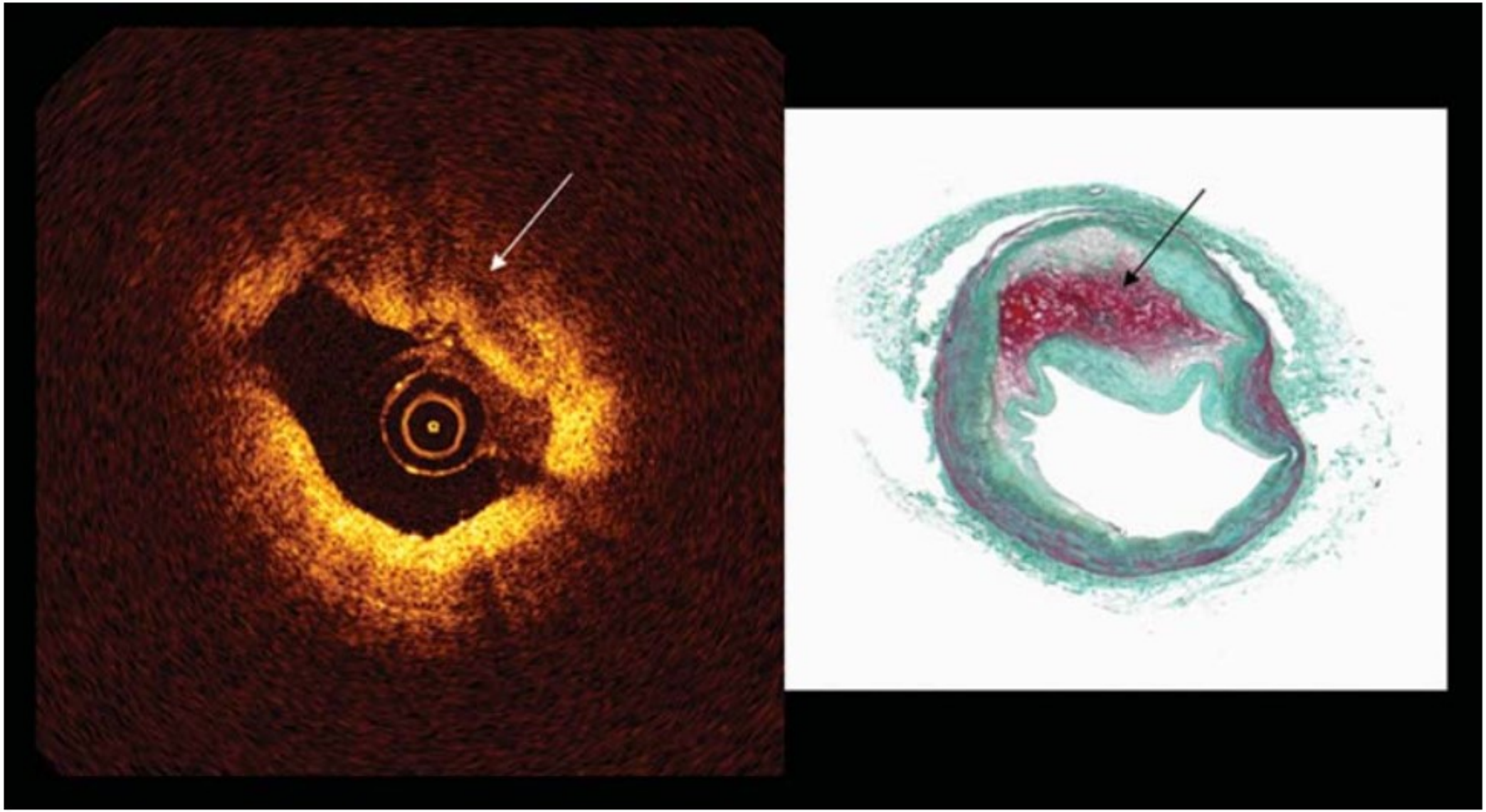

Optical coherence tomography detection of plaque hemorrhage. The left panel **shows a signal poor region** (arrow) which corresponds to an **haemorragic plaque region at histology** (arrow in the right panel).

European Heart Journal (2010) 31, 401–415 doi:10.1093/eurheartj/ehp433.

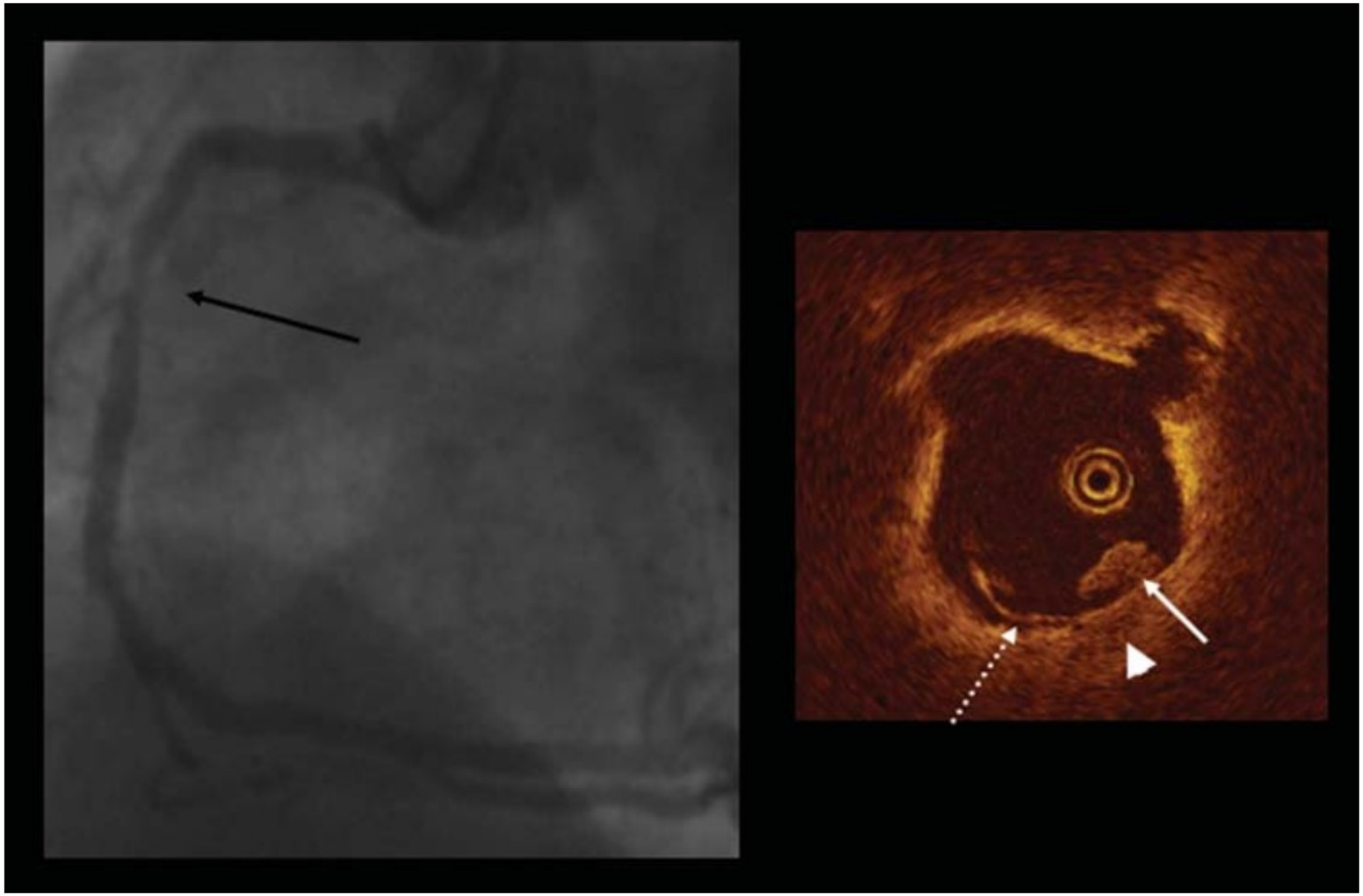

Identification of culprit lesion at the site of non-significant narrowing with angiographic haziness (A).
Optical coherence tomography shows a mild dissection (dotted arrow) and thrombus (white arrow), facing a small lipid pool (arrow-head).
A large portion of thrombus has been likely cleared by the adoption of anti-thrombotic treatment.

European Heart Journal (2010) 31, 401–415 doi:10.1093/eurheartj/ehp433.

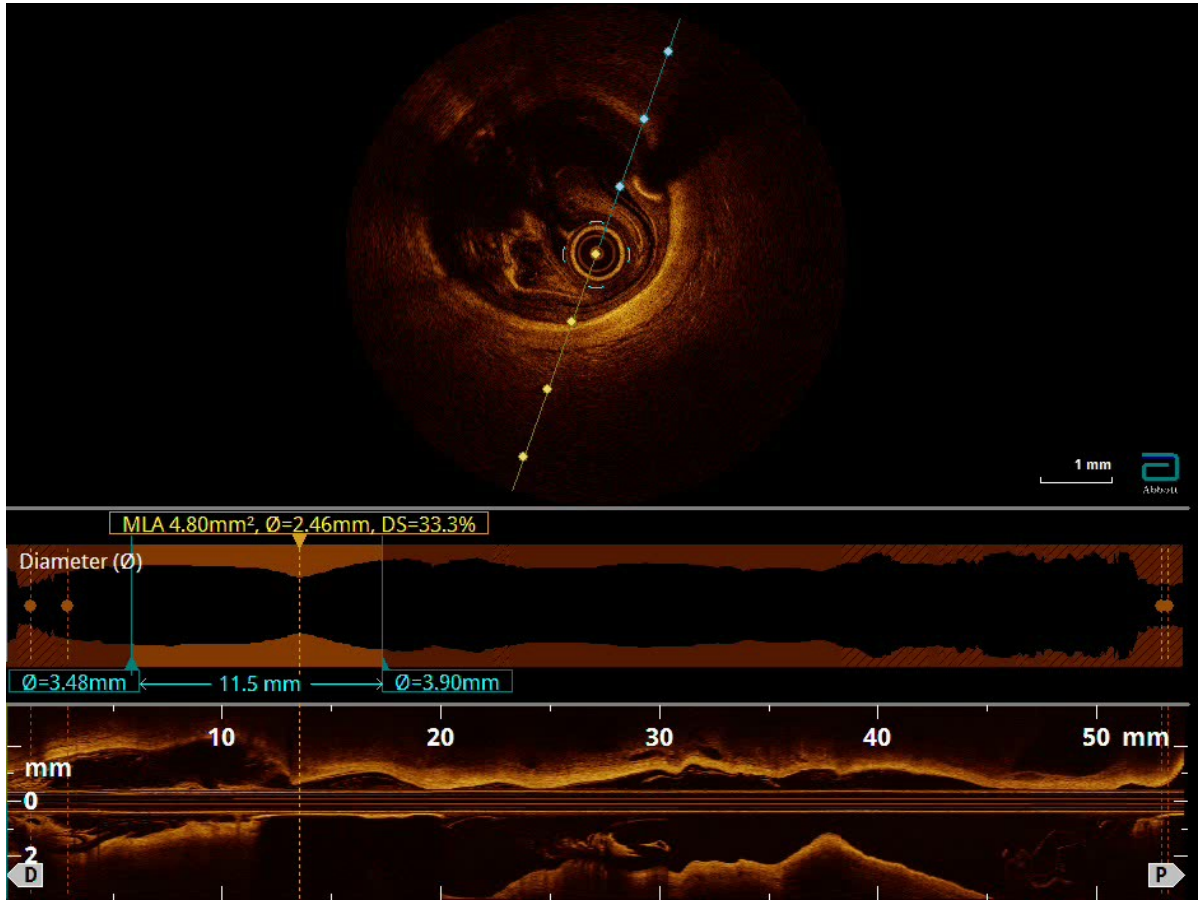
1 mm
MLA 4.80mm², Ø=2.46mm, DS=33.3%
Diameter (Ø)
Ø=3.48mm
11.5 mm
Ø=3.90mm
10
20
30
40
50 mm
mm
0
2
D
P

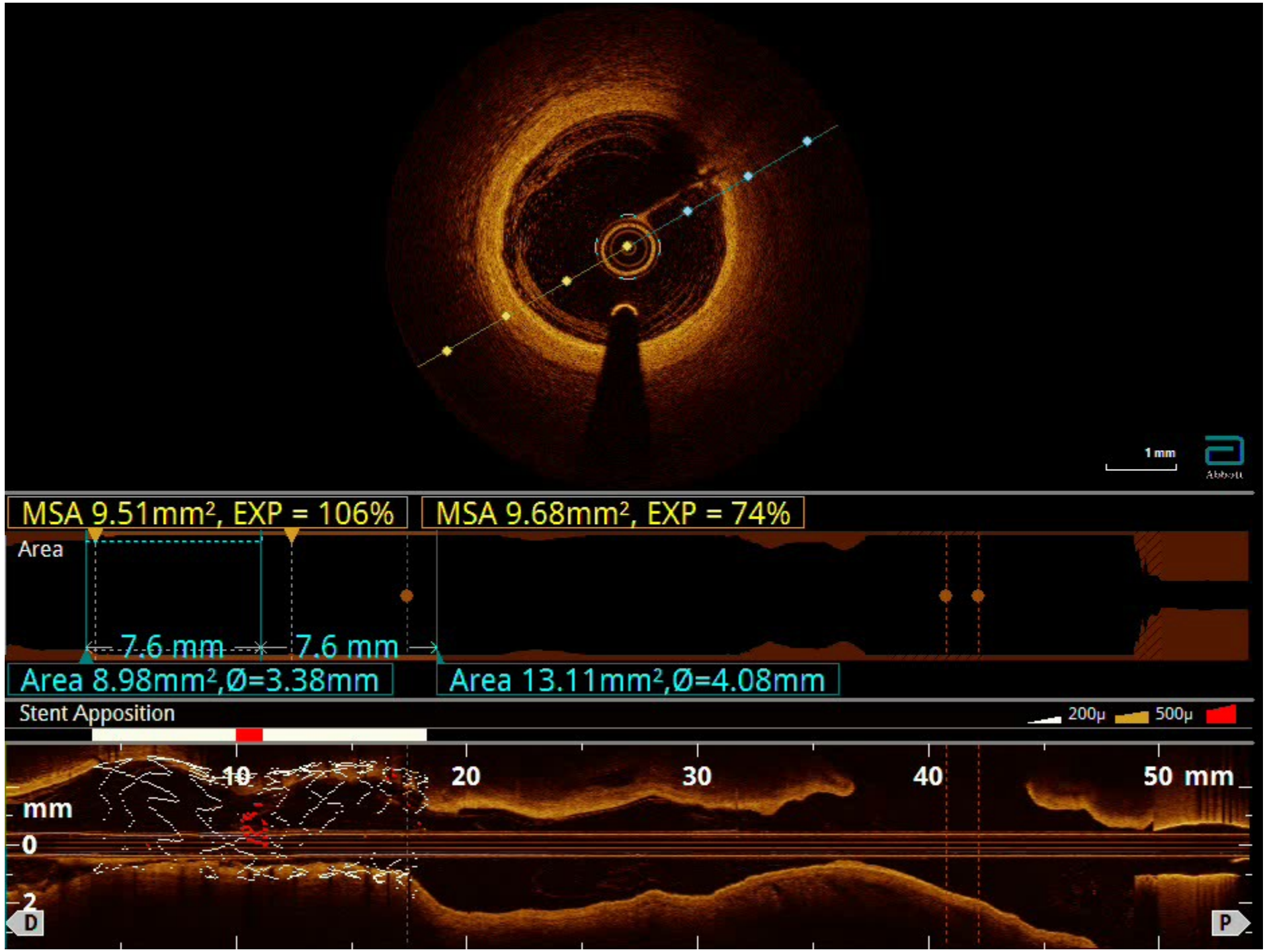
1 mm
MSA 9.51mm², EXP = 106%
MSA 9.68mm², EXP = 74%
Area
7.6 mm
7.6 mm
Area 8.98mm²,Ø=3.38mm
Area 13.11mm²,Ø=4.08mm
Stent Apposition
200µ
500µ
10
20
30
40
50 mm
mm
0
2
D
P

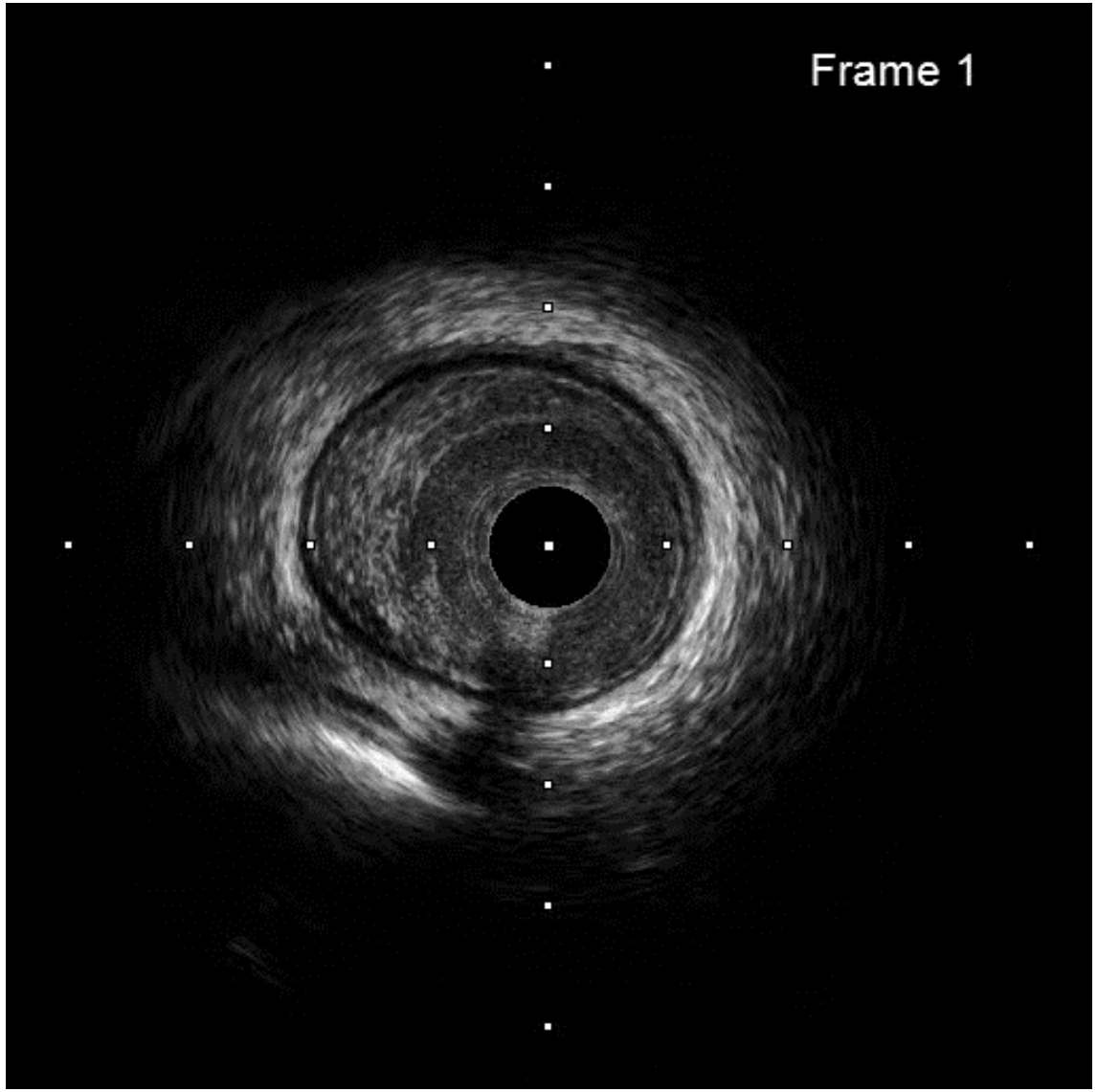
Frame 1

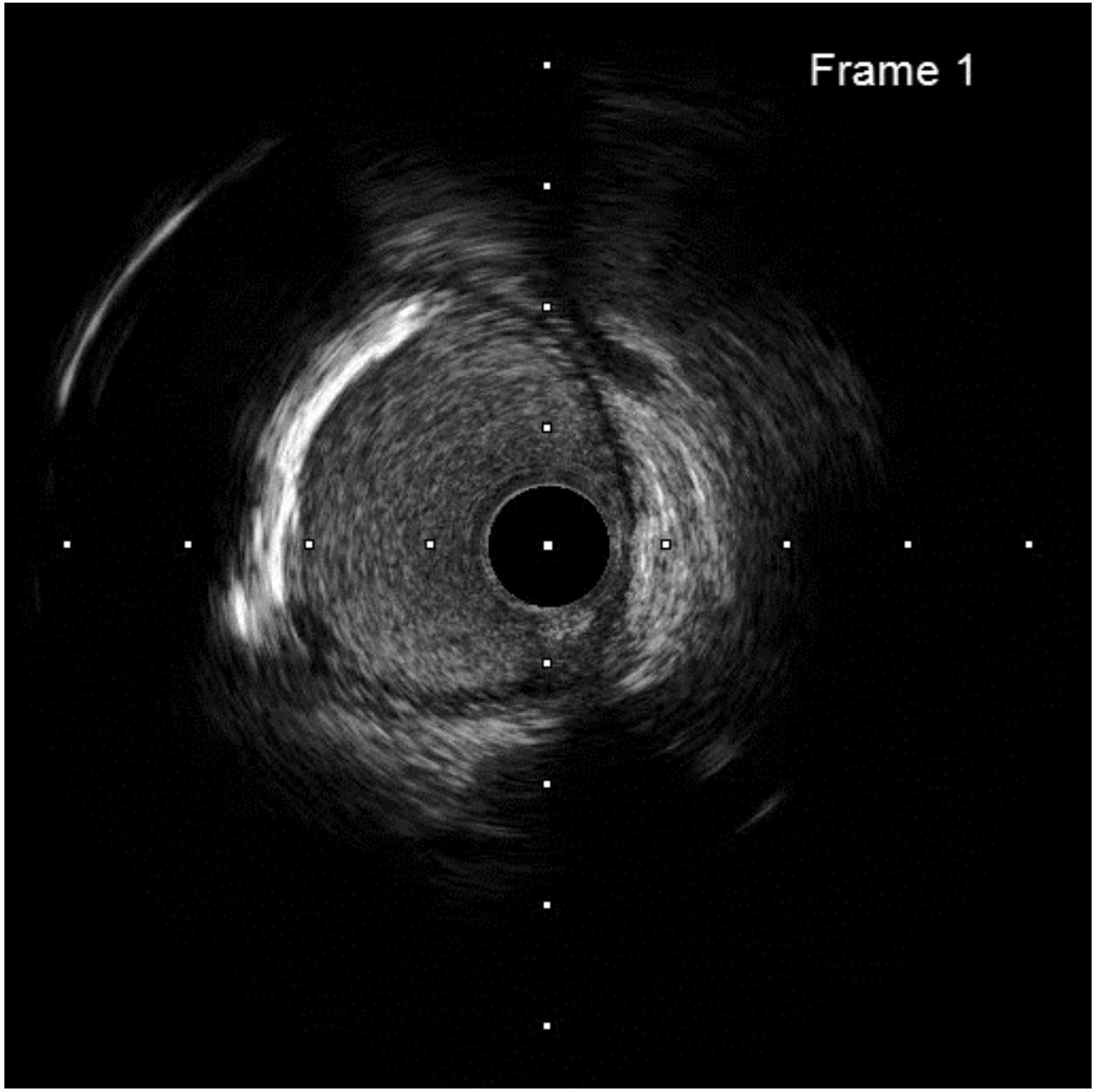
Frame 1

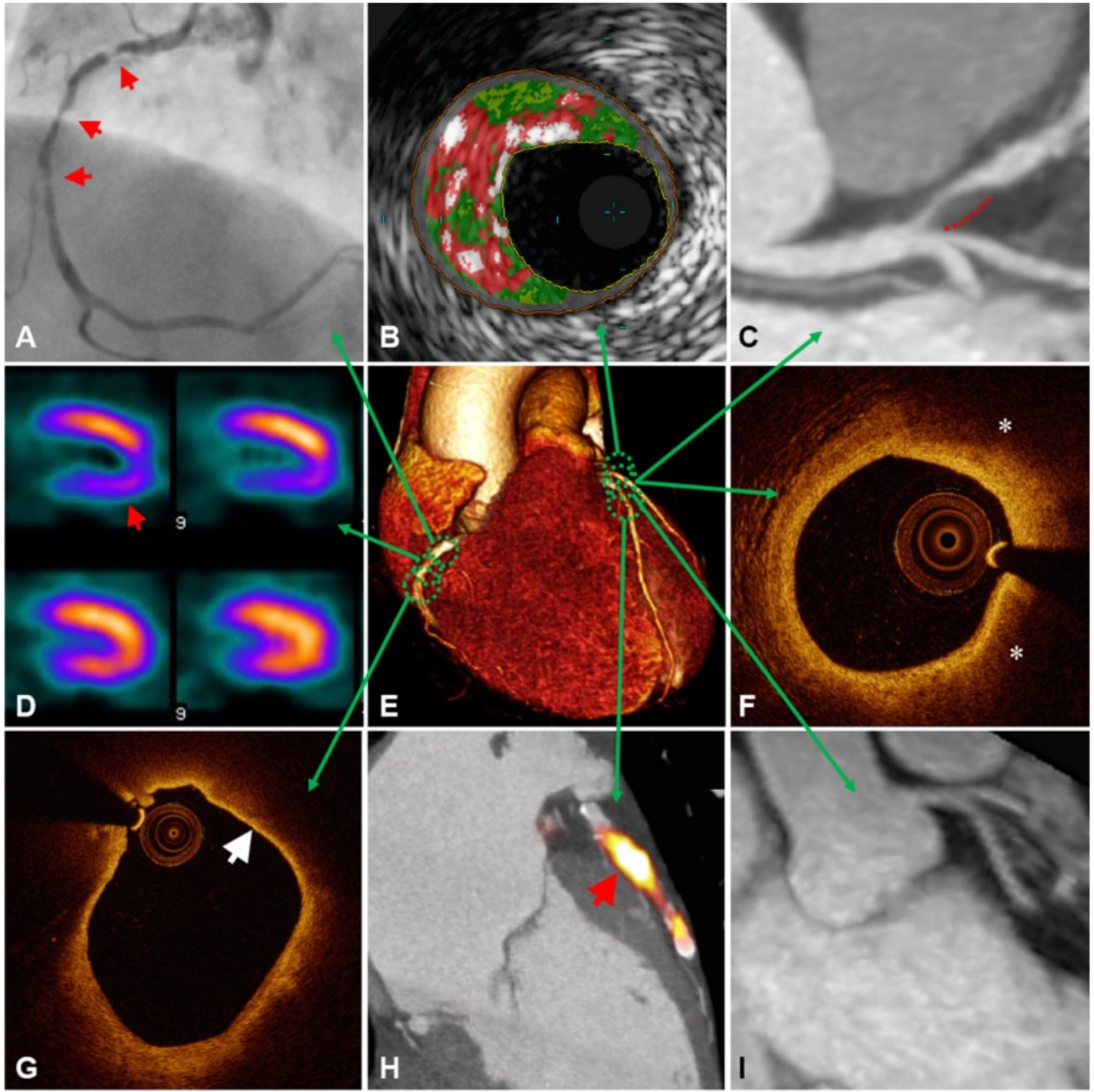

Multimodal approach to atherosclerosis imaging.
Each modality offers unique measurements of disease severity. Together, this information can be used to determine anatomic and hemodynamic consequences of atherosclerosis, complimented by detail on plaque composition, overall disease burden, and current metabolic activity acting within an individual patient.

A, X-ray angiography showing multiple right coronary artery atherosclerotic lesions (arrows) resulting in significant luminal narrowing; **B,** virtual histology intravascular ultrasound (VH-IVUS) demonstrating coronary plaque with high content of necrotic core (red), as well as dense calcium (white) and fibro-fatty regions (dark/ light green);
C, Computed tomographic (CT) angiography showing noncalcified plaque in the left anterior descending artery with positive remodeling (dashed line);
D, single-photon emission computed tomography (SPECT) myocardial perfusion scan with stress-induced perfusion defect (arrow);
E, 3D volume rendered CT whole-heart image;
F, optical coherence tomography (OCT) image of a coronary plaque showing lipid (*), characterized as signal-poor regions with poorly demarcated borders;
G, OCT image of a lipid-rich coronary plaque displaying thin overlying fibrous cap (arrow), indicative of thin-cap fibroatheroma;
H, Fused 18F-NaF positron emission tomography (PET)–CT image showing high left anterior descending artery tracer uptake (arrow) revealing active plaque microcalcification;
I, 3-T magnetic resonance (MR) contrast-angiography performed with dual ECG and respiratory navigator gating showing clear delineation of the proximal left-sided coronary vessels.

Circ Res. 2016;118:750-769. DOI: 10.1161/CIRCRESAHA.115.306247.